Dissolution behavior of silver nanoparticles in environmental samples using single particle inductively coupled plasma mass spectrometry

Mehrnoosh Azodi

Doctor of Philosophy

Department of Civil Engineering and Applied Mechanics,
McGill University
Montreal, Quebec, Canada
April 2017

A thesis submitted to McGill University in partial fulfillment of the requirements of the degree of Doctor of Philosophy

Copyright © Mehrnoosh Azodi, 2017

TABLE OF CONTENTS

LIST OF FIGURES

LIST OF TABLES

ABSTRACT

Silver nanoparticles (nAg) are used in various consumer products due to their distinct antimicrobial and antibacterial properties. However, there is growing concern about the environmental fate of the engineered nanoparticles (ENPs) and the potential risks to various biota. A significant fraction of nAg in usage is released from various products slowly but persistently, and eventually discharged with municipal wastewater (WW). The chemical transformation (i.e. dissolution of nAg) during the treatment processes and the accurate detection of environmentally relevant concentrations of Ag (nAg, and dissolved) in WW is a knowledge gap. Dissolution of nAg and the ion release over time has been shown to contribute to the toxicity of nAg in aquatic environments. Thus one objective of the research was to assess the dissolution rate and extent of nAg in municipal WW using arelatively new technique, single particle inductively coupled plasma mass spectrometry (spICP-MS). In addition, the surface speciation of nAg in WW and the fate of dissolved Ag after release were assessed.

The dissolution of nAg in municipal wastewater (WW) collected from the secondary aeration tank and the effluent of a treatment facility was characterized. After 168 h the concentration of dissolved (ionic and complexed with natural organic matter or other dissolved moieties in wastewater) Ag in WW effluent was 71% of the dissolved Ag in deionized (DI) water, in batch reactors spiked with 5×10^6 PVP-nAg particles/mL (10 µg/L), an environmentally relevant concentration. Dissolved Ag in WW was partly reformed into ~22 nm nAg_xS_y by inorganic sulfides and organosulfur fractions of dissolved organic carbon (DOC) after 120 h. Reformation of nAg_xS_y from Ag^+ also occurred in cysteine solutions but not in DI water, or humic and fulvic acid solutions. Dissolution experiments with nAg in WW mixed liquor showed qualitatively similar dissolution trends. Time-of-Flight Secondary Ion Mass Spectrometry (ToF-

SIMS) and X-ray photoelectron spectroscopy (XPS) analyses indicated binding of thiol- and amine-containing DOC as well as inorganic sulfides with nAg.

Reaction of nAg with inorganic sulfides resulted in the formation of insoluble Ag_2S and resulted in 97% lower dissolution of nAg as compared to DI water system. However, there is a lack of understanding how dissolved organic matter influences the extents of sulfidation and dissolution. Therefore, to assess the dissolution patterns of sulfidated nAg under environmentally relevant conditions nAg (30, 50 and 100 nm) was contacted over 648 h with sulfides before (pre-sulfidation), after (post-sulfidation) and simultaneously with DOC compounds (humic acids, and fulvic acids, alginate, and a mixture of cysteine and methionine) . The inorganic sulfides were a mixture of metal sulfides of copper and zinc at S to Ag mole ratios of 0.4 and 10. The results suggested that the presence of humic substances significantly enhanced the dissolution of sulfidated nAg up to 400% for 30 nm nAg in post-sulfidation systems compared to that in DI water systems. Humic and fulvic acids were able to enhance dissolution of nAg in systems containing sulfides through two pathways: binding to the sulfides in solution, and complexation to the surface of nAg and blocking sites for sulfidation reaction. However, alginate did not bind to dissolved sulfides and was only able to suppress sulfidation of nAg when it was contacted with NPs prior to sulfides. No dissolved Ag was measured in the mixture of amino acids (i.e. cysteine and methionine) while reformation of small nAg was observed in this system.

nAg in environmental samples is polydisperse and have a wide size distribution from very small diameters to large aggregates which are difficult to detect with many of present techniques. This study developed a method to improve the characterization of very small nAg (10 nm) and very large nAg (200 nm) with spICP-MS. First, the transport efficiency of NPs was determined by using a standard nAu with a mean size close to the test nAg samples; second, a

NP calibration curve using the standard sized nAg was applied both of which significantly improved the analysis of 10 nm and 200 nm nAg. Conventionally, transport efficiency is assessed using 60 nm nAu for the analysis of various nAg diameters, and calibration curves are prepared using dissolved Ag. nAg of a wide range of diameters from 10 nm to 200 nm at short and long dwell times (10-3000 μs) using spICP-MS in DI water, and in WW media, were performed under the modified settings to demonstrate their relevance to accurate estimations on nAg sizes and concentrations.

Overall, this research demonstrates nAg dissolution behavior in complex environmental aqueous samples, and systems with various concentrations of DOC and inorganic sulfides at environmentally relevant concentration of nAg. spICP-MS analyses parameters were optimized for analysis nAg of various sizes so as to be able to accurately track the mean size, the dissolved fraction and particle number concentration in complex environmental matrices.

RÉSUMÉ

Les nanoparticules Ag (nAg) sont utilisées dans divers produits de consommation en raison de leurs activités antimicrobiennes et antibactériennes attrayantes. Cependant, on s'inquiète de plus en plus du devenir environnemental de ces nanoparticules artificielles (PEV) et des risques potentiels pour divers biota dus à leur rejet dans l'environnement aquatique. On sait qu'une fraction importante de nAg pendant l'utilisation est libérée des produits et éventuellement déchargée dans des eaux usées municipales (WW). Ainsi, la transformation chimique (c'est-à-dire la dissolution de nAg) au cours des processus de traitement et la détection précise de très faible concentration d'Ag (nAg et dissous) dans la matrice complexe de WW sont les lacunes actuelles. La dissolution de nAg et la libération d'ions dans le temps est attribuée à la toxicité de nAg dans la littérature précédente. L'objectif de la recherche était d'évaluer le taux de dissolution et l'étendue de nAg dans la WW municipale et dans l'environnement avec une concentration considérable de carbone organique dissous (DOC) et de sulfures inorganiques en utilisant une spectrométrie de masse par plasma à couplage inductif à une seule particule (spICP-MS). De plus, on évalue la spéciation de surface de nAg dans WW et le devenir de l'Ag dissous après libération.

Nous avons évalué la dissolution de nAg dans les eaux usées municipales (WW) collectées à partir de la cuve d'aération secondaire et de l'effluent de l'installation de traitement. La concentration en Ag dissous (non-particulaire) dans l'effluent WW était de 71% de l'Ag dissous dans de l'eau désionisée (DI) à 168 h, dans des réacteurs discontinus additionnés de 5 x 106 particules de PVP-nAg / mL (10 μg / L), une concentration environnementale pertinente. L'AG dissout dans WW a été partiellement réformé en ~ 22 nm nAg_xS_y par des sulfures inorganiques et organosulfur DOC après 120 h. La réformation de nAg_xS_y à partir d'Ag + s'est

également produite dans des solutions de cysteine, mais pas dans l'eau DI, ni dans des solutions d'acide humique et fulvique. Des expériences de dissolution avec nAg dans une liqueur mixte WW ont montré des tendances de dissolution qualitativement similaires. Des analyses de spectrométrie de masse d'ions secondaires de temps de vol (ToF-SIMS) et de spectroscopie de photoélectrons de rayons X (XPS) ont indiqué une liaison de DOC contenant du thiol et de l'aminé ainsi que des sulfures inorganiques avec nAg.

La réaction de nAg avec des sulfures inorganiques a entraîné la formation d'Ag_2S insoluble et donc une dissolution inférieure de 97% de nAg par rapport au système d'eau DI. Par conséquent, pour évaluer le comportement de dissolution de nAg sulfuré dans des conditions environnementales pertinentes, nous avons évalué l'exposition de nAg (30, 50 et 100 nm) aux sulfures avant (pré-sulfuration), après (post-sulfuration) et simultanément à l'addition de composés de DOC sur 648 h période d'étude. Les sulfures inorganiques étaient un mélange de sulfures métalliques de cuivre et de zinc à deux taux de sulfure en rapport molaire Ag (S: Ag=0,4 et 10). Les résultats suggèrent que la présence de substances humiques améliore significativement la dissolution de nAg sulfuré jusqu'à 400% pour nAg de 30 nm dans des systèmes de post-sulfuration. Les substances humiques ont pu améliorer la dissolution par deux voies; d'abord par l'accumulation des sulfures métalliques et d'autre part par complexation de la surface de nAg et réduction des sites actifs pour la réaction de sulfures métalliques libres avec nAg. Alors que l'alginate n'a été capable de supprimer la sulfuration de nAg que lorsqu'il a été mis en contact avec des NP avant les sulfures. Aucune concentration en solution de Ag n'a été mesurée dans le mélange d'acides aminés (c'est-à-dire de cystéine et de méthionine) tandis qu'une réformation de nAg faible a été observée dans ce système.

Cette étude a analysé nAg avec une large gamme de diamètres de 10 nm à 200 nm à court et long temps de séjour (10-3000 μs) en utilisant spICP-MS dans l'eau DI, et dans les milieux WW. nAg dans les échantillons environnementaux est polydispersé et présente une distribution de grande taille, de très petits diamètres à de grands agrégats qui sont difficiles à détecter avec de nombreuses techniques actuelles. Cette étude a développé une méthode pour améliorer la caractérisation de nAg très petit (10 nm) et très grand nAg (200 nm) avec spICP-MS. Tout d'abord, l'efficacité de transport des NP a été modifiée en utilisant un nAu standard avec une taille moyenne proche de l'échantillon d'essai nAg; deuxièmement, on a appliqué une courbe d'étalonnage de NP utilisant le nAg de taille standard qui a amélioré de manière significative l'analyse de nAg de 10 nm et de 200 nm. Alors que dans le procédé classique, on a utilisé un rendement de transport de 60 nm nAu pour l'analyse de divers diamètres de nAg, ce qui a affecté négativement l'estimation de la taille moyenne des NP avec des diamètres beaucoup plus petits ou plus grands que 60 nm.

Dans l'ensemble, cette recherche démontre le comportement de dissolution de nAg dans une matrice complexe de WW, et des systèmes avec une concentration variée de DOC et de sulfures inorganiques à une concentration de nAg respectueuse de l'environnement. SPICP-MS est optimisé et appliqué avec succès pour analyser nAg de différentes tailles afin de pouvoir suivre avec précision la taille moyenne, la fraction dissoute et la concentration du nombre de particules dans des matrices environnementales complexes.

Dedication

To my parents, Sina, Maral and Maris

ACKNOWLEDGEMENTS

I would like to acknowledge my supervisor Prof. Subhasis Ghoshal. I greatly appreciate the opportunity that I was given, his continuous support and insights during various stages of my PhD.

I would like to express my sincere thanks to Dr. Flavio Piccapietra at the Benedek Environmental Engineering Laboratories, at McGill for his support, inspiration, encouragement and valued suggestions with spICP-MS, and all the great discussion on my research. I also would like to thank Dr. Emma Jeong at Benedek Laboratories for her help and advice.

I would like to thank Prof. Cavus Falamaki at Amirkabir University of Technology (Tehran), for his invaluable advice. In addition, I would like to thank Prof. Jalal Shayegan at Sharif University of Technology for his warm support.

I would like to thank Prof. Audrey Moores, and Jacqueline Farrell for very useful CREATE seminars and workshops during which I learned a lot. Thanks to Prof. Nathalie Tufenkji for having me using the instrumentation in her laboratory at the Chemical Engineering department.

I would like to thank Ailin Mir for helping translate my thesis abstract in French and being there for me at all cost as a friend and her warm support just like a sister in Canada.

I would like to acknowledge the financial support from McGill Engineering Doctoral Award (MEDA), and CREATE in Green Chemistry.

I would also like to thank Dr. Ali Akbari, who truly is a patient listener and a great helper. I would acknowledge my colleagues and friends here at Benedek Laboratories, Sarayu Rao, Arshath Abdul Rahim, Mariana Umpiérrez, Aleksandra Kasprzyk. I would like to express my sincere thanks to Sanaz Alizadeh at École Polytechnique Montréal for her warm support and all encouraging words.

Sincere thanks to Josianne Lefebvre, École Polytechnique Montréal, for not hesitating to analyze my samples in a timely manner and spending time to answer my endless questions.

A special thanks to David Liu, Dentistry at McGill, for spending many hours on my complicated samples. Thanks to Jacinthe Mailly, water treatment lab at Polytechnique de Montreal; Andrew Golsztajn, at Chemical engineering; Jorge Sayat and the administrative staff at the department of civil and applied mechanics for their support.

Thanks my amazing friend, life partner and my only family in Canada, Maris Jukss, for being there for me through the hardest and loneliest times. Thank you for the encouragement and inspiration, for all the great moments we shared at McGill. Last but not the least, my wonderful parents, Tahereh and Ali, who are the most impressive people I have ever known. No words of appreciation can describe how much I owe it to you, how much you sacrificed, and how loving you are. Finally, to my younger sister and brother who cheered with me and cheered me up every single day of the past four years. Thank you, thank you and thank you. I do not know what I would do without you.

PREFACE

In accordance with the "*Guidelines for Thesis Preparation*", this thesis is presented in a manuscript-based format. Chapters 1 presents a general introduction to the topic and is followed by the literature review in Chapter 2. Chapters 3 to 5 presents 3 related but independent studies with descriptions of the experimental methods, and discussions of the experimental results. In the final chapter (Chapter 6), conclusion and future work are presented. The results presented in these chapters are or will be submitted to different journals. In all the publications, the author of the manuscript is the primary author of this thesis. Below is a detailed description of the efforts of each contributing author:

Contributions to New Knowledge

The specific contributions to new knowledge of this work are listed below:

1. **Dissolution rates and extents of nAg in WW are controlled by the presence of both, DOC and acid volatile sulfides.** Recent studies that have observed decreased dissolution as a result of sulfidation of nAg have suggested that dissolution in WW and sludge is limited by sulfidation reactions alone. The research reported here demonstrates that nAg in WW dissolves to a significant extent, but slower than in DI water as the control system, even though the WW specimens contained considerable levels of inorganic (acid volatile) sulfides. Further investigation of surface of nAg with EDX, XPS, ToF-SIMs showed that both organosulfur and inorganic sulfides were associated with the surface of nAg.

2. **Silver ions in WW are reformed into particulate nAg_xS_y due to the presence of inorganic or organosulfur compounds.** As nAg is dissolved over time, it was demonstrated that new nanoparticles of Ag (nAg_xS_y) reformed from the dissolved silver by complexation and reduction of silver ions with inorganic sulfide or organosulfur compounds. Although, the

reformation of nAg from dissolved silver in pure solutions of organosulfur compounds such as cysteine, or humic acids has been reported before under selected conditions of high Ag^+ concentrations, presence of light etc.; this phenomenon was not reported before in WW systems. Characterization of the secondary particles with spICP-MS was performed to determine their mean size, concentration and stability over time. EDX analysis showed the presence of sulfur and carbon on the surface of secondary particles.

3. **Humic and fulvic acids and alginate did not alter the equilibrium dissolved silver concentrations as compared to DI water systems and only slowed the dissolution rate of nAg compared to dissolution in DI water during the first several days of contact. .** Earlier studies have reported that the presence of alginate or humic substances in the system inhibited the extents of dissolution of nAg, and those studies assessed dissolution over relatively short time periods. In this study, we show that although the initial dissolution rate of nAg in alginate and humic subtances solutions was slower than in DI water, dissolution continued up to 648 h and eventually the equilibrium concentrations reached were similar to those in DI water. In the first 3 days diffusional limitations to Ag dissolutions due to interactions of organics with nAg surfaces, as evidenced by changes in plasmonic responses in UV-vis spectra, affected dissolution rates, but longer periods, equilibration in dissolution was achieved.

4. **Presence of humic substances considerably improved the dissolution extent of sulfidated nAg.** Studies have shown that sulfidation reaction of nAg severely diminished the dissolution of the NPs even at S to Ag mole ratios lower than 0.5 (Ag_2S is an essentially insoluble solid). In this study, it was demonstrated that the presence of humic and fulvic acids significantly enabled dissolution of Ag from sulfidated nAg (S:Ag=0.4) . The least impact of sulfidation on nAg dissolution was attained when the nAg was first contacted with humic and

fulvic acids first and then reacted with the sulfides, although notable dissolution of nAg also occurred when humic and fulvic acids were added simultaneously with sulfides or after addition of sulfides. The humic substances limited the impact of sulfidation on dissolution of nAg by complexing the surface of nAg and therefore blocking the active sites for reaction with the sulfides. Furthermore, the humic substances bound to the dissolved sulfide, and diminished the availability of sulfides for reaction with nAg. Unlike humic and fulvic acids, cysteine and methionine induced NP aggregation and destabilized nAg and negligible dissolved Ag was measured. Alginate inhibited sulfidation reactions to a significant extent only when nAg was contacted with nAg prior to the sulfides. This suggests that different DOC components in aquatic environments can have very different impacts both on sulfidation of nAg and on dissolution of Ag from sulfidated nAg. To date, there are no studies of impacts of DOC on nAg sulfidation other than with humic acids.

5. **Improvement of spICPMS methods for detection of nAg less than 20 nm.** Current optimization procedure for spICP-MS limits the instrument to size detection of about 20 nm for nAg. Previous literature suggested use of 60 nm nAu to determine the transport efficiency of the NPs into the plasma regardless of the size of the nAg to be analyzed. Although this method works well for the NPs within the size range of 60 nm nAu, it does not represent the actual transport efficiency of much smaller NPs (<20 nm) and overestimate its size. In this study, it was shown that the transport efficiency of NPs change with the mean size of NPs. Small NPs have significantly smaller transport efficiency. As a result, the mean size determined by the system for 10 nm nAg can be adversely affected. Using 20 nm nAu significantly improved the mean size attained by spICP-MS for 10 nm nAg and was in good agreement with the mean size attained by TEM.

Publications

(1) Findings from Chapter 3 are published as:

Azodi, M., Sultan, Y., Ghoshal, S. (2016), "Dissolution Behavior of Silver Nanoparticles and Formation of Secondary Silver Nanoparticles in Municipal Wastewater by Single Particle ICP-MS." Environmental Science and Technology, 50 (24), pp 13318–13327.

Azodi, M.: Experimental design and execution of the experimental, analysis of data, wrote the manuscript drafts.

Ghoshal, S.: Discussions on conception of the study, experimental procedure and methods, research supervision and revisions of the manuscript drafts.

Sultan, Y.: Discussions on conception of the study, and discussion of the results.

(2) Findings from Chapters 4 are in preparation for submission to following journals:

Azodi, M. and Ghoshal, S. (2017), "Dissolved Organic Carbon Enhances Dissolution of Sulfidated Silver Nanoparticles." In preparation for submission to Environmental Science and Technology.

Azodi, M.: Experimental design and execution of the experimental, analysis of data, wrote the manuscript drafts.

Ghoshal, S.: Discussions on conception of the study, experimental procedure and methods, research supervision and revisions of the manuscript drafts.

(3) Findings from Chapters 5 are in preparation for submission to following journals:

Azodi, M. and Ghoshal, S. (2017), "Characterization of 10 and 200 nm Ag nanoparticles in environmental samples with SPICP-MS." In preparation for submission to Journal of Analytical Atomic Spectrometry.

Azodi, M.: Conception of the study, experimental design and execution of the experimental, analysis of data, wrote the manuscript drafts.

Ghoshal, S.: Discussions on experimental procedure and methods, research supervision and revisions of the manuscript drafts.

Chapter 1 INTRODUCTION

1.1. Introduction

1.1.1 Background

Since Richard Feynman brought attention to the world of nanomaterials in his famous talk “There is plenty of room at the bottom” in 1959, nanotechnology has come a long way very rapidly (Nogi 2012). Nanomaterials are defined by the International Organization for Standardization (ISO) as the materials with at least one physical dimension in the size range of 1-100 nm; nanoparticles (all three dimensions between 1 and 100 nm); nanofibers (two dimensions between 1 and 100 nm); and nanoplates (one dimension between 1 and 100 nm). The principal parameters of nanomaterials are their shape, size, composition and morphological sub-structure.

The use of engineered nanoparticles (ENPs) is significantly increasing. ENPs are used by various industries, e.g., electronic, biomedical, pharmaceutical, cosmetic, energy, environmental, and materials. The number of nanoenabled consumer products registered by Woodrow Wilson Institute (Project on Emerging Nanotechnologies) jumped from only 212 in 2006 to 1400 in 2011. Metal ENPs (e.g. TiO_2, ZnO, Ag) are some of the most commonly used nanomaterials; for example, Ag ENPs (nAg throughout the thesis) as an antimicrobial agent in textiles (Reidy et al. 2013). It is certain that increasing amounts of ENPs will be released from various products and introduced into the environment in increasing amounts in coming years (Nowack and Bucheli 2007, Bystrzejewska-Piotrowska et al. 2009, Mueller and Nowack 2008).

While the unique nanoparticle properties, such as small size, high specific surface area and reactivity, makes the nAg an incredibly attractive generation of new materials, it could potentially lead to unexpected hazards to environment and humans (Wiesner et al. 2006). Some recent toxicological studies confirmed the uptake and toxicity of the nAg to a range of biota including bacteria (Jiang et al. 2009), fish (Asharani et al. 2008, Griffitt et al. 2009) and other

aquatic species (Choi and Hu 2008). Furthermore, ions silver are known to be toxic to aquatic organisms in the nanomolar range (Greulich et al. 2012).

ENPs such as nAg are released from point sources such as factories and landfills, and from nonpoint sources, such as the wet deposition from atmosphere, and storm-water runoff. Release of nAg from various products such as garments, cleaning products and personal care products during washing is a major route of nAg release into the sewer system and finally to the wastewater (WW) treatment plants (Gottschalk and Nowack 2011). nAg are then discharged into the environment with WW sludge (Brar et al. 2010) that is landfilled, incinerated, or land-applied on agricultural lands (Pradas del Real et al. 2016) or with WW effluents released into receiving water bodies (Adams and Kramer 1999).

To assess the impact of nAg released from WW treatment plants into the environment, it is important to determine the concentration released to the environment from various sources and also the physical and chemical changes to nAg after release from products (Mueller and Nowack 2008). For instance, nAg in WW may be transformed by dissolution, agglomeration/aggregation, changes in surface composition through reactions with WW constituents, and sorption to biomass (Tiede et al. 2010).

1.1.2 Fate of metal nAg in WW and sludge

nAg may transform chemically and physically while passing through various processes in the WWTP (Brar et al. 2010). In the preliminary treatment processes consisting of bar screens and grit removal, part of the nAg are likely to adsorb to the debris and other large particles and are removed. Usage of coagulants and flocculants in primary settling may lead to the agglomeration/aggregation and adsorption of the nAg and further settling in WW sludge. The nAg enter into the secondary treatment unit where they may adhere to the microbial cell surfaces

or microbe-associated extracellular polymeric substances (EPS) (Kiser et al. 2010). Moreover, during anaerobic digestion of WW, nAg is exposed to the inorganic sulfide species at 200-300 times in excess of nAg (Vaiopoulou et al. 2005) and NPs quickly react with inorganic sulfides and form silver sulfide complexes (Kaegi et al. 2011). One of abundant phases formed is silver sulfide (Ag_2S) which has very low solubility, limited mobility and bioavailability (Levard et al. 2013a). Hence, inorganic sulfide species and natural organic matter found abundantly in WWTPs (Imai et al. 2002) and after discharge in the aquatic and terrestrial environment significantly impact the mobility, solubility and toxicity of nAg.

1.1.3 Toxicological implications of nAg and their dissolved ions

Dissolution of nAg in an aqueous medium is described as the liberation of ions from the surface into the medium (Dokoumetzidis and Macheras 2006). Dissolution of nAg is strongly dependant on solvent properties, the availability of molecular oxygen for oxidation of Ag, as well as on physiochemical properties of nAg such as, size, crystal structure, surface morphology, and surface modifications (Misra et al. 2012).

nAg may pose risks to various environmental receptors due to the toxicity associated with metal ions released by dissolution, biouptake of NPs and generation of reactive oxygen species (Miller et al. 2010, He et al. 2012, Kim et al. 2007). The uptake path and toxicity of Ag ions and the ions bound to the soluble ligands is different from nAg (Borm et al. 2006). Having a clear understanding of the dissolution behavior and amount in environmental media such as WW, surface waters, etc. is important for risk assessment of nAg on the potential receptors. Dissolution of nAg not only releases toxic dissolved silver into the aquatic medium but also results in much smaller nAg due to silver mass loss over time, which might have very different uptake and toxicity pathway than pristine nAg.

1.1.4 Characterization and detection of nAg

Detection, identification and quantification of nAg in complex media such as wastewater (WW) is challenging. The variability and complexity of aqueous waste streams, as well as the number of insoluble salts and complexes, causes the speciation of NPs in WW and sludge to be varied and complex (Brar et al. 2010). Numerous techniques for the characterization of nAg have different capabilities and detection limits. For instance, the light scattering techniques such as nanparticle tracking analysis (NTA), and dynamic light scattering (DLS) are reliable techniques for the detection of nAg in aqueous media. However, it poses some challenges for polydisperse samples, and for low particle concentrations. Microscopy techniques such as SEM, TEM provide advanced images of nAg morphology and reveal their size, but do not easily provide information on the concentration of ENPs in the specific medium.

A rapidly developing technique for characterization of ENP size and concentrations in aqueous media is Single Particle Inductively Coupled Plasma Mass Spectroscopy (spICP-MS) which is capable of quantifying the dissolved, and nanoparticle concentrations of a target element as well as the nanoparticle size distribution (Lee et al. 2014, Mitrano et al. 2012a, Montaño et al. 2016, Pace et al. 2012). spICP-MS atomizes and ionizes the masses of elements by the high temperature argon plasma (Degueldre et al. 2006). The ions created by the plasma are separated by their mass to charge ratios, enabling the identification and quantification of unknown materials by the detector (Hineman and Stephan 2014). This technique is capable of distinguishing between dissolved and particulate forms of an element based upon their differing signal intensities in a highly diluted sample (Mitrano et al. 2014a). Recent studies have reported on application of spICP-MS for characterization of nAg and improving the detection in environmental samples (Tuoriniemi et al. 2012, Laborda et al. 2011) and complex matrices

(Peters et al. 2015). Analysis of nAg in a wide range of aqueous media such as WW and natural waters (Proulx et al. 2016, Yang et al. 2016a), drinking water (Donovan et al. 2016), and biological tissue (Gray et al. 2013) has been achieved using spICP-MS.

1.1.1 Current challenges and knowledge gaps

Detection, identification and quantification of nAg in complex media such as sludge and wastewater (WW) are is a challenge due to very low concentration (ppb-ppt) of the nAg and the complexity of the background medium interfering with many characterization techniques (Von der Kammer et al. 2012). Even though the sulfidation of nAg in WW has been investigated (Kaegi et al. 2013), the presence other WW constituents such as dissolved organic carbons (DOC) on the speciation and dissolution behavior of nAg is largely unknown.

With the technology for detection and quantification of nAg advancing, more in depth studies on the fate and transformation of nAg in the environment is becoming more feasible. Research and extensive studies on this topic are needed for thorough risk assessment, and regulatory consideration of nanomaterials releases to the environment. Nanotechnology has great potential for solving many technological challenges, yet if not used and implemented responsibly, can pose serious risks to the environment and human health.

1.2. Research Objectives

The overall objective of the research is to assess the dissolution behavior of nAg at environmentally relevant concentrations in aquatic environments such as WW and lake water containing DOC. An associated objective was to improve the detection and characterization of nAg and dissolved silver at low concentrations with spICP-MS.

The specific objectives of the research are:

1. To characterize the dissolution rate of nAg at low and high concentration in various WW matrices such as WW mixed liquor and effluent.
2. To investigate the changes in surface chemsitry of nAg upon exposure to WW and the changes in particle sizes of nAg.
3. To assess how major constituents of WW, such as acid volatile sulfides and dissolved organic carbon, impact the dissolution rate and extent of nAg of various sizes and surface coatings. To evaluate the influence of DOC compounds, such as humic substances, polysaccharides, and amino acids, on the dissolution of partially sulfidated nAg.

   To assess how the sequence of exposure to DOC and sulfides to nAg affects the dissolution of nAg.
4. To optimize spICP-MS methods and sample preparation for characterization of various sizes of nAg in complex, environmental aquatic media.

1.3. Thesis Organization

Chapter 1- presents an introduction, the objectives, thesis structure and contribution of authors.

Chapter 2- provides a detailed literature review on the fate and transformation of nAg in various aquatic and terrestrial environment including the WW, sludge and biosolids. The dissolution behavior and kinetics of nAg and sulfidated nAg, the toxicity of various chemical forms of nAg and dissolved silver complexes are discussed. In addition, detailed literature review on characterization techniques for detection of nAg, evaluation of dissolution, and surface speciation of nAg are presented.

Chapter 3- discusses the dissolution behavior of nAg in WW matrix and the changes in surface chemistry of nAg after exposure to WW. Batch experiments containing two concentration of nAg (10 and 1000 ppb) in two WW media (effluent and mixed liquor) were conducted under various dissolved oxygen concentrations. This research showed that nAg dissolved over time and the free silver ions were complexed with thiol containing organic and inorganic sulfides and reformed into small secondary particles (nAg_xS_y). The particle concentration and dissolved oxygen levels influenced the dissolution rates. The impact of DOC and inorganic sulfides in WW on the reduced dissolution of nAg in WW is discussed. Additional surface characterization of the nAg and secondary nAg_xS_y was performed using TEM-EDS, XPS, UV-vis spectroscopy, ToF-SIMs to better understand the surface chemistry of NPs following exposure to aqueous media rich in DOC and sulfides. This chapter discusses the dissolution of nAg in WW and shows the reformation of nAg_xS_y particles from the dissolved silver ions.

Chapter 4- analyzes the effect of DOC compounds of natural organic matter on the dissolution of sulfidated nAg. Both inorganic sulfides and dissolved organic carbon compounds greatly impact the solubility and mobility of nAg. Both DOC and inorganic sulfides species are abundantly found in WW, sludge, and surface waters and it was hypothesized that the sequence of exposure of nAg can influence the rate and extent of dissolution. To investigate this, nAg was subjected to three different exposure scenarios to inorganic sulfides before, after and simultaneous to addition of DOC compounds. Three DOC solutions containing alginate, a mixture of humic and fulvic acids, and a mixture of cysteine and methionine were examined. Characterization and quantification of dissolved silver fractions were performed using spICP-

MS. The extent of sulfidation and evaluation of DOC sorption on nAg was examined using ICP-OES and TOC analyzer.

Chapter 5- presents the optimization of spICP-MS methods for more accurate characterization of small (10 nm) and large (200 nm) nAg. Very small nAg (10 nm) has very different transport efficiency as compared to larger size nAg (80 nm). Calibrating the spICP-MS with 60 nm nAu for transport efficiency works well for particles between the size 30 to 100 nm, however for nAg (10 nm) it overestimates the transport efficiency of NPs into plasma and thus it adversely affects the sizing of particles. Applying similar size nAu for transport efficiency results in more accurate mean size of both nAg 10 and 200 nm.

Chapter 6- contains the overall summary of the thesis and general conclusions of this doctoral research work.

1.4. References

1. Nogi, K. (2012) Nanoparticle technology handbook, Elsevier.
2. Woodrow Wilson International Center for Scholars, Project on Emerging Nanotechnologies http://www.nanotechproject.org/.
3. Reidy, B., Haase, A., Luch, A., Dawson, K.A. and Lynch, I. (2013) Mechanisms of silver nanoparticle release, transformation and toxicity: a critical review of current knowledge and recommendations for future studies and applications. Materials 6(6), 2295-2350.
4. Nowack, B. and Bucheli, T.D. (2007) Occurrence, behavior and effects of nanoparticles in the environment. Environmental Pollution 150(1), 5-22.
5. Bystrzejewska-Piotrowska, G., Golimowski, J. and Urban, P.L. (2009) Nanoparticles: their potential toxicity, waste and environmental management. Waste Management 29(9), 2587-2595.
6. Mueller, N.C. and Nowack, B. (2008) Exposure modeling of engineered nanoparticles in the environment. Environmental Science & Technology 42(12), 4447-4453.
7. Wiesner, M.R., Lowry, G.V., Alvarez, P., Dionysiou, D. and Biswas, P. (2006) Assessing the risks of manufactured nanomaterials. Environmental Science & Technology 40(14), 4336-4345.
8. Jiang, W., Mashayekhi, H. and Xing, B. (2009) Bacterial toxicity comparison between nano-and micro-scaled oxide particles. Environmental Pollution 157(5), 1619-1625.
9. Asharani, P., Wu, Y.L., Gong, Z. and Valiyaveettil, S. (2008) Toxicity of silver nanoparticles in zebrafish models. Nanotechnology 19(25), 255102.
10. Griffitt, R.J., Hyndman, K., Denslow, N.D. and Barber, D.S. (2009) Comparison of molecular and histological changes in zebrafish gills exposed to metallic nanoparticles. Toxicological Sciences 107(2), 404-415.
11. Choi, O. and Hu, Z. (2008) Size dependent and reactive oxygen species related nanosilver toxicity to nitrifying bacteria. Environmental Science & Technology 42(12), 4583-4588.
12. Greulich, C., Braun, D., Peetsch, A., Diendorf, J., Siebers, B., Epple, M. and Köller, M. (2012) The toxic effect of silver ions and silver nanoparticles towards bacteria and human cells occurs in the same concentration range. RSC Advances 2(17), 6981-6987.
13. Gottschalk, F. and Nowack, B. (2011) The release of engineered nanomaterials to the environment. Journal of Environmental Monitoring 13(5), 1145-1155.
14. Brar, S.K., Verma, M., Tyagi, R. and Surampalli, R. (2010) Engineered nanoparticles in wastewater and wastewater sludge–Evidence and impacts. Waste Management 30(3), 504-520.
15. Pradas del Real, A.E., Castillo-Michel, H.A., Kaegi, R., Sinnet, B., Magnin, V., Findling, N., Villanova, J., Carriere, M., Santaella, C. and Fernandez-Martinez, A. (2016) Fate of Ag-NPs in sewage sludge after application on agricultural soils. Environmental Science & Technology.
16. Adams, N.W. and Kramer, J.R. (1999) Silver speciation in wastewater effluent, surface waters, and pore waters. Environmental Toxicology and Chemistry 18(12), 2667-2673.
17. Tiede, K., Boxall, A.B., Wang, X., Gore, D., Tiede, D., Baxter, M., David, H., Tear, S.P. and Lewis, J. (2010) Application of hydrodynamic chromatography-ICP-MS to investigate the fate of silver nanoparticles in activated sludge. Journal of Analytical Atomic Spectrometry 25(7), 1149-1154.
18. Kiser, M.A., Ryu, H., Jang, H., Hristovski, K. and Westerhoff, P. (2010) Biosorption of nanoparticles to heterotrophic wastewater biomass. Water Research 44(14), 4105-4114.
19. Vaiopoulou, E., Melidis, P. and Aivasidis, A. (2005) Sulfide removal in wastewater from petrochemical industries by autotrophic denitrification. Water Research 39(17), 4101-4109.
20. Kaegi, R., Voegelin, A., Sinnet, B., Zuleeg, S., Hagendorfer, H., Burkhardt, M. and Siegrist, H. (2011) Behavior of metallic silver nanoparticles in a pilot wastewater treatment plant. Environmental Science & Technology 45(9), 3902-3908.

21. Levard, C., Hotze, E.M., Colman, B.P., Dale, A.L., Truong, L., Yang, X., Bone, A.J., Brown Jr, G.E., Tanguay, R.L. and Di Giulio, R.T. (2013) Sulfidation of silver nanoparticles: natural antidote to their toxicity. Environmental Science & Technology 47(23), 13440-13448.
22. Imai, A., Fukushima, T., Matsushige, K., Kim, Y.-H. and Choi, K. (2002) Characterization of dissolved organic matter in effluents from wastewater treatment plants. Water Research 36(4), 859-870.
23. Dokoumetzidis, A. and Macheras, P. (2006) A century of dissolution research: from Noyes and Whitney to the biopharmaceutics classification system. International Journal of Pharmaceutics 321(1), 1-11.
24. Misra, S.K., Dybowska, A., Berhanu, D., Luoma, S.N. and Valsami-Jones, E. (2012) The complexity of nanoparticle dissolution and its importance in nanotoxicological studies. Science of the Total Environment 438, 225-232.
25. Miller, R.J., Lenihan, H.S., Muller, E.B., Tseng, N., Hanna, S.K. and Keller, A.A. (2010) Impacts of metal oxide nanoparticles on marine phytoplankton. Environmental Science & Technology 44(19), 7329-7334.
26. He, D., Dorantes-Aranda, J.J. and Waite, T.D. (2012) Silver nanoparticle・algae interactions: oxidative dissolution, reactive oxygen species generation and synergistic toxic effects. Environmental Science & Technology 46(16), 8731-8738.
27. Kim, J.S., Kuk, E., Yu, K.N., Kim, J.-H., Park, S.J., Lee, H.J., Kim, S.H., Park, Y.K., Park, Y.H. and Hwang, C.-Y. (2007) Antimicrobial effects of silver nanoparticles. Nanomedicine: Nanotechnology, Biology and Medicine 3(1), 95-101.
28. Borm, P., Klaessig, F.C., Landry, T.D., Moudgil, B., Pauluhn, J., Thomas, K., Trottier, R. and Wood, S. (2006) Research strategies for safety evaluation of nanomaterials, part V: role of dissolution in biological fate and effects of nanoscale particles. Toxicological Sciences 90(1), 23-32.
29. Lee, S., Bi, X., Reed, R.B., Ranville, J.F., Herckes, P. and Westerhoff, P. (2014) Nanoparticle size detection limits by single particle ICP-MS for 40 elements. Environmental Science & Technology 48(17), 10291-10300.
30. Mitrano, D.M., Lesher, E.K., Bednar, A., Monserud, J., Higgins, C.P. and Ranville, J.F. (2012) Detecting nanoparticulate silver using single-particle inductively coupled plasma–mass spectrometry. Environmental Toxicology and Chemistry 31(1), 115-121.
31. Montaño, M.D., Olesik, J.W., Barber, A.G., Challis, K. and Ranville, J.F. (2016) Single Particle ICP-MS: Advances toward routine analysis of nanomaterials. Analytical and Bioanalytical Chemistry 408(19), 5053-5074.
32. Pace, H.E., Rogers, N.J., Jarolimek, C., Coleman, V.A., Gray, E.P., Higgins, C.P. and Ranville, J.F. (2012) Single particle inductively coupled plasma-mass spectrometry: A performance evaluation and method comparison in the determination of nanoparticle size. Environmental Science & Technology 46(22), 12272-12280.
33. Mitrano, D., Ranville, J., Bednar, A., Kazor, K., Hering, A. and Higgins, C. (2014) Tracking dissolution of silver nanoparticles at environmentally relevant concentrations in laboratory, natural, and processed waters using single particle ICP-MS (spICP-MS). Environmental Science: Nano 1(3), 248-259.
34. Degueldre, C., Favarger, P.-Y. and Wold, S. (2006) Gold colloid analysis by inductively coupled plasma-mass spectrometry in a single particle mode. Analytica Chimica Acta 555(2), 263-268.
35. Hineman, A. and Stephan, C. (2014) Effect of dwell time on single particle inductively coupled plasma mass spectrometry data acquisition quality. Journal of Analytical Atomic Spectrometry.
36. Tuoriniemi, J., Cornelis, G. and Hassellöv, M. (2012) Size discrimination and detection capabilities of single-particle ICPMS for environmental analysis of silver nanoparticles. Analytical Chemistry 84(9), 3965-3972.

37. Laborda, F., Jiménez-Lamana, J., Bolea, E. and Castillo, J.R. (2011) Selective identification, characterization and determination of dissolved silver (I) and silver nanoparticles based on single particle detection by inductively coupled plasma mass spectrometry. Journal of Analytical Atomic Spectrometry 26(7), 1362-1371.
38. Peters, R., Herrera-Rivera, Z., Undas, A., van der Lee, M., Marvin, H., Bouwmeester, H. and Weigel, S. (2015) Single particle ICP-MS combined with a data evaluation tool as a routine technique for the analysis of nanoparticles in complex matrices. Journal of Analytical Atomic Spectrometry 30(6), 1274-1285.
39. Proulx, K., Hadioui, M. and Wilkinson, K.J. (2016) Separation, detection and characterization of nanomaterials in municipal wastewaters using hydrodynamic chromatography coupled to ICPMS and single particle ICPMS. Analytical and Bioanalytical Chemistry, 1-9.
40. Yang, Y., Long, C.-L., Li, H.-P., Wang, Q. and Yang, Z.-G. (2016) Analysis of silver and gold nanoparticles in environmental water using single particle-inductively coupled plasma-mass spectrometry. Science of the Total Environment 563, 996-1007.
41. Donovan, A.R., Adams, C.D., Ma, Y., Stephan, C., Eichholz, T. and Shi, H. (2016) Single particle ICP-MS characterization of titanium dioxide, silver, and gold nanoparticles during drinking water treatment. Chemosphere 144, 148-153.
42. Gray, E.P., Coleman, J.G., Bednar, A.J., Kennedy, A.J., Ranville, J.F. and Higgins, C.P. (2013) Extraction and analysis of silver and gold nanoparticles from biological tissues using single particle inductively coupled plasma mass spectrometry. Environmental Science & Technology 47(24), 14315-14323.
43. Von der Kammer, F., Ferguson, P.L., Holden, P.A., Masion, A., Rogers, K.R., Klaine, S.J., Koelmans, A.A., Horne, N. and Unrine, J.M. (2012) Analysis of engineered nanomaterials in complex matrices (environment and biota): General considerations and conceptual case studies. Environmental Toxicology and Chemistry 31(1), 32-49.
44. Kaegi, R., Voegelin, A., Ort, C., Sinnet, B., Thalmann, B., Krismer, J., Hagendorfer, H., Elumelu, M. and Mueller, E. (2013) Fate and transformation of silver nanoparticles in urban wastewater systems. Water Research.

Chapter 2 LITERATURE REVIEW

2.1. Fate and transport of nAg after release from consumer products

Ag nanomaterials are integrated into many consumer products, due to its long known antibacterial and antimicrobial effects. Ag nanomaterials are therefore one of the nanomaterials with the highest level of commercialization activity recorded in nano-product databases. Ag nanomaterials used in textiles and plastics makes up the main source of silver in the environment (Walser et al. 2011). Furthermore, Ag nanomaterials are used in disinfecting sprays, deodorants, cosmetics (Lorenz et al. 2011), in water purification systems (Nowack et al. 2011) and electronic devices (Zeng et al. 2010). Other applications under research and development for Ag nanomaterials is in food packaging (Cushen et al. 2012), in medical devices and implants (Trop et al. 2006, Vlachou et al. 2007).

As the number of materials functionalized with Ag nanomaterials increases, the release of silver from these products in the environment is of concern. The properties of Ag nanomaterials such as small size and greater specific surface area results in a more rapid dissolution; potentially leading to increased toxicity of nAg compared to its bulk forms (Reidy et al. 2013). A few studies showed the release of nAg from textiles (Benn and Westerhoff 2008, Geranio et al. 2009) such as socks in both nano and ionic form (Mitrano et al. 2014b, Mitrano et al. 2015). The amount and form of nAg released was strongly depended on the way the nAg was incorporated into the fabric (Geranio et al. 2009). In another example, Kaegi *et al.* found significant release of nAg (30% of the initial silver mass) in one year from paint during several run off events (Kaegi et al. 2010).

In a study by Mueller and Nowack (Mueller and Nowack 2008), the quantities of several engineered nanomaterials (ENMs) including nAg released to the environment were modelled showing that waste incineration plants and landfills account for the primary flow of

nanomaterials due to high rates of removal of ENMs during WW treatment and the subsequent incineration of sludge. However, the transformation, such as dissolution and sedimentation of nAg was not taken into account in this study. In a later study, Gottschalk *et al.* (Gottschalk and Nowack 2011, Gottschalk et al. 2009) expanded the model using Monte Carlo simulation to determine the concentrations of nAg and other ENPs for U.S., Europe and Switzerland and found much smaller concentration of nAg in surface waters than Mueller and Nowack, because they accounted for sedimentation of nAg.

Keller *et al.* assessed the life cycle emission of ten ENPs including nAg to the environmental compartments of air, water and soil plus landfills (Keller et al. 2013). Emissions during manufacturing, use, disposal through WW treatment plant and waste incineration were estimated. Their investigation suggested that applications such as coatings, paint and cosmetics dominate nAg releases into the environment and likely currently contribute 150 (metric tons/year) of total nAg emissions to soil and 63 (metric tons/year) to water. Brar *et al.* showed that the majority of nAg after release from consumer products joins the sewer system and eventually ends up in the wastewater (WW) treatment facilities (Brar et al. 2010). Therefore, to understand the toxicological implications of nAg and to assess the risk posed by the release of silver ions, it is necessary to find out the fate and transport of nAg in WW and the potential physical and chemical transformation they may go through.

2.2. nAg transformation and speciation in WW treatment plant

WW treatment facilities are known to be the major receptors of nAg released from different sources, such as households and industries (Gottschalk and Nowack 2011). nAg may transform chemically and physically while passing through various processes in the WWTP. In the preliminary treatment processes consisting of bar screens and grit removal, part of the NPs

are likely to adsorb to the debris and other large particles and are removed. Usage of coagulants and flocculants in the primary settling process leads to the agglomeration/aggregation and adsorption of the nAg and further settling in WW sludge. The nAg that are not removed in the primary treatment processes enter into the secondary treatment unit comprising of fixed film or suspended growth bioreactors and secondary sedimentation systems, where they may adhere to the microbial cell surfaces or microbe-associated extracellular polymeric substances (EPS) (Lytle 1984). nAg are largely associated with sludge in secondary treatment systems. Tiede *et al.* found that more than 90% nAg in activated sludge was partitioned to the sewage sludge solids using HDC-ICP-MS (Tiede et al. 2010). Choi *et al.* observed attachment of nAg to the microbial cells in WW (Choi et al. 2008).

Several studies have examined the fate and speciation of nAg during WW treatment (Kent et al. 2014). Kaegi *et al*. spiked nAg in a pilot WWTP and they also reported that after the initial pulse of nAg that passed through the system, nAg was largely (97-98%) associated with the biosolids and very little nAg was found in the effluent (Kaegi et al. 2011). Adams and Kramer measured silver in the municipal WW effluent and receiving waters in three size fractions; particulate (>0.45 μm), colloidal (10 kDa–0.45 μm), and dissolved (<10 kDa) and reported that particulate silver quickly decreased after reaching receiving waters likely due to particle settling, sorption, and uptake by organisms whereas the concentration of dissolved silver remains constant.

In another part of their study Kaegi *et al.* (Kaegi et al. 2011, Kaegi et al. 2013) also observed that a large amount of NPs transformed to Ag_2S NPs in a non-aerated secondary treatment reactor. Kaegi *et al.* and Brunetti *et al.* reported that sulfidation of nAg also happens to a great extent in the sewer systems (Kaegi et al. 2015, Brunetti et al. 2015). Kim *et al.* found

Ag_2S NPs with the size 5-20 nm in the final sewage sludge product using high resolution TEM (Kim et al. 2010). Scanning transmission electron microscopy-high angle annular dark field (STEM-HAADF) image of Ag_2S NP aggregates showed that Ag_2S NPs were as small as five nm in diameter. Furthermore, there have been several attempts to characterize nAg after sludge stabilization treatment processes. Lombi *et al.* (Lombi et al. 2013) studied the transformation of nAg with three types of surface functionalization, nAgCl, $AgNO_3$, in a bench scale anaerobic digester and found that all forms of silver transformed into Ag_2S. The Ag_2S in sludge was stable over six month in a simulated composting reactor. In another study, the fate of nAg in a sludge that was treated under both aerobic and anaerobic conditions was determined using X-ray absorption spectroscopy (XAS) (Doolette et al. 2013). XAS showed that after aerobic digestion only about 15% of Ag was in metallic form whereas the rest was bound to sulfur, whereas after anaerobic digestion all the nAg was transformed to Ag-S phases.

A few studies have investigated the transformation of nAg during sludge and waste incineration. Currently, incineration and agricultural land application are the main routes for sewage sludge disposal in many western countries (Fytili and Zabaniotou 2008). Impellitteri *et al.* (Impellitteri et al. 2013) spiked biosolids with nAg, Ag ions, and Ag_2S and found that they were all transformed to Ag sulfide or sulfhydryl species in fresh and aged (one month) biosolids. In contrast, after incineration of biosolids 30-50% of total silver was found in the form of elemental silver, 25% in the form of $AgSO_4$ and 26-50% associated with sulfhydryl groups. In another similar study, Meier *et al.* spiked nAg in to a pilot WW treatment plant, digested the sludge anaerobically, then incinerated on a bench-scale fluidized bed reactor (Meier et al. 2016a). XAS analyses showed that nAg(0) was identified as a major Ag component in the ashes but Ag_2S was clearly absent.

2.3. Dissolution of nAg and toxicological implications of dissolution

2.3.1. Dissolution kinetics of NPs and factors affecting dissolution of nAg

Dissolution of a particulate substance means the constituent molecules of the dissolving solid migrate from the surface to the bulk solution through a diffusion layer (Borm et al. 2006). The driving force for dissolution depends on the materials solubility within a given environment as well as the concentration gradient between the particle surface and the bulk solution phase. Hence, the kinetics of dissolution of a particle is surface area dependent. The kinetics of dissolution of particulate materials is often described by Noyes-Whitney equation (Borm et al. 2006):

$$C_t = C_s \times (1 - e^{kt}) \quad (2\text{-}1)$$

Where C_t is the concentration of a solute molecule in bulk solution, C_s is the solubility or saturation concentration of solute molecule in bulk solution, t is the time and k is the rate constant of dissolution which is described as:

$$k = \frac{A \times D}{V \times h} \quad (2\text{-}2)$$

Where D is the diffusion coefficient of solute molecule, V is the volume of solution, h is the thickness of diffusion layer, and A is the cross-sectional area through which diffusive the diffusive flux occurs. The rate constant of dissolution, k, decreases with increasing the total silver concentration (Liu and Hurt 2010). The dissolution process slows as the concentration in the bulk solution phase reaches equilibrium (solubility) levels. Solubility depends on the size of NPs according to Ostwald-Freundlich equation (Ma et al. 2011):

$$\frac{RT\rho}{M} ln \frac{C_{s1}}{C_{s2}} = 2\sigma(\frac{1}{r_1} - \frac{1}{r_2}) \quad (2\text{-}3)$$

Where R is the gas constant, T is the absolute temperature, M is the molecular weight of the solid in solution, σ is the interfacial tension between solid and liquid, ρ is the density of solid, and S_1 and S_2 are the solubility of particle of radius r_1 and r_2, respectively. This equation states that solubility increases as particle size decreases, and this is attributable to the higher energy state of surface atoms in smaller particles.

Solubility also depends on other physiochemical properties of NPs such as, crystal structure, and surface morphology, and surface area. Surface functionalization of NPs with surfactants or other capping agents can also affect the rates of dissolution in ultra-pure water shown by Kittler *et al.* (Kittler et al. 2010). For example, Polyvinylpyrrolidone (PVP)-capped nAg was shown to dissolve less than the citrate-capped nAg over one week exposure to natural, pure and tap waters (Mitrano et al. 2014a). Ma *et al.* (Ma et al. 2011) found that other factors such as coating type and synthesis method did not affect the solubility as much as the NP size.

Dissolution of NPs is an important property which influences their bioavailability, toxicity, mobility, and environmental impact (Misra et al. 2012). Dissolution of NPs such as nAg not only depends on intrinsic properties (e.g. size, chemical and surface properties) as discussed earlier; it also is strongly dependant on solvent properties such as pH, ionic strength, dissolved organic and inorganic constituents. Thermodynamic analysis of ion release from nAg was first discussed by Liu and Hurt (Liu and Hurt 2010) showing that dissolution of nAg is an oxidation process involving protons and dissolved oxygen. Those authors described the reaction stoichiometry of dissolution of nAg as below in an aqueous phase containing oxygen no other oxidant or reductant. According to this equation, proton (Liu and Hurt 2010) or oxygen depletion (i.e. anaerobic condition or high particle concentration) (Xiu et al. 2012) would limit dissolution of nAg.

$$2Ag_{(s)} + \frac{1}{2}O_{2(aq)} + 2H^{+}_{(aq)} \leftrightarrow 2Ag^{+}_{(aq)} + H_2O_{(l)} \quad (2\text{-}4)$$

Studies show that characteristics of surrounding media can affect suspension stability and as a result the agglomeration/aggregation of nAg by which the surface area and the dissolution of NPs change (Badawy et al. 2010, Baalousha et al. 2013, Huynh and Chen 2011, Li et al. 2011). Furthermore, the ionic composition of the aqueous media impacts the dissolution of nAg (Huynh and Chen 2011). Chloride (Cl^-) is shown to impact the dissolution of nAg due to strong affinity to oxidized silver and the formation of solid or soluble Ag-Cl species depending on Cl to Ag ratio (Levard et al. 2013b, Kent and Vikesland 2012). In another instance absorption of ambient CO_2 enhanced the dissolution of nAg due to decrease in pH of solution (Fujiwara et al. 2015).

2.3.2. The impact of sulfides and DOC on dissolution of nAg

Several studies have investigated the influence of dissolved organic carbon (Mitrano et al. 2014a, Chappell et al. 2011, Aiken et al. 2011, Pokhrel et al. 2013) and inorganic sulfides (Levard et al. 2011) species on the dissolution of nAg. Dissolved organic carbon (DOC) such as humic substances, amino acids, polysaccharides are common constituents of natural waters, and WW (Ma et al. 2001, Accardi-Dey and Gschwend 2002). DOC can control nAg surface chemistry, mobility and bioavailability (Baker 1973) by complexing silver ions, or Ag atoms on the surface of nAg (Sikora and Stevenson 1988, Veronesi et al. 2015). Interactions of nAg with DOC can influence its colloidal stability (Gunsolus et al. 2015), induce precipitation reactions (Gondikas et al. 2012), or drive redox reactions (Akaighe et al. 2011, Khan and Talib 2010, Akaighe et al. 2012). In a few studies Suwannee river humic and fulvic acids were found to reduce dissolution depending on nAg to carbon ratio (Mitrano et al. 2014a, Liu and Hurt 2010).

Navarro *et al.* (Navarro et al. 2008), and He *et al.* (He et al. 2012) reported that cysteine, an amino acid found in natural waters (Shea and MacCrehan 1988), inhibited dissolution of nAg by strongly binding Ag^{+}. However, Gondikas *et al.* (Gondikas et al. 2012) reported on increased dissolution of citrate coated nAg in the presence of cysteine.

The impact of inorganic sulfides on the reduced dissolution of nAg due to formation of insoluble Ag_2S has been extensively studied (Levard et al. 2013a, Levard et al. 2011, Liu et al. 2011). The reaction of nAg and silver ions with HS^{-} and with metal sulfides (Thalmann et al. 2014) with smaller stability constant (i.e. CuS, log K=22.3 and ZnS, log K=25.1) is thermodynamically favored. Ag(I) is Group 11 element and has a single *s* electron outside the filled *d* shell and is particularly prone to reacting with sulfide because of the relatively small energy difference between the frontier orbitals of the ion (Rickard 2012, Rickard and Luther 2006). Thus, chemical equilibrium constants for the sulfides of Ag(I) are high (log K=50.1 at 25 ºC) (Bell and Kramer 1999);

$$2Ag^{+1} + S^{-2} = Ag_2S_{(s)} \quad (2\text{-}5)$$

$$2Ag^{+1} + HS^{-1} = Ag_2S_{(s)} + H^{+} \quad (2\text{-}6)$$

The large equilibrium constant of the Ag_2S and low solubility suggest that these species are more stable than nAg. However, recent studies found that in case of incomplete sulfidation (S:Ag< 0.5), unreacted surface of nAg is prone to oxidation and ion release (Kent et al. 2014). In addition, Zhang *et al.* showed that sulfidation kinetics of nAg slowed in the presence of humic substances (Zhang et al. 2016). The presence of organosulfur ligands (i.e. thiols) increased the dissolved silver concentration and disrupted the sulfidation reaction of silver in iron sulfide solution (Adams and Kramer 1998).

2.3.3. Toxicity of nAg and dissolved silver

Extensive toxicological studies have demonstrated the toxicity of nAg to various organisms. To explain this observation, some studies have suggested increased toxicity of nAg as compared to bulk silver material due to a nanoscale effect. Other studies argue that dissolution of nAg is the sole cause of toxicological responses to nAg (Kittler et al. 2010). Therefore, dissolution of nAg in the exposure media and speciation of ions with other ligands can change their bioavailability, and toxicity (Misra et al. 2012). Recent studies however provide evidence for a complex interplay between nAg and dissolved silver (Navarro et al. 2008). Dissolved ions of nAg use the ion transporters or ion channels preferably for cellular entry (Piccapietra et al. 2012). Another route for transport of Ag ions is dissolution of nAg associated with biological membranes (Xiu et al. 2012, Park et al. 2010). Other pathways of toxicity arise from direct uptake of nAg into cells (Morones et al. 2005) and reactive oxygen species generation (Jones et al. 2011, Carlson et al. 2008). Toxicity of nAg to various biota such as zebra fish (Asharani et al. 2008), algae (Miao et al. 2009), and to various bacteria such as *Escherichia coli* (Levard et al. 2013b) and nitrifying bacteria (Choi and Hu 2008), and worms such as Caenorhabditis elegans (Collin et al. 2016, Yang et al. 2011) has been reported.

Toxicity of nAg to biological processes in WW treatment facilities is also studied (Choi and Hu 2008, Farkas et al. 2011). Choi and Hu found that 1 ppm of nAg inhibited the activity of nitrifying bacteria by 80% (Choi and Hu 2008) and Liang *et al.* (Liang et al. 2010) showed that nAg was more toxic to nitrifying bacteria in activated sludge than silver ions.

2.4. Analytical techniques for quantification of NPs and their dissolved ions in aquatic environment

It may seem that we can generally apply the analytical methods and experimental dissolution protocols used for macroscopic materials to study the dissolution of NPs. However, there are two main challenges in quantification of dissolution of NPs in complex media such as WW and DOC, (i) separation of NPs from dissolved component and (ii) instrumentation available to measure dissolution at environmentally relevant concentrations (ppt-ppb levels) in complex matrices. There are several direct and indirect techniques for measuring the dissolution of nAg. Many of metal analysis techniques such as ICP-MS, ICP-OES, and GF-AAS need separation of dissolved portion from the NPs. Dialysis membrane (Kittler et al. 2010) and centrifugal ultrafiltration (Ma et al. 2011, Li et al. 2011) have seen increased application for the separation of nAg from ions with high recovery in clean systems. Then the dissolved silver is quantified by analyzing the filtrate with ICP-MS, or GF-AAS. However, an ineffective method of separation can lead to over/under estimation of dissolved silver. For example, Ag ions complexed to DOC molecules can be retained in the filter or settled by centrifugation, which can lead to underestimation of dissolution extents. Furthermore, separation methods do not provide any information on the state of particles so for that other characterization techniques such as TEM or light scattering is used. Recent studies have used techniques such as single particle inductively coupled plasma mass spectrometry (spICP-MS) (Mitrano et al. 2014a), or ion selective electrodes (ISE) (Hadioui et al. 2012), by which no separation process of nAg from dissolved species is required. spICP-MS enables the analysis of nAg and dissolved silver at trace concentration (ppt-ppb) simultaneously with great accuracy.

2.4.1. Single Particle ICP-MS

spICP-MS provides a rapid and sensitive elemental analysis at trace concentrations (ppt-ppb) which makes it a great technique for characterization of nAg in the environmental samples. The basic methodology of spICP-MS was established initially by Degueldre *et al.* for the analysis of colloids (Degueldre et al. 2006, Degueldre and Favarger 2003, 2004). Liquid samples are introduced to spICP-MS on a particle-by-particle basis assuming that a single particle generates a discrete transient pulse whereas the dissolved species generate a continuous baseline signal. The system first aspirates the liquid sample through a nebulization system that produces an aerosol of droplets. The droplets are then desolvated, atomized and ionized by passing through the plasma, then they are sorted according to their mass to charge ratio in a mass spectrometer. **s**pICP-MS is able to provide thorough information on the particle number concentrations, and particle diameter and dissolved fraction. This technique has been employed for the analysis of nAg and other metal NPs in a wide range of media such as such biological tissues (Gray et al. 2013), plant tissues (Dan et al. 2015), food (fruit juices) (Witzler et al. 2016), lake water (Furtado et al. 2014), WW effluent (Yang et al. 2016a) and sea water (António et al. 2015).

2.5. Reference

1. Woodrow Wilson International Center for Scholars, Project on Emerging Nanotechnologies http://www.nanotechproject.org/.
2. Walser, T., Demou, E., Lang, D.J. and Hellweg, S. (2011) Prospective environmental life cycle assessment of nanosilver T-shirts. Environmental Science & Technology 45(10), 4570-4578.
3. Lorenz, C., Hagendorfer, H., von Goetz, N., Kaegi, R., Gehrig, R., Ulrich, A., Scheringer, M. and Hungerbühler, K. (2011) Nanosized aerosols from consumer sprays: experimental analysis and exposure modeling for four commercial products. Journal of Nanoparticle Research 13(8), 3377-3391.
4. Nowack, B., Krug, H.F. and Height, M. (2011) 120 years of nanosilver history: implications for policy makers. Environmental Science & Technology 45(4), 1177-1183.
5. Zeng, X.Y., Zhang, Q.K., Yu, R.M. and Lu, C.Z. (2010) A new transparent conductor: silver nanowire film buried at the surface of a transparent polymer. Advanced Materials 22(40), 4484-4488.
6. Cushen, M., Kerry, J., Morris, M., Cruz-Romero, M. and Cummins, E. (2012) Nanotechnologies in the food industry–Recent developments, risks and regulation. Trends in Food Science & Technology 24(1), 30-46.
7. Trop, M., Novak, M., Rodl, S., Hellbom, B., Kroell, W. and Goessler, W. (2006) Silver-coated dressing acticoat caused raised liver enzymes and argyria-like symptoms in burn patient. Journal of Trauma and Acute Care Surgery 60(3), 648-652.
8. Vlachou, E., Chipp, E., Shale, E., Wilson, Y.T., Papini, R. and Moiemen, N.S. (2007) The safety of nanocrystalline silver dressings on burns: a study of systemic silver absorption. Burns 33(8), 979-985.
9. Reidy, B., Haase, A., Luch, A., Dawson, K.A. and Lynch, I. (2013) Mechanisms of silver nanoparticle release, transformation and toxicity: a critical review of current knowledge and recommendations for future studies and applications. Materials 6(6), 2295-2350.
10. Benn, T.M. and Westerhoff, P. (2008) Nanoparticle silver released into water from commercially available sock fabrics. Environmental Science & Technology 42(11), 4133-4139.
11. Geranio, L., Heuberger, M. and Nowack, B. (2009) The behavior of silver nanotextiles during washing. Environmental Science & Technology 43(21), 8113-8118.
12. Mitrano, D.M., Rimmele, E., Wichser, A., Erni, R., Height, M. and Nowack, B. (2014a) Presence of nanoparticles in wash water from conventional silver and nano-silver textiles. ACS nano 8(7), 7208-7219.
13. Mitrano, D.M., Arroyo Rojas Dasilva, Y. and Nowack, B. (2015) Effect of variations of washing solution chemistry on nanomaterial physicochemical changes in the laundry cycle. Environmental Science & Technology 49(16), 9665-9673.
14. Kaegi, R., Sinnet, B., Zuleeg, S., Hagendorfer, H., Mueller, E., Vonbank, R., Boller, M. and Burkhardt, M. (2010) Release of silver nanoparticles from outdoor facades. Environmental Pollution 158(9), 2900-2905.
15. Mueller, N.C. and Nowack, B. (2008) Exposure modeling of engineered nanoparticles in the environment. Environmental Science & Technology 42(12), 4447-4453.
16. Gottschalk, F. and Nowack, B. (2011) The release of engineered nanomaterials to the environment. Journal of Environmental Monitoring 13(5), 1145-1155.
17. Gottschalk, F., Sonderer, T., Scholz, R.W. and Nowack, B. (2009) Modeled environmental concentrations of engineered nanomaterials (TiO2, ZnO, Ag, CNT, fullerenes) for different regions. Environmental Science & Technology 43(24), 9216-9222.
18. Keller, A.A., McFerran, S., Lazareva, A. and Suh, S. (2013) Global life cycle releases of engineered nanomaterials. Journal of Nanoparticle Research 15(6), 1-17.

19. Brar, S.K., Verma, M., Tyagi, R. and Surampalli, R. (2010) Engineered nanoparticles in wastewater and wastewater sludge–Evidence and impacts. Waste Management 30(3), 504-520.
20. Kent, R., Oser, J. and Vikesland, P.J. (2014) Controlled Evaluation of Silver Nanoparticle Sulfidation in a Full-Scale Wastewater Treatment Plant. Environmental Science & Technology.
21. Kaegi, R., Voegelin, A., Sinnet, B., Zuleeg, S., Hagendorfer, H., Burkhardt, M. and Siegrist, H. (2011) Behavior of metallic silver nanoparticles in a pilot wastewater treatment plant. Environmental Science & Technology 45(9), 3902-3908.
22. Kaegi, R., Voegelin, A., Ort, C., Sinnet, B., Thalmann, B., Krismer, J., Hagendorfer, H., Elumelu, M. and Mueller, E. (2013) Fate and transformation of silver nanoparticles in urban wastewater systems. Water Research.
23. Kaegi, R., Voegelin, A., Sinnet, B., Zuleeg, S., Siegrist, H. and Burkhardt, M. (2015) Transformation of AgCl nanoparticles in a sewer system—A field study. Science of the Total Environment 535, 20-27.
24. Brunetti, G., Donner, E., Laera, G., Sekine, R., Scheckel, K.G., Khaksar, M., Vasilev, K., De Mastro, G. and Lombi, E. (2015) Fate of zinc and silver engineered nanoparticles in sewerage networks. Water Research 77, 72-84.
25. Kim, B., Park, C.-S., Murayama, M. and Hochella Jr, M.F. (2010) Discovery and characterization of silver sulfide nanoparticles in final sewage sludge products. Environmental Science & Technology 44(19), 7509-7514.
26. Lombi, E., Donner, E., Taheri, S., Tavakkoli, E., Jämting, Å.K., McClure, S., Naidu, R., Miller, B.W., Scheckel, K.G. and Vasilev, K. (2013) Transformation of four silver/silver chloride nanoparticles during anaerobic treatment of wastewater and post-processing of sewage sludge. Environmental Pollution 176, 193-197.
27. Doolette, C.L., McLaughlin, M.J., Kirby, J.K., Batstone, D.J., Harris, H.H., Ge, H. and Cornelis, G. (2013) Transformation of PVP coated silver nanoparticles in a simulated wastewater treatment process and the effect on microbial communities. Chemistry Central Journal 7(1), 1.
28. Fytili, D. and Zabaniotou, A. (2008) Utilization of sewage sludge in EU application of old and new methods—a review. Renewable and Sustainable Energy Reviews 12(1), 116-140.
29. Impellitteri, C.A., Harmon, S., Silva, R.G., Miller, B.W., Scheckel, K.G., Luxton, T.P., Schupp, D. and Panguluri, S. (2013) Transformation of silver nanoparticles in fresh, aged, and incinerated biosolids. Water Research 47(12), 3878-3886.
30. Meier, C., Voegelin, A., Pradas del Real, A., Sarret, G., Mueller, C.R. and Kaegi, R. (2016) Transformation of Silver Nanoparticles in Sewage Sludge during Incineration. Environmental Science & Technology 50(7), 3503-3510.
31. Borm, P., Klaessig, F.C., Landry, T.D., Moudgil, B., Pauluhn, J., Thomas, K., Trottier, R. and Wood, S. (2006) Research strategies for safety evaluation of nanomaterials, part V: role of dissolution in biological fate and effects of nanoscale particles. Toxicological Sciences 90(1), 23-32.
32. Liu, J. and Hurt, R.H. (2010) Ion release kinetics and particle persistence in aqueous nano-silver colloids. Environmental Science & Technology 44(6), 2169-2175.
33. Ma, R., Levard, C.m., Marinakos, S.M., Cheng, Y., Liu, J., Michel, F.M., Brown Jr, G.E. and Lowry, G.V. (2011) Size-controlled dissolution of organic-coated silver nanoparticles. Environmental Science & Technology 46(2), 752-759.
34. Misra, S.K., Dybowska, A., Berhanu, D., Luoma, S.N. and Valsami-Jones, E. (2012) The complexity of nanoparticle dissolution and its importance in nanotoxicological studies. Science of the Total Environment 438, 225-232.
35. Xiu, Z.-m., Zhang, Q.-b., Puppala, H.L., Colvin, V.L. and Alvarez, P.J. (2012) Negligible particle-specific antibacterial activity of silver nanoparticles. Nano Letters 12(8), 4271-4275.

36. Zhang, W., Yao, Y., Sullivan, N. and Chen, Y. (2011) Modeling the primary size effects of citrate-coated silver nanoparticles on their ion release kinetics. Environmental Science & Technology 45(10), 4422-4428.
37. Radniecki, T.S., Stankus, D.P., Neigh, A., Nason, J.A. and Semprini, L. (2011) Influence of liberated silver from silver nanoparticles on nitrification inhibition of< i> Nitrosomonas europaea</i>. Chemosphere 85(1), 43-49.
38. Li, X., Lenhart, J.J. and Walker, H.W. (2011) Aggregation kinetics and dissolution of coated silver nanoparticles. Langmuir 28(2), 1095-1104.
39. Kittler, S., Greulich, C., Diendorf, J., Koller, M. and Epple, M. (2010) Toxicity of silver nanoparticles increases during storage because of slow dissolution under release of silver ions. Chemistry of Materials 22(16), 4548-4554.
40. Mitrano, D., Ranville, J., Bednar, A., Kazor, K., Hering, A. and Higgins, C. (2014b) Tracking dissolution of silver nanoparticles at environmentally relevant concentrations in laboratory, natural, and processed waters using single particle ICP-MS (spICP-MS). Environmental Science: Nano 1(3), 248-259.
41. Badawy, A.M.E., Luxton, T.P., Silva, R.G., Scheckel, K.G., Suidan, M.T. and Tolaymat, T.M. (2010) Impact of environmental conditions (pH, ionic strength, and electrolyte type) on the surface charge and aggregation of silver nanoparticles suspensions. Environmental Science & Technology 44(4), 1260-1266.
42. Baalousha, M., Nur, Y., Römer, I., Tejamaya, M. and Lead, J. (2013) Effect of monovalent and divalent cations, anions and fulvic acid on aggregation of citrate-coated silver nanoparticles. Science of the Total Environment 454, 119-131.
43. Huynh, K.A. and Chen, K.L. (2011) Aggregation kinetics of citrate and polyvinylpyrrolidone coated silver nanoparticles in monovalent and divalent electrolyte solutions. Environmental Science & Technology 45(13), 5564-5571.
44. Pokhrel, L.R., Dubey, B. and Scheuerman, P.R. (2014) Natural water chemistry (dissolved organic carbon, pH, and hardness) modulates colloidal stability, dissolution, and antimicrobial activity of citrate functionalized silver nanoparticles. Environmental Science: Nano 1(1), 45-54.
45. Levard, C., Mitra, S., Yang, T., Jew, A.D., Badireddy, A.R., Lowry, G.V. and Brown Jr, G.E. (2013a) Effect of chloride on the dissolution rate of silver nanoparticles and toxicity to E. coli. Environmental Science & Technology 47(11), 5738-5745.
46. Kent, R.D. and Vikesland, P.J. (2012) Controlled evaluation of silver nanoparticle dissolution using atomic force microscopy. Environmental Science & Technology 46(13), 6977-6984.
47. Fujiwara, K., Sotiriou, G.A. and Pratsinis, S.E. (2015) Enhanced Ag+ Ion Release from Aqueous Nanosilver Suspensions by Absorption of Ambient CO2. Langmuir 31(19), 5284-5290.
48. Chappell, M.A., Miller, L.F., George, A.J., Pettway, B.A., Price, C.L., Porter, B.E., Bednar, A.J., Seiter, J.M., Kennedy, A.J. and Steevens, J.A. (2011) Simultaneous dispersion–dissolution behavior of concentrated silver nanoparticle suspensions in the presence of model organic solutes. Chemosphere 84(8), 1108-1116.
49. Aiken, G.R., Hsu-Kim, H. and Ryan, J.N. (2011) Influence of dissolved organic matter on the environmental fate of metals, nanoparticles, and colloids. Environmental Science & Technology 45(8), 3196-3201.
50. Pokhrel, L.R., Dubey, B. and Scheuerman, P.R. (2013) Impacts of select organic ligands on the colloidal stability, dissolution dynamics, and toxicity of silver nanoparticles. Environmental Science & Technology 47(22), 12877-12885.
51. Levard, C., Reinsch, B.C., Michel, F.M., Oumahi, C., Lowry, G.V. and Brown Jr, G.E. (2011) Sulfidation processes of PVP-coated silver nanoparticles in aqueous solution: impact on dissolution rate. Environmental Science & Technology 45(12), 5260-5266.

52. Ma, H., Allen, H.E. and Yin, Y. (2001) Characterization of isolated fractions of dissolved organic matter from natural waters and a wastewater effluent. Water Research 35(4), 985-996.
53. Accardi-Dey, A. and Gschwend, P.M. (2002) Assessing the combined roles of natural organic matter and black carbon as sorbents in sediments. Environmental Science & Technology 36(1), 21-29.
54. Baker, W. (1973) The role of humic acids from Tasmanian podzolic soils in mineral degradation and metal mobilization. Geochimica et Cosmochimica Acta 37(2), 269-281.
55. Sikora, F. and Stevenson, F. (1988) Silver complexation by humic substances: conditional stability constants and nature of reactive sites. Geoderma 42(3), 353-363.
56. Veronesi, G., Aude-Garcia, C., Kieffer, I., Gallon, T., Delangle, P., Herlin-Boime, N., Rabilloud, T. and Carrière, M. (2015) Exposure-dependent Ag+ release from silver nanoparticles and its complexation in AgS 2 sites in primary murine macrophages. Nanoscale 7(16), 7323-7330.
57. Gunsolus, I.L., Mousavi, M.P., Hussein, K., Buhlmann, P. and Haynes, C.L. (2015) Effects of Humic and Fulvic Acids on Silver Nanoparticle Stability, Dissolution, and Toxicity. Environmental Science & Technology.
58. Gondikas, A.P., Morris, A., Reinsch, B.C., Marinakos, S.M., Lowry, G.V. and Hsu-Kim, H. (2012) Cysteine-induced modifications of zero-valent silver nanomaterials: implications for particle surface chemistry, aggregation, dissolution, and silver speciation. Environmental Science & Technology 46(13), 7037-7045.
59. Akaighe, N., MacCuspie, R.I., Navarro, D.A., Aga, D.S., Banerjee, S., Sohn, M. and Sharma, V.K. (2011) Humic acid-induced silver nanoparticle formation under environmentally relevant conditions. Environmental Science & Technology 45(9), 3895-3901.
60. Khan, Z. and Talib, A. (2010) Growth of different morphologies (quantum dots to nanorod) of Ag-nanoparticles: role of cysteine concentrations. Colloids and Surfaces B: Biointerfaces 76(1), 164-169.
61. Akaighe, N., Depner, S.W., Banerjee, S., Sharma, V.K. and Sohn, M. (2012) The effects of monovalent and divalent cations on the stability of silver nanoparticles formed from direct reduction of silver ions by Suwannee River humic acid/natural organic matter. Science of the Total Environment 441, 277-289.
62. Navarro, E., Piccapietra, F., Wagner, B., Marconi, F., Kaegi, R., Odzak, N., Sigg, L. and Behra, R. (2008) Toxicity of silver nanoparticles to Chlamydomonas reinhardtii. Environmental Science & Technology 42(23), 8959-8964.
63. He, D., Dorantes-Aranda, J.J. and Waite, T.D. (2012) Silver nanoparticle・algae interactions: oxidative dissolution, reactive oxygen species generation and synergistic toxic effects. Environmental Science & Technology 46(16), 8731-8738.
64. Shea, D. and MacCrehan, W.A. (1988) Determination of hydrophilic thiols in sediment porewater using ion-pair liquid chromatography coupled to electrochemical detection. Analytical Chemistry 60(14), 1449-1454.
65. Liu, J., Pennell, K.G. and Hurt, R.H. (2011) Kinetics and mechanisms of nanosilver oxysulfidation. Environmental Science & Technology 45(17), 7345-7353.
66. Levard, C., Hotze, E.M., Colman, B.P., Dale, A.L., Truong, L., Yang, X., Bone, A.J., Brown Jr, G.E., Tanguay, R.L. and Di Giulio, R.T. (2013b) Sulfidation of silver nanoparticles: natural antidote to their toxicity. Environmental Science & Technology 47(23), 13440-13448.
67. Thalmann, B., Voegelin, A., Sinnet, B., Morgenroth, E. and Kaegi, R. (2014) Sulfidation kinetics of silver nanoparticles reacted with metal sulfides. Environmental Science & Technology 48(9), 4885-4892.
68. Rickard, D. (2012) Sulfidic Sediments and Sedimentary Rocks, Newnes.
69. Rickard, D. and Luther, G.W. (2006) Metal sulfide complexes and clusters. Reviews in mineralogy and geochemistry 61(1), 421-504.

70. Bell, R.A. and Kramer, J.R. (1999) Structural chemistry and geochemistry of silver-sulfur compounds: Critical review. Environmental Toxicology and Chemistry 18(1), 9-22.
71. Zhang, Y., Xia, J., Liu, Y., Qiang, L. and Zhu, L. (2016) Impacts of Morphology, Natural Organic Matter, Cations, and Ionic Strength on Sulfidation of Silver Nanowires. Environmental Science & Technology 50(24), 13283-13290.
72. Adams, N.W. and Kramer, J.R. (1998) Reactivity of Ag+ ion with thiol ligands in the presence of iron sulfide. Environmental Toxicology and Chemistry 17(4), 625-629.
73. Piccapietra, F., Allué, C.G., Sigg, L. and Behra, R. (2012) Intracellular silver accumulation in Chlamydomonas reinhardtii upon exposure to carbonate coated silver nanoparticles and silver nitrate. Environmental Science & Technology 46(13), 7390-7397.
74. Park, E.-J., Yi, J., Kim, Y., Choi, K. and Park, K. (2010) Silver nanoparticles induce cytotoxicity by a Trojan-horse type mechanism. Toxicology in Vitro 24(3), 872-878.
75. Morones, J.R., Elechiguerra, J.L., Camacho, A., Holt, K., Kouri, J.B., Ramírez, J.T. and Yacaman, M.J. (2005) The bactericidal effect of silver nanoparticles. Nanotechnology 16(10), 2346.
76. Jones, A.M., Garg, S., He, D., Pham, A.N. and Waite, T.D. (2011) Superoxide-mediated formation and charging of silver nanoparticles. Environmental Science & Technology 45(4), 1428-1434.
77. Carlson, C., Hussain, S.M., Schrand, A.M., K. Braydich-Stolle, L., Hess, K.L., Jones, R.L. and Schlager, J.J. (2008) Unique cellular interaction of silver nanoparticles: size-dependent generation of reactive oxygen species. The journal of physical chemistry B 112(43), 13608-13619.
78. Asharani, P., Wu, Y.L., Gong, Z. and Valiyaveettil, S. (2008) Toxicity of silver nanoparticles in zebrafish models. Nanotechnology 19(25), 255102.
79. Miao, A.-J., Schwehr, K.A., Xu, C., Zhang, S.-J., Luo, Z., Quigg, A. and Santschi, P.H. (2009) The algal toxicity of silver engineered nanoparticles and detoxification by exopolymeric substances. Environmental Pollution 157(11), 3034-3041.
80. Choi, O. and Hu, Z. (2008) Size dependent and reactive oxygen species related nanosilver toxicity to nitrifying bacteria. Environmental Science & Technology 42(12), 4583-4588.
81. Collin, B., Tsyusko, O.V., Starnes, D.L. and Unrine, J.M. (2016) Effect of natural organic matter on dissolution and toxicity of sulfidized silver nanoparticles to Caenorhabditis elegans. Environmental Science: Nano.
82. Yang, X., Gondikas, A.P., Marinakos, S.M., Auffan, M., Liu, J., Hsu-Kim, H. and Meyer, J.N. (2011) Mechanism of silver nanoparticle toxicity is dependent on dissolved silver and surface coating in Caenorhabditis elegans. Environmental Science & Technology 46(2), 1119-1127.
83. Farkas, J., Peter, H., Christian, P., Urrea, J.A.G., Hassellöv, M., Tuoriniemi, J., Gustafsson, S., Olsson, E., Hylland, K. and Thomas, K.V. (2011) Characterization of the effluent from a nanosilver producing washing machine. Environment International 37(6), 1057-1062.
84. Liang, Z., Das, A. and Hu, Z. (2010) Bacterial response to a shock load of nanosilver in an activated sludge treatment system. Water Research 44(18), 5432-5438.
85. Hadioui, M., Leclerc, S. and Wilkinson, K. (2012) Multimethod quantification of Ag< sup>+</sup> release from nanosilver. Talanta.
86. Degueldre, C. and Favarger, P.-Y. (2003) Colloid analysis by single particle inductively coupled plasma-mass spectroscopy: a feasibility study. Colloids and Surfaces A: Physicochemical and Engineering Aspects 217(1), 137-142.
87. Degueldre, C. and Favarger, P.-Y. (2004) Thorium colloid analysis by single particle inductively coupled plasma-mass spectrometry. Talanta 62(5), 1051-1054.
88. Degueldre, C., Favarger, P.-Y. and Wold, S. (2006) Gold colloid analysis by inductively coupled plasma-mass spectrometry in a single particle mode. Analytica Chimica Acta 555(2), 263-268.

89. Gray, E.P., Coleman, J.G., Bednar, A.J., Kennedy, A.J., Ranville, J.F. and Higgins, C.P. (2013) Extraction and analysis of silver and gold nanoparticles from biological tissues using single particle inductively coupled plasma mass spectrometry. Environmental Science & Technology 47(24), 14315-14323.
90. Dan, Y., Zhang, W., Xue, R., Ma, X., Stephan, C. and Shi, H. (2015) Characterization of gold nanoparticle uptake by tomato plants using enzymatic extraction followed by single-particle inductively coupled plasma–mass spectrometry analysis. Environmental Science & Technology 49(5), 3007-3014.
91. Witzler, M., Küllmer, F., Hirtz, A. and Guenther, K. (2016) Validation of Gold and Silver Nanoparticle Analysis in Fruit Juices by sp-ICP-MS Without Sample Pre-Treatment. Journal of Agricultural and Food Chemistry.
92. Furtado, L.M., Hoque, M.E., Mitrano, D.M., Ranville, J.F., Cheever, B., Frost, P.C., Xenopoulos, M.A., Hintelmann, H. and Metcalfe, C.D. (2014) The persistence and transformation of silver nanoparticles in littoral lake mesocosms monitored using various analytical techniques. Environmental Chemistry 11(4), 419-430.
93. Yang, Y., Long, C.-L., Li, H.-P., Wang, Q. and Yang, Z.-G. (2016) Analysis of silver and gold nanoparticles in environmental water using single particle-inductively coupled plasma-mass spectrometry. Science of the Total Environment 563, 996-1007.
94. António, D.C., Cascio, C., Jakšić, Ž., Jurašin, D., Lyons, D.M., Nogueira, A.J., Rossi, F. and Calzolai, L. (2015) Assessing silver nanoparticles behaviour in artificial seawater by mean of AF4 and spICP-MS. Marine environmental research 111, 162-169.

Chapter 3 DISSOLUTION BEHAVIOR OF SILVER NANOPARTICLES IN MUNICIPAL WASTEWATER AND THE IMPACT OF PARTICLE CONCENTRATION, DISSOLVED OXYGEN, AND PARTICLE COATING ON DISSOLUTION BY SINGLE PARTICLE ICP-MS

Connecting text: nAg are incorporated into many nano-enabled products and its growing use has raised concern about the environmental implications of their release. nAg and free silver ions are both shown to be toxic to a wide range of organisms. Dissolution of nAg can release toxic silver ions in the aquatic environment and it results in considerably smaller NPs than the pristine particles, which may have different bio-uptake and toxicity pathways. A significant fraction of the nAg are released into sewer systems and end up in WW treatment facilities. However, up to now there has been no study on the dissolution behavior of nAg in different WW streams. In this chapter, dissolution kinetics and extent of nAg in WW is examined over periods that are representative of WWTP hydraulic and sludge retention times. The changes in surface speciation were characterised using TEM- Energy-dispersive X-ray spectroscopy (TEM-EDX) and X-ray photoelectron spectroscopy (XPS) and ToF-SIMs

The Chapter was published in Environmental Science and Technology as:

Azodi, A., Sultan, Y. and Ghoshal, S. (2016) Dissolution Behavior of Silver Nanoparticles and Formation of Secondary Silver Nanoparticles in Municipal Wastewater by Single Particle ICP-MS. **Environmental Science and Technology,** 2016, 50 (24), pp 13318–13327

3.1. Introduction

The uses of nAg in commercial products (e.g., medical devices, coating and paints, textiles, and cosmetics) are growing very rapidly primarily because of their excellent antimicrobial properties (Kim et al. 2007, Rai et al. 2009). However, nAg once released into aquatic environments may pose risks to various environmental receptors due to the toxicity associated with Ag^+ released by dissolution (Misra et al. 2012), nAg bio-uptake (Navarro et al. 2008, Morones et al. 2005) and reactive oxygen species generated (Jones et al. 2011). Based on materials flow analyses of nAg released from various products in the environment, it has been suggested that a significant fraction of nAg released from consumer goods will enter municipal WW treatment plants (WWTPs) (Keller et al. 2013),(Gottschalk et al. 2009).

In assessing the environmental risks of nAg, it is important to consider the environmental transformations of nAg that affect their size, and surface or bulk chemistry. Dissolution of nAg is an important environmental transformation process because it releases Ag^+ into the aquatic environment and also alters the size of nAg, both of which can influence the toxicity characteristics of nanoparticles (NPs) (Park et al. 2011),(Carlson et al. 2008),(Choi and Hu 2008),(Kittler et al. 2010). The rates and extents of dissolution depend on the intrinsic properties of NPs such as size (Ma et al. 2011, Zhang et al. 2011), particle concentration (Liu and Hurt 2010), nature of surface capping agents (Li et al. 2011, Dobias and Bernier-Latmani 2013) as well as on the chemistry of the aqueous medium. Previous studies have investigated the dissolution of nAg in simple aqueous media compositions with various pH (Liu and Hurt 2010) and ionic strength (Huynh and Chen 2011), various concentrations of dissolved organic matter (Chappell et al. 2011, Ostermeyer et al. 2013), inorganic sulfide (Levard et al. 2011, Liu et al. 2011), chloride (Levard et al. 2013b), oxygen (Liu and Hurt 2010) or carbonate (Fujiwara et al.

2015) and have determined that these factors influence dissolution rates. It is difficult to extrapolate the dissolution behavior from those systems of simple composition to a complex, multicomponent media such as municipal WW.

To date, a detailed characterization of nAg dissolution in WW has not been reported. Dissolved organic carbon (DOC) such as humic acids (HA) and fulvic acids (FA), polysaccharides, proteins and amino acids are present at ppm levels in municipal WW (Imai et al. 2002, Ma et al. 2001), (Drewes and Croue 2002). Furthermore, sulfides and chloride ions can be present in WW at concentrations of a few hundred ppm (Du and Parker 2013). Therefore, the WW matrix is likely to influence dissolution of nAg. Several studies have reported the sulfidation of nAg in wastewater streams (Kaegi et al. 2013) and during sludge treatment (Ma et al. 2013). Sulfidation has been shown to hinder dissolution partly or completely (Levard et al. 2011). Recent investigations have found that sulfidation is not uniform over the nAg surface even at high sulfide concentrations (Kent and Vikesland 2012, Baalousha et al. 2015) and some Ag^+ release may still occur.

Past approaches for measuring the dissolution of NPs is the separation of dissolved Ag from the NPs by methods such as centrifugation (Chappell et al. 2011), dialysis membrane (Kittler et al. 2010), or centrifugal ultrafiltration (Liu and Hurt 2010, Ma et al. 2011, Huynh and Chen 2011, Navarro et al. 2008) and then quantification of the dissolved metal concentrations by total metal analysis by ICP-MS (Huynh and Chen 2011, Chappell et al. 2011, Gondikas et al. 2012), ICP-AES (Miller et al. 2010), and GF-AAS (Liu and Hurt 2010). Organic macromolecules in WW may bind Ag^+ and those complexes may be filtered out with nAg during phase separation, leading to the underestimation of dissolved Ag. In this study we used ICP-MS

in single particle mode (spICP-MS) which is capable of simultaneous quantification of nAg size and concentration and dissolved Ag concentrations (Mitrano et al. 2012a, Mitrano et al. 2014a, Laborda et al. 2011, Degueldre and Favarger 2003, Mitrano et al. 2012b). Although spICP-MS has been used for characterization of metal NPs and dissolved metals in aqueous solutions of relatively simple chemistry (Mitrano et al. 2014a, Hadioui et al. 2012), its implementation for environmental complex samples such as WW has been very limited (Peters et al. 2015, Yang et al. 2016b, Hadioui et al. 2015)

We assessed the dissolution of sulfidated and unsulfidated Citrate-nAg and PVP-nAg (80 nm) in aerated and non-aerated WW samples from an urban municipal activated sludge WWTP, over time periods representative of the hydraulic residence time (HRT) and solids retention time (SRT). Dissolution of the nAg was also evaluated in DI water, which served as a control medium. Dissolution of nAg requires dissolved oxygen or strongly oxidizing conditions (Liu and Hurt 2010), and many WW treatment processes are aerobic. The rationale for studying dissolution of unsulfidated nAg under aerobic conditions was to characterize the rates and extents of dissolution under favorable conditions. The presence of unsulfidated nAg may relate to scenarios such as the release of nAg from NP-functionalized matrices (e.g. polymer composites, fibers) present in influent WW, after entering the WWTP. Dissolution of the nAg was also evaluated in air-saturated DI water, which served as a control medium. Dissolution of nAg requires dissolved oxygen or strongly oxidizing conditions (Liu and Hurt 2010), and many WW treatment processes are aerobic.

This study presents for the first time a detailed investigation of the dissolution of nAg because not only were the amounts of Ag dissolved assessed, the changes in nAg particle size

distributions and surface composition during dissolution were also assessed. Characterization of the changes in surface chemistry was performed by ToF-SIMS and XPS. Furthermore, the fate of the dissolved Ag in WW was investigated and our results suggest its re-precipitation into substantially smaller (~ 22 nm) NPs. A spICP-MS methodology for the detection of the smaller nAg formed was developed, as those sizes are below the detection limits of instrument settings reported in prior studies (Donovan et al. 2016). Dissolution was assessed at nAg concentrations of 10 ppb which is close to the range of predicted concentrations in municipal WWTPs (Gottschalk et al. 2009, Keller et al. 2013). Most previous studies have only reported on the dissolution of Ag with NPs concentrations only at ppm levels (Ma et al. 2011, Gondikas et al. 2012). Comparison of the dissolution experiments performed with nAg concentrations of 5×10^6 particles/mL (10 ppb) and 5×10^8 particles/mL (1 ppm) demonstrated that the initial concentration of nAg influenced not only the dissolved Ag concentrations but also the size of the nAg. The impacts of common DOC macromolecules (alginate, HA and FA) on the dissolution rates and extents were investigated to determine how those WW constituents influence dissolution.

3.2. Materials and Methods

3.2.1. Chemicals

Silver NPs. Citrate-coated NanoXact nAg (TedPella), and PVP-coated NanoXact nAg (NanoComposix) at a stock concentration of 20 ppm and nominal diameter of 80 nm were purchased. TEM analysis yielded a mean size of 74.1±5.3 nm (n=120) and 79.0±7.5 nm (n=120) for the cit- and PVP-nAg, respectively. These measurements were in agreement with spICP-MS

(Perkin Elmer NexION 300X) measurements of mean particle sizes of 74.8±0.24 nm and 81.7±0.06 nm for the cit- and PVP-nAg, respectively.

WW samples. The WW samples were collected from an activated sludge, secondary municipal WW treatment plant near Montreal (La Prairie, QC, Canada). Samples were collected from the secondary settling tank overflow (WW effluent) and the secondary aeration tank (WW mixed liquor) in a clean dark glass bottle (acid washed, rinsed with DI water, and dried) and were sealed completely. WW characteristics such as total Ag after acid digestion, pH, conductivity, total organic carbon (TOC), DOC, redox potential, total sulfur, acid volatile sulfides (AVS) and total suspended solids were measured within 24 h after the WW was sampled and are listed in Table 3-1 S1. The methods for measurement are stated in Supplementary Information (SI).

Dissolution experiments with nAg in WW and DOC solutions. Dissolution experiments were conducted in batch systems comprised of 15 or 50 mL polypropylene, conical-bottom tubes. The WW effluent and mixed liquor samples were first filtered using 0.45 µm cellulose acetate filters to eliminate suspended solids, which can adversely impact the performance of the spICP-MS. The DI water (double deionized, Millipore) and one set of WW effluent and mixed liquor samples were aerated for 15 min to ensure that all systems had identical DO (9.5 mg/L). In parallel, a second set of WW samples were prepared by purging the WW samples with N_2 to achieve DO concentrations similar to those typically recorded at the treatment plant. In that set, WW effluent samples were adjusted to a DO of 5.3 and 7.7 mg/L and the mixed liquor samples were adjusted to 2.3 mg/L.

Citrate- and PVP-nAg stock solutions were dispersed in 10 mL aliquots in triplicate vials of DI water and filtered WW at specific DO, to attain a final concentration of 10 or 1000 ppb

nAg in all the systems. The samples were continuously mixed on a horizontal shaker and were periodically sampled up to 168 h, a time range which includes the HRT and SRT of typical activated sludge systems (Metcalf 2003). The error bars in all the graphs therefore, are the standard deviation of three sample replicates.

Several dissolution experiments were conducted with sulfidated nAg. A sulfide stock solution was prepared by dissolving 1 mM Na_2S (Sigma Aldrich) solution in 0.5 mM $NaNO_3$ in an anaerobic chamber according to methods reported elsewhere (Levard et al. 2011). The solution was diluted in de-aerated DI water and added to tubes each containing 10 or 1000 ppb nAg and capped in the anaerobic chamber to yield S/Ag mole ratios of 0.5, 5, and 50. The suspensions were placed in an end-over-end mixer overnight and then the sulfidated nAg was separated by centrifugal ultrafiltration, performed three times at 4600 g for 20 min. The sulfidated nAg was then used in dissolution experiments that were performed as described above.

Additional nAg dissolution experiments were conducted with DOC solutions. Solutions of alginate (Sigma, sodium salt of alginic acid from brown algae), FA (Suwannee River Fulvic Acids standard II, International Humic Substances Society), and HA (Suwannee River Humic Acids standard II) were prepared in DI water. Alginate was dissolved in DI water by mixing with an end-over-end for 1 h. FAs and HAs were prepared in DI water by overnight shaking and filtering (0.45 μm). Then the alginate, FA and HA solutions were diluted to obtain final concentrations of 1, 6, and 10 ppm and nAg was spiked to obtain a final concentration of 10 ppb. The dissolution experiments were otherwise identical to those described above for the WW samples. All dissolution experiments and analyses were conducted at room temperature (21 °C).

3.2.2. Instrumentation and characterization

A Perkin Elmer NexION 300X ICP-MS supported by Syngistix software (ver1.1.) was used in single particle mode for nAg characterization (Degueldre and Favarger 2003). The dissolved silver measured by spICP-MS includes the any free silver ions, soluble silver complexes, as well as small nAg <10 nm which are not detectable and count as dissolved silver. Therefore, throughout this study dissolved silver is referred to any free silver ions, to soluble inorganic and organic silver complexes and all particulate silver species smaller than 10 nm. The integration dwell time of 1000 µs was generally used, but several samples were also analyzed at 100 µs in order to compare the particle size distribution, and mean size from the two dwell times. In order to detect the secondary nAg in the range of 10 to 30 nm, torch alignment and nebulizer gas flow of spICP-MS were optimized for the highest sensitivity to Ag. In addition, a dwell time of 100 µs was used and the total data collection time was increased to 150 s for sample analysis. A total data collection time of 100 s (but 150 s for time point 168 h) was set for all the other samples. Other instrumental parameters are presented in Table 3-2 S2. The standard reference nAu (NIST), with a nominal 60 nm diameter at a concentration of 9.5×10^4 particles/mL in DI water provided a transport efficiency of between 5 to 7% at dwell time of 1000 µs and 7 to 9% at dwell time of 100 µs for different runs.

Stock solutions of 20 ppm PVP-coated NanoXact nAg (nanoComposix) of nominal size of 10 nm and 20 nm at concentrations of 0.1 ppb were used to determine the particle mean size detection limit of spICP-MS analysis. The detection limit for nAg size by spICP-MS was established to be about 10 nm in DI water. The minimum detectable particle concentration for 80 nm nAg was 6250 particles/mL and for dissolved silver in DI water was 30 ppt in single particle mode.

Sample dilutions were done immediately before the analysis. In addition, many control samples were run to ensure the dilution factors of 10, 100 and 1000 times did not trigger any immediate ion release from nAg. Further details on spICP-MS optimization and data quality (Figures 3-5 S1, 3-6 S2) as well as the total silver mass balance are discussed in SI (Table 3-8 S8).

Transmission Electron Microscopy (TEM). TEM analysis was performed using a FEI Tecnai G2 F20 S/TEM equipped with Gatan Ultrascan 4000 4k × 4k CCD Camera System (Model 895). An EDAX Octane T Ultra W /Apollo XLT2 SDD system was used for energy dispersive X-ray spectroscopy (EDS) measurements. To image the WW samples to which nAg and Ag^+ ions were added, the samples were concentrated by centrifugation at 4600 g for 20 min. Then 10 µL of the concentrate was deposited on the Cu TEM substrates (Electron Microscopy Sciences, Carbon film 200 mesh Cu grids). The grids were kept in dark and air dried. The samples were rinsed with DI water a few times to clean background WW debris, and air dried again prior to analysis.

Time-of-flight secondary ion mass spectrometry (ToF-SIMS). A ToF-SIMS IV (IONTOF GmbH) instrument was used. The primary ion beam was rastered over a 50 µm × 50 µm area with a spectral resolution of 128 × 128 pixels. The mass resolution $m/\Delta m$ was > 8000 on $^{29}Si^+$ and the width of the H^+ peak on silicon was 0.7 ns. H^+, H_2^+, H_3^+, $C_2H_3^+$, $C_2H_5^+$, $C_3H_5^+$, $C_3H_7^+$, $C_4H_7^+$, and $C_4H_9^+$ were used to calibrate the positive spectra, while H^-, C^-, CH^-, C_2^-, and C_2H^- were used to calibrate the negative spectra. Samples for ToF-SIMS analyses were prepared by suspending 10 mg/L PVP-nAg in WW samples for 72 h, and air drying several drops of the suspension on silicon substrates (Electron Microscopy Sciences) prior to analysis. Instrument operating conditions are stated in SI.

X-ray photoelectron spectroscopy (XPS). Analysis was performed using a XPS VG Escalab 3 Mk II with a non-monochromatic Al K-α source at 300 W. The analyzed surface was 2 mm × 3 mm and depth was 50-100 Å. High resolution scans were performed at a pass energy of 20 eV with 0.05 eV energy step size. The spectra were charge corrected with respect to Ag3d5/2 at 368.3 eV for analyzing nAg suspended in WW, and to C1s at 285 eV for analyzing sulfidated nAg. PVP-nAg at 10 mg/L were suspended in WW effluent and mixed liquor for 72 h and then several drops of each sample were deposited on Cu grids.

UV-vis spectroscopy The optical absorption spectra of Ag were measured in a wavelength range of 200-800 nm by a SpectraMax M5 Multimode Plate Reader.

3.3. Results and Discussion

3.3.1. Dissolution of nAg in WW mixed liquor and effluent samples.

spICP-MS analyses of the filtered WW samples performed promptly after sample collection showed no detectable nAg or dissolved silver in effluent and mixed liquor.

Figures 3-1 A, B show changes in nAg particle sizes and dissolved Ag concentrations over time from spICP-MS analyses of suspensions of 80 nm PVP-nAg at an initial particle Ag concentration of 10 ppb (5×10^6 particles/mL). The results demonstrated that the nAg dissolved to a greater extent in air-saturated DI water (DO 9.5 mg/L) than in WW mixed liquor and effluent. Dissolution of PVP-nAg over 168 h in DI water resulted in the largest decrease in particle diameter of 42.06±3.6 nm (82.4 to 40.3 nm) and a dissolved Ag concentration of 3.1±0.18 ppb. Dissolution of the PVP-nAg in the air-saturated mixed liquor and effluent samples did not change significantly beyond 72 h, and yielded a decrease of 17±0.9 and 15.8±0.55 nm,

respectively, in mean diameter over 72 h. The dissolved Ag concentrations at 72 h in the mixed liquor and effluent samples were 1.15±0.04 and 0.9±0.02 ppb, respectively. The effluent and mixed liquor WW had very similar composition after pre-filtration although the mixed liquor had four times higher DOC levels (Table 3-1 S1). The total dissolved concentrations measured by spICP-MS, as shown in Figure 3-1A, comprised Ag^+ and Ag complexed to DOC or other agents (e.g., anions).

One reason for the reduced dissolution in the air-saturated WW effluent and mixed liquor as compared to DI water could be the presence of reduced sulfur. Inorganic sulfides in WW can sulfidate nAg and impact its dissolution (Kaegi et al. 2013). In this study, inorganic sulfides which include HS^- and acid soluble metal sulfides were quantified, as described in supporting information (SI), for WW effluent and mixed liquor samples before and after sample pre-treatment (0.45 µm filtration and aeration for 15 min). The sample treatment, particularly filtration, resulted in removal of some inorganic sulfides, but sufficient sulfides (1.88-2.84 ppm) remained in the aerated filtrate to which nAg at was added (mole ratio S/Ag = 632 for 10 ppb nAg; or S/Ag = 6.32 for 1 ppm nAg; Table 3-2 S2).

Decrease in DO concentrations reduced the rates and extents of dissolution of nAg, similar to trends observed elsewhere. (Liu and Hurt 2010) The dissolved silver concentration decreased by more than 50% at DO levels of 5.3 and 2.2 mg/L in WW effluent and mixed liquor, respectively. The dissolved silver concentrations in WW samples with DO at 7.7 mg/L were however similar to those in the air-saturated WW samples (Figure 3-1A).

The changes in particle size distributions of nAg for air-saturated DI water and effluent samples over 72 h are shown in Figure 3-1C. Particle sizes diminished due to dissolution and there was no evidence of nAg aggregation. In order to verify the nAg mean sizes attained by

spICP-MS, TEM analyses were performed for PVP-nAg immediately after exposure to DI water and those exposed to effluent WW for 72 h, and the results were in good agreement (Table 3-4 S4 and Figure 3-7 S3).

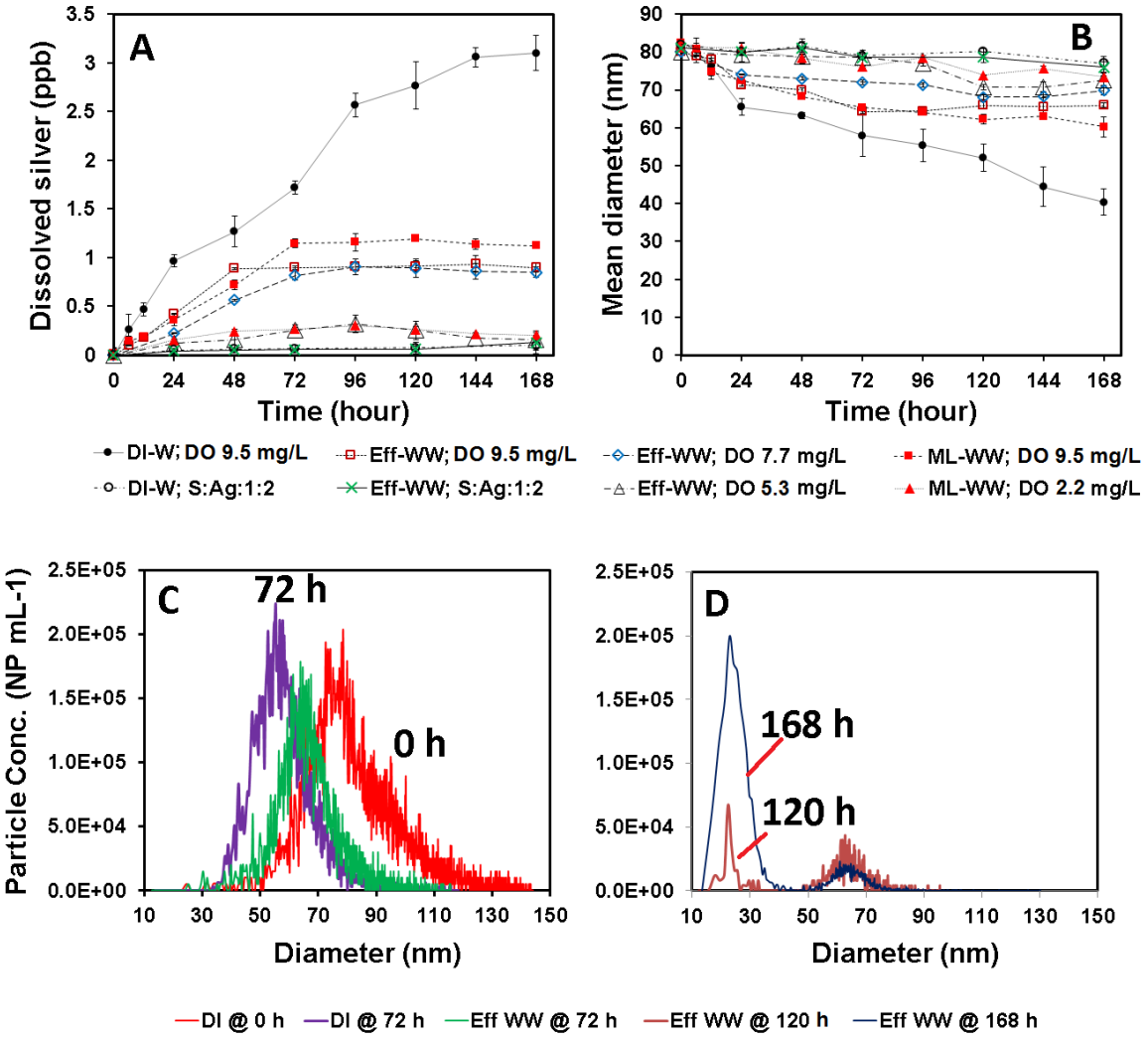

Figure 3-1- Changes in dissolved Ag concentrations and nAg mean diameters with time in dissolution experiments with PVP-nAg at initial concentration of 10 ppb. (A) Dissolved silver concentrations over time in DI water (DI-W), WW effluent (Eff-WW) and WW mixed liquor (ML-WW) (B) Change in mean size over time. (C) Changes in particle size distribution of PVP-nAg in DI water and WW effluent over 72 h. (D) Particle size distribution of PVP-nAg in WW effluent at 120 and 168 h.

Figures 3-1D shows the particle size distribution of nAg in effluent samples at 120 and 168 h, and a noteworthy feature is that a peak for particle sizes centered at 22.7 nm appeared

starting at 120 h that was non-existent at the particle size distribution of pristine nAg (Figure 3-8 S4). The nAg in DI water did not show the appearance of such a secondary peak under any spICP-MS settings of dwell time and sample time. The mean size of the primary particles decreased to 65.9±2.4 and 60.2±1.1 nm for air-saturated effluent and mixed liquor, respectively, over 168 h (Figure 3-1B). Similar bi-modal particle size distributions were observed with the mixed liquor samples at 120 and 168 h (Figures 3-9 S5, 3-10 S6). The formation of the secondary NPs was observed in vials maintained both in the dark and under laboratory light (Figure 3-11 S7). Several control experiments were conducted to explain the mechanism of the formation of the secondary NPs, and are discussed in the following section.

Citrate-nAg dissolved to a smaller extent than PVP-nAg (Figure 3-12 S8) but the patterns were qualitatively similar. The dissolution patterns of the citrate- and PVP-nAg is consistent with results reported by Dobias *et al.* (Dobias and Bernier-Latmani 2013) and Kittler *et al.* (Kittler et al. 2010). Those authors attributed the lower dissolution of citrate-nAg to higher binding of Ag^+ to the carboxylic groups of citrate (Dobias and Bernier-Latmani 2013).

In addition, PVP-nAg were reacted with Na_2S (S/Ag mole ratio 0.5, 5, 50) and re-suspended in DI water and WW effluent to evaluate the dissolution of sulfidated nAg. TEM and XPS characterization of the sulfidated nAg (S/Ag=0.5) are presented in Figure 3-13 S9. Sulfidated PVP-nAg (S/Ag mole ratio 0.5) dissolved the least, and yielded a small, but measurable dissolved Ag concentration of 0.1±0.08 ppb in DI water and 0.13±0.07 ppb in effluent samples, over 168 h (Figure 3-1A). It should be noted that the mean size calculated with spICP-MS for sulfidated PVP-nAg in Figure 3-1B, is based on the mass of Ag and not the actual particle diameter accounting for both S and Ag. In samples containing higher concentrations of sulfide (S/Ag equal to 5 and 50), no detectable dissolved Ag was observed.

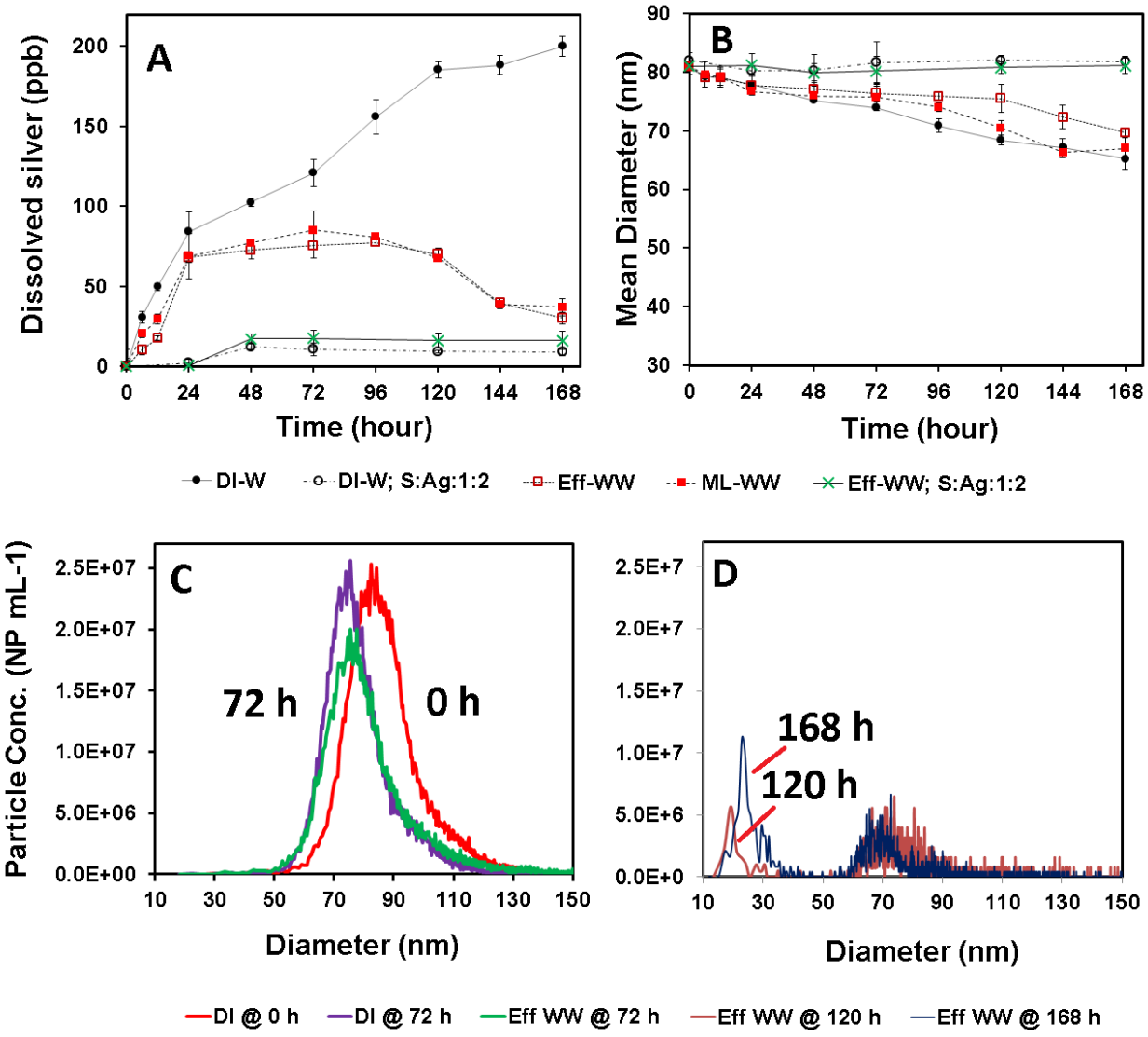

Figure 3-2- Changes in dissolved Ag concentrations and nAg mean diameters with time in dissolution experiments with PVP-nAg at initial concentration of 1000 ppb. (A) Dissolved silver concentrations over time in DI water, WW effluent and WW mixed liquor (B) Change in mean size over time (C) Changes in particle size distribution of PVP-nAg in DI water and WW effluent over 72 h. (D) Particle size distribution of PVP-nAg in WW effluent at 120 and 168 h. The DO in systems was 9.5 mg/L.

Particles sizes reduced to a substantially smaller extent with dissolution in the systems spiked with 1000 ppb (5×10^8 particles/mL) nAg, than in the systems where 10 ppb (5×10^6 particles/mL) nAg was added (Figure 3-1 B, C and 3-2 B, C). nAg at a nominal concentration of

1000 ppb attained higher dissolved Ag concentrations than nAg at 10 ppb for both coatings of PVP (Figure 3-2 B) and citrate (Figure 3-12 S8 B) in all three air-saturated aqueous media. However, the surface area normalized dissolution rates in DI water were 3.77×10^{-8} and 1.63×10^{-8} g cm^{-2} sec^{-1} for 10 and 1000 ppb nAg respectively over 72 h. Liu and Hurt demonstrated that at high nAg concentrations dissolution is hindered because of high proton depletion (Liu and Hurt 2010). Their thermodynamic analyses suggest that the extent of dissolution would have been limited in our 1000 ppb nAg test systems. This resulted in a relatively smaller percentage of Ag in dissolved form in the 1000 ppb test systems and caused smaller changes in the mean particle sizes than in the 10 ppb systems.

In air-saturated effluent and mixed liquor WW the dissolved Ag concentration was 20.1±3.7 and 36.9±5.4 ppb, respectively, at 168 h, which surprisingly was lower than what was measured at 72 h (75.3±7.9 ppb in effluent, and 85.0±12.1 ppb in mixed liquor samples). Yet the dissolved silver in DI water reached up to 200.1±6.2 ppb at 168 h. The emergence of smaller (~22 nm mean diameter) secondary NPs was also observed in the WW systems containing 1000 ppb PVP-nAg starting at 120 h (Figure 3-9 S5 B and 3-10 S6 B) as shown in Figure 2D. The mean size of PVP-nAg in WW effluent and mixed liquor samples reached 69.7±0.8 and 67±1.9 nm at 168 h.

The decrease in dissolved Ag concentrations in the WW samples can be attributed to the reformation of the secondary NPs from dissolved Ag. The appearance of these secondary NPs coincided with the decrease in dissolved Ag and the decrease dissolved Ag mass closely matched the Ag mass in that population discussed in SI.

Similar to the 10 ppb systems, DO concentrations of 2.2 and 5.3 mg/L decreased dissolution of nAg, but concentrations of 7.7 mg/L did not (Figure 3-14 S10).

3.3.2. Characterization of secondary NPs in WW effluent and mixed liquor

To confirm that the secondary peak in the nAg particle size distribution at 168 h was in fact due to the formation of secondary NPs from dissolved Ag, several control experiments were conducted.

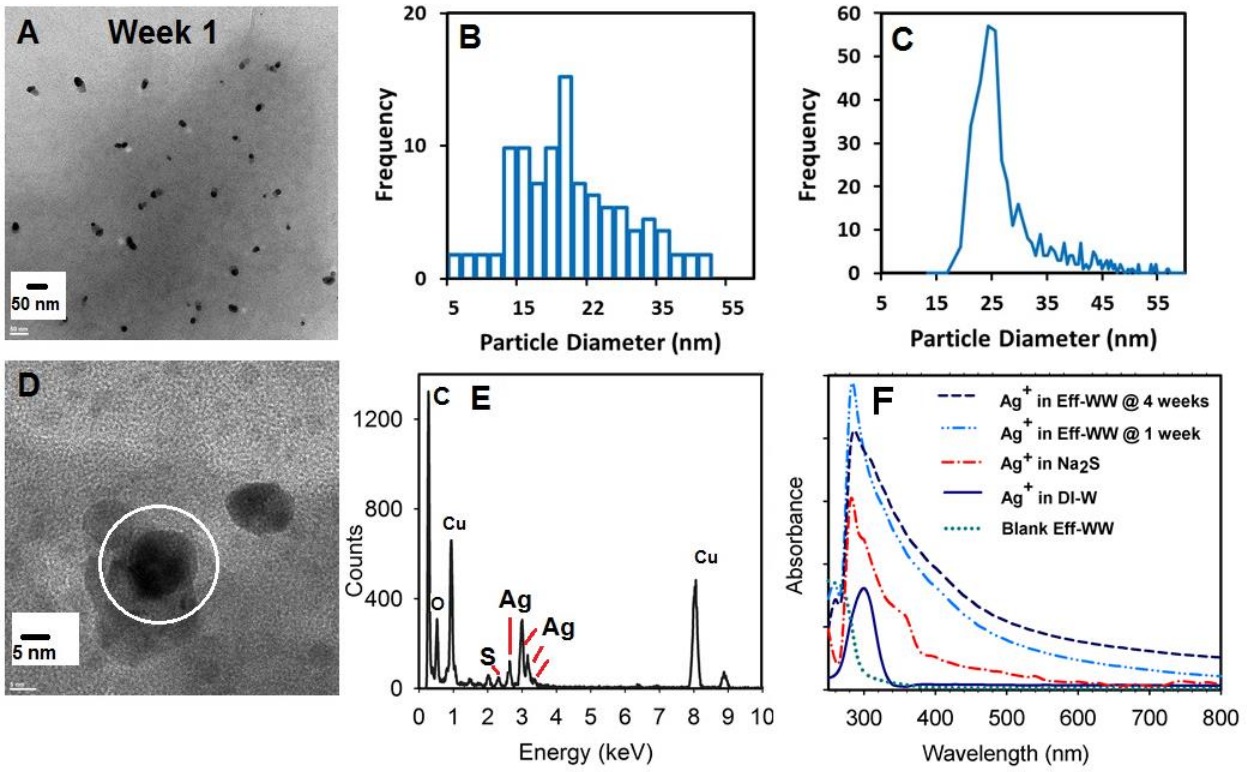

Figure 3-3- (A, D) TEM images of nAg formed in wastewater effluent samples at 168 h after addition of 1000 ppb Ag^+ ions. (B) The particle size distribution of the nAg formed in samples described in (A) as analyzed by spICP-MS, and (C) by TEM (n>100 particles). (E) EDS analysis of the nAg shown in (D); (F) UV absorbance spectra of DI water (at time 0) and WW effluent samples (after 1 and 4 weeks contact time) spiked with 1000 ppb Ag^+.

First, the spICP-MS was optimized for detection of very small nAg by analyzing standard 20 nm PVP-nAg. At dwell time of 100 µs and sample time of 100 s, spICP-MS provided a mean size of about 22±0.47 nm for the standard nAg (Figure 3-15 S11). The minimum detectable mass of Ag was less than 10 ppt (5.5×10^5 particles/mL) for 20 nm nAg.

A dissolved Ag standard solution was added to WW effluent to provide a range of concentrations of Ag^+ (10, 100, 1000 and 10^4 ppb). The effluent samples were then analyzed with spCP-MS at 72 and 168 h, and thereafter every week up to four weeks, to detect any NP formation. The analyses of Ag in WW effluent with spICP-MS immediately after sample preparation showed no presence of nAg and the dissolved Ag concentrations matched (>95%) the amounts of Ag^+ added. However, at 72 h and all time points thereafter, spICP-MS analyses showed formation of NPs in all samples.

TEM analyses also confirmed the presence of 3 to 30 nm diameter NPs (Figure 3-3 A, D) in samples with various Ag^+ concentrations. The mean diameter of the NPs detected with spICP-MS was 25.6±3.5 nm and 20.6±9.07 nm with TEM (n=110) in WW effluent samples spiked with 1000 ppb Ag^+ ions and stored for 168 h (Figure 3-3 B, C). The difference in size distribution of nAg by TEM and spICP-MS is due to their different detection limits. TEM detected particles as small as 2 nm whereas spICP-MS did not register any particle events smaller than 10 nm. There was no observed change in mean size of these NPs between 168 h and 4 weeks based on TEM and spICP-MS measurements. The formation of these NPs was observed in either the presence or absence of ambient laboratory light (Figure 3-16 S12). Therefore, the formation of NPs was not due to the photo reduction of dissolved Ag (Courrol et al. 2007).

EDS spectra showed the presence of sulfur in the NPs formed (Figure 3-3E) which could belong to both inorganic sulfides (HS^-, metal sulfides) or DOC containing thiol functional groups. Moreover, the peak for carbon was large and could be attributed to the carbon in the grid or to DOC associated with surface of secondary NPs. Chloride was not detected in any of the EDS analyses which suggests that the nAg formed were not silver chloride precipitates.

Figure 3-3F compares the UV-Vis spectrum of Ag^+ in WW effluent after 1 and 4 week of contact (containing formed NPs); Ag^+ in fresh DI water and Na_2S solutions; and unspiked (blank) WW effluent. Samples containing Ag^+ in WW effluent after 1 and 4 week of mixing showed high absorbance between 375-500 nm whereas the spectrum of Ag^+ freshly dispersed in DI water showed zero absorbance at these wavelengths. UV absorbance at this range is attributed to nAg_2S (Akamatsu et al. 2000),(León-Velázquez et al. 2010). To verify that, Ag^+ ions (10 ppm) and 20 nm PVP-nAg (10 ppm) were separately dispersed in Na_2S solution. The UV-vis spectra of these samples were qualitatively similar to that of the NPs formed in WW effluent (Figure 3-3 F, and 3-17 S13). In the spectrum of Ag^+ in WW effluent, the absorbance at 300 nm is attributable to dissolved silver and the absorbance at 250 nm could likely be due to absorbance of soluble organic or colloids in WW (Litvin et al. 2012).

A possible scenario for the formation of secondary particles during dissolution of nAg in WW is formation of various nanoparticulate silver sulfides. Sulfides can dissociate from other metals and react with Ag^+ and nAg due to the higher stability constants of silver sulfides (Thalmann et al. 2014). Several studies have shown that HAs and FAs are able to reduce dissolved Ag to form nAg, particularly in the co-presence of strong reducing agents, high pH, high temperature and UV light (Akaighe et al. 2011, Adegboyega et al. 2012). Furthermore previous literature suggested that the thiol in cysteine strongly binds to Ag^+ and forms nAg (Khan and Talib 2010, Siriwardana et al. 2015). To investigate whether DOC compounds such as humic substances and amino acids (i.e. cysteine) can be responsible for the formation of secondary particles several control experiments were performed. Ag^+ ions at 10 to 10^4 ppb were added to 38, 126, and 378 ppm of HA and FA solutions, both in the dark and under laboratory light and contacted for up to 4 weeks. Neither spICP-MS, nor TEM could detect any nAg in

these systems. In addition, Ag^+ ions were added to cysteine (L-Cysteine Sigma-Aldrich) dissolved in DI water at cysteine:Ag mole ratios of 0.44, 0.89, 4.4, 8.9, and 44.5. spICP-MS analysis of Ag^+ in exposure to cysteine after 24 and 168 h showed particles of silver with a mean size between 40-50 nm both in the presence and absence of laboratory light (Figure 3-18 S14). Furthermore, UV-vis spectra of Ag^+ in cysteine after 1-week contact showed a peak at 400 nm for plasmonic NPs formed in cysteine solution (Figure 3-17 S13). The WW samples contained 8.8 and 39.7 ppm DOC of which a percentage could be due to presence of amino acids containing thiol groups. Thus, amino acids such as cysteine if present can play a role in the formation of secondary particles.

3.3.3. Surface chemistry of nAg contacted with WW effluents.

The lower rates and extents of dissolution of nAg in WW samples compared to DI water suggest changes in the surface composition in contact with WW. Thus, the surface chemistry of nAg was contacted with effluent WW samples was characterized by complementary techniques. Figure 3-4 shows some of the peaks identified for both positive and negative ions in the ToF-SIMS spectra obtained for PVP-nAg exposed to WW effluent samples for 72 h. A more detailed list of secondary ions identified in the spectra, along with their ion attribution and peak intensity is presented in Tables 3-9 S5, 3-10 S6 and 3-10 S7. The presence of sulfide species associated with the nAg are suggested by the presence of positive ions such as AgS^+, AgS_2^+, at 138.87, 170.85, mass (u) respectively and negative ions such as AgS^-, $AgHS^-$, AgS_2^-, at 138.87, 139. 88, 170.84 mass (u) respectively. One possible source of such silver sulfide ions could be the presence of Ag_2S and other silver sulfide species on the surface of nAg. Goh *et al.* showed that the ToF-SIMS analysis of Ag_2S surfaces generated ions such as AgS^-, AgS_2^-, $Ag_2S_2^-$, $AgHS^-$

(Goh et al. 2006). Another possible source of such ions is the ionization of Ag-organosulfur species (Advanced Powder TechnologyGoh et al. 2008, Gades and Urbassek 1995).

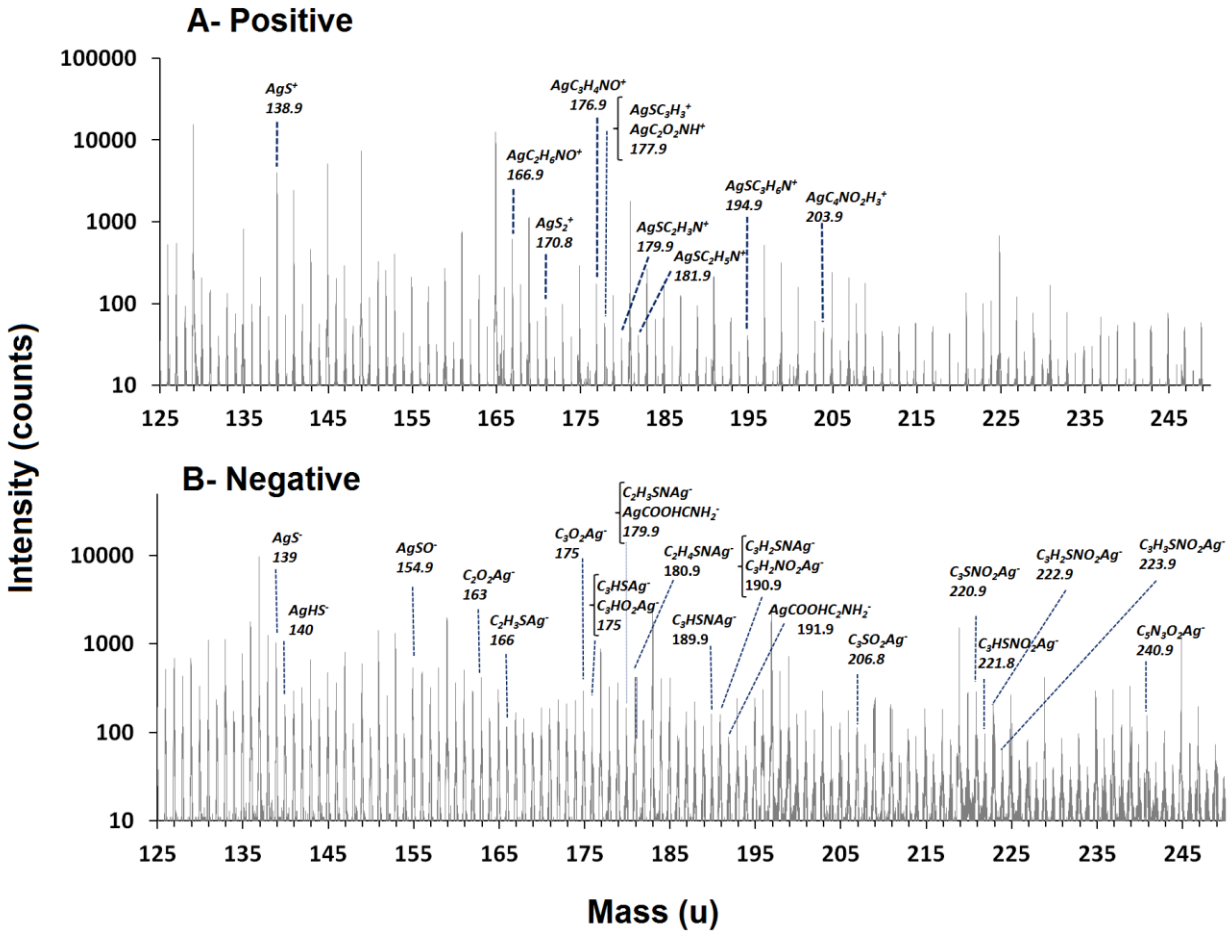

Figure 3-4- ToF-SIMS analysis of PVP-nAg suspended in WW effluent for 72 h (A) positive ion spectrum and (B) negative ion spectrum in the mass region of 125-245. A description of all the positive and negative ions associated with silver can be found in supplementary information (Table S4, 5, and 6).

Complementary analyses of the sulfide species on the surface of nAg, were performed with XPS. The XPS analyses of nAg in WW effluent indicated S2p doublets which are similar peaks and which can be deconvoluted into three components with S2p3/2 levels centered at binding energies of 161.6 and 163.1 eV that were attributed to the inorganic sulfides Ag_2S and

Ag-S-H, and 164.2 eV that was attributed to Ag-S-C organosulfur bonds (Figure 3-19 S15). The total sulfur analysis of WW effluent samples with ICP-OES indicated the presence of 64.9±2.6 ppm sulfur (Table 3-1 S1) and AVS concentration after filtration and aeration of WW were 1.88-2.84 ppm in effluent and mixed liquor respectively (Table 3-2 S2). Thus the sulfur was present as stable metal sulfides (e.g., FeS, CuS, and ZnS) (Adams and Kramer 1999) as well as organosulfur compounds in WW effluent and mixed liquor. The bonding of inorganic and organic S to nAg would have contributed to the lower dissolution of nAg in the WW mixed liquor and effluent samples observed in Figures 1 and 2.

Several species of silver bound to organic molecules containing S and N functional groups were detected by ToF-SIMs (Tables 3-4 S4, 3-5 S5). Some of the silver amine positive ions were $AgC_2H_6NO^+$, $AgC_3H_4NO^+$, $AgC_4NO_2H_3{}^+$ at 167, 177, 203.9 mass (u) and negative ions included $AgCOOHCNH_2^-$, $C_3H_2NO_2Ag^-$, $C_5N_3O_2Ag^-$ at 179.91, 192, 241 mass (u). Ag bonds with S functional groups generated positive ions such as $AgSC_2H_3N^+$, $AgSC_3H_6N^+$ at 179.90 and 194.93, mass (u), respectively, and negative ions such as $AgC_2H_3SN^-$, $C_3H_2SNAg^-$, $C_3H_7SNO_2Ag^-$ at 179.89, 190.89 and 227.92 mass (u). These ions were exclusively detected in nAg samples suspended in WW effluent and did not exist in spectra of the reference sample of pure PVP-nAg. Ag has strong affinity to N and S functional groups in organic moieties (Stumm and Morgan 1981) (Cotton et al. 1999, Morf et al. 1974) and the Ag-organosulfur bonds are likely due to DOC containing N and S functional groups (e.g. proteins, amino acids, thiols) identified in Tables 3-4 S4 and 3-5 S5 that are commonly found in WW effluents (Drewes and Croue 2002)·(Goh et al. 2006). Given the strong evidence of interaction of DOC to the nAg, experiments were conducted to assess if DOC affected dissolution rates and extents.

3.3.4. The effect of natural DOC on the dissolution of nAg.

The extent of dissolution of PVP over 72 h in the presence of alginate decreased with increasing alginate concentrations (Figure 3-20 S16). Although the dissolved Ag concentrations (1.4±0.06 ppb) measured in the presence of 1 ppm alginate were close to that in DI water, with an increase in concentration of alginate to 10 ppm the dissolution of PVP-nAg over 72 h was almost completely inhibited (0.04±0.02) and that of Citrate-nAg was reduced to 50% as compared in DI water (0.5±0.01).

PVP and Citrate-nAg suspended in HA or FA solutions showed decreased dissolved Ag concentrations and smaller changes in nAg mean diameters as compared to the dissolution in DI water or alginate solutions (Figure 3-20 S16). The extent of dissolution of PVP-nAg in 1 and 10 ppm HA solutions over 72 h was reduced by between 74 and 84% compared to DI water, and in FA solutions, it was reduced by between 60 and 73%. The decrease in dissolved Ag concentration and particle size change was more substantial in HA than in FA solutions, particularly for PVP-nAg. This is likely because HAs have higher affinity than FA for nAg surfaces (Furman et al. 2013). Suwannee River HA used in this research was reported to contain 1.19 and 0.58 %(w/w) (of a dry, ash free sample) of N and S and Suwannee river FA contains 0.72 and 0.44 %(w/w) N and S respectively according to the manufacturer, International Humic Substances Society (IHSS). The concentration of HA and FA increased to 6 and 10 ppm, no statistically significant difference in the dissolved silver concentrations were observed. Thus, no clear trend between HA and FA concentrations and dissolved Ag concentrations was observed. Reduced dissolution of Citrate-nAg in HA (56-67%) and FA (33-57%) solutions compared in DI water was also observed (Figure 3-20 S16).

Hindered dissolution of nAg in the presence of HA and FA was also reported in previous studies (Aiken et al. 2011, Gunsolus et al. 2015, Furman et al. 2013, Delay et al. 2011). For example, Liu *et al.* showed that HA and FA (0-50 ppm) inhibited the dissolution of nAg in a dose dependent manner (Liu and Hurt 2010). Ostermeyer *et al.* also reported that high alginate concentrations (100-1000 ppm) reduced the extent of dissolution of 1000 ppb nAg by 20% after 3 h exposure (Ostermeyer et al. 2013). Those authors suggested that alginate sorbs onto the surface of nAg and inhibits dissolution by either hindering diffusion of Ag^+ from the surface of nAg or by blocking the active sites for oxidation of nAg surface. The inhibition of dissolution may also be due to a reversible reaction of released Ag^+ to Ag(0) due to chemical reduction by HA and FA (Sal'nikov et al. 2009).

3.4. Conclusions

New insights into the fate of Ag as a result of dissolution of nAg were provided by this study. Dissolution of 80 nm PVP-nAg resulted in the release of dissolved Ag that reacted with sulfides in WW resulting in the reformation of new (secondary) NPs of approximately ~20 nm in diameter after approximately 3 days. ToF-SIMS and XPS analyses suggest that Ag interacted with S from various inorganic and organic sources, and thus the secondary NPs formed in WW likely have a complex composition of various sulfides that may be represented as nAg_xS_y. Reformation of nAg_xS_y was not observed during dissolution in DI water or in HA and FA solutions. Furthermore, dissolution of nAg at lower, environmentally relevant concentrations (10 ppb) yielded much smaller primary nAg particle sizes (~40 nm) than with 1000 ppb nAg (~65 nm). Smaller nAg can have significant different hetero- or homo-aggregation behavior, bio-uptake and other environmental fate processes compared to larger particles, and thus the dissolution conditions that result in generation of small nAg have environmental significance and

should be considered in risk assessment studies. The association of WW DOC (e.g. with amine and thiol groups), DO concentrations, as well as inorganic sulfides with nAg control the rates of dissolution, and it appears that inorganic sulfides and organosulfur DOC are responsible for formation of the 20 nm nAg. The dissolved Ag is also complexed by DOC (further details in SI) or inorganic sulfides and thus direct toxicity from Ag^+ is unlikely in WW systems. It is important to note that the WW samples were filtered in our experiments and therefore the effect of WW colloids retained on 0.45 μm filters on dissolution may contribute to different dissolution patterns and this needs to be investigated using different analytical approaches than spICP-MS. Our study also shows that spICP-MS can be used to detect nAg as small as 20 nm (simultaneously with dissolved Ag) in complex aqueous matrices such as wastewater, at sub ppb levels.

3.5. Acknowledgments

We thank David Liu, McGill, for TEM/EDS analysis of nAg; Josianne Lefebvre, Université de Montréal, for XPS and ToF-SIMS analyses, La Prairie WWTP for assistance with WW sampling and Flavio Piccapietra, McGill, for help with spICP-MS optimization protocols. Funding from Natural Sciences and Engineering Research Council, Canada (Grants STPGP 430659–12, RGPIN 2016-05022, 413978-12), Environment and Climate Change Canada, Perkin Elmer Health Sciences Canada, and SNC Lavalin Environnment, is gratefully acknowledged.

3.6. Supplementary Data

Table 3-1- S1- Characteristics of WW mixed liquor and effluent collected.

WW Sample	pH	Conductivity (µS/m)	ORP (mV)	DOC (mg/L)	TOC (mg/L)	Suspended solids (TSS) (mg/L)	Total Ag after acid digestion (unfiltered) (µg/L)
Secondary aeration tank (WW mixed liquor)	7.13± 0.01	1030±2	+257±1	39.7	2131.5	1823.3±60.3	0.37±0.05
Secondary settling tank (WW effluent)	7.28±0.01	1002±1	+264±2	8.85	34.7	10±4.26	0.025±0.001

Table 3-2- S2- Acid volatile sulfide, total sulfur and dissolved oxygen (D.O.) concentrations in the WW effluent and mixed liquor samples before and after filtration and aeration.

Sample	Total sulfur (mg/L)	AVS (mg/L)	D.O. (mg/L)
Effluent WW	40.10±0.3	**9.77±0.04**	5.0-7.0
Filtered+Aerated Effluent WW	36.93±0.9	**2.84±0.05**	9.5
Mixed liquor WW	58.33±0.3	**12.06±0.05**	2.0-5.0
Filtered+Aerated Mixed liquor WW	30.91±1.2	**1.88±0.07**	9.55

3.6.1. WW analysis

The total Ag analysis was done by ICP-MS (Perkin Elmer NexION 300X) after acid digestion of the WW samples. Conductivity was determined by a digital conductivity meter (Fisher Scientific). The redox potential was determined using an Accumet AP71 (Fisher Scientific) at 25 ºC calibrated at 215 mV Ag/AgCl with the ORP standard calibration solution. A TOC Analyser (Sievers Innovox Laboatory, GE) was used to measure the levels of DOC and TOC in WW samples. For TSS, the 0.45 µm, the filters were washed and dried beforehand to stabilize their weight connected to a vacuum pump. The filters were weighed after drying at 150 C over-night to establish the TSS. Total sulfur was analyzed for WW effluent and mixed liquor as they arrived in the lab after filtration and aeration using ICP-OES. AVS was quantified using a modified method of Berner (1964). Briefly, 6 N HCl was added to the samples and brought to a

boiling temperature to release AVS to the atmosphere as H_2S gas. Total sulfur in the WW samples before and after filtration and aeration was analyzed using ICP-OES after acid digestion with aqua regia (HNO_3:HCl=1:3) in a microwave at 90 ^oC for 75 min. A calibration curve for ICP-OES analysis (25 ppb-5 ppm) were prepared by diluting Atomic Spectroscopy Standard Sulfur (1000 μg/mL, Perkin Elmer Pure) in 5% HNO_3. The weight change before and after acid digestion in the microwave, as well as the total sulfur measurements were used to calculate the AVS. ICP-OES was used because of the high accuracy for sulfur measurement with a detection limit of 25 ppb.

Table 3-3- S3- Single Particle ICP-MS Instrumental Parameters

Parameter	**Value**
Sample Uptake Rate	0.3 mL/min
Nebulizer	Glass Concentric
Spray Chamber	Glass Cyclonic
RF Power	1600 W
Analyte	Ag107
Analysis time	100-150 sec
Dwell time	100 & 1000 μsec

3.6.2. SP and standard mode ICP-MS calibration and verification of data quality

A dissolved Ag standard solution of 1001±4 ppm in 4% HNO_3 (PlasmaCAL) was used for preparing the ICP-MS calibration curve including one blank and 4-5 dissolved Ag solutions (0-5 ppb) in 1% HNO_3 in both standard and single particle modes. The nAg suspensions in WW or DOC samples were diluted 10 times in DI water (~1 ppb nominal) to establish the dissolved

Ag concentration and diluted 100 times (~0.1 ppb nominal) to obtain the particle size distribution for the samples spiked with 10 ppb nAg and was compared with the particle size distribution at 1 ppb. No difference in mean particle size was observed between the two dilution factors that means the dilution and detection were reliable.

All the samples from all the time points were analyzed on one day with the same instrument setting and optimization. Moreover, every 10-15 samples, one quality control sample containing 100 ppt dissolved Ag in 1% HNO_3 was analyzed from the stock of 100 ppm dissolved Ag solution (PlasmaCAL, Q.C. Standard 4, in 5% HNO_3). Every 5 analyses, a sample of 1% HNO_3 in DI water was analyzed in order to indicate any drift (>20%) in intensity of counts by the instrument and in case of any contamination occurred.

3.6.3. Centrifugal Ultrafiltration and ICP-MS

To verify the accuracy of the dissolved Ag measurements by spICP-MS, centrifugal ultrafiltration at 4600g for 30 min for three sequential filtrations (Amicon, NMWL 3 kDa) was performed to separate the nAg from the aqueous phase in the DI water samples, and some of the WW-effluent samples followed by ICP-MS analyses of the acidified (1% HNO_3) filtrate. The dissolved concentrations obtained from dissolution of nAg in DI water by two techniques were in excellent agreement (Figure 3-6 S2). Moreover, in a few control experiments Ag^+ (1 ppb) in DI water passed through 3 kDa filters more than 96%. However, more than 90% of dissolved Ag^+ ions added to WW effluent were retained on the filter likely due to complexation of dissolved Ag^+ ions with the DOC compounds in WW. The analysis was done immediately after spiking WW effluent with Ag^+ and therefore there was no formation of nAg in these samples yet. It is hypothesized that the centrifugal ultrafiltration at 3 kDa removes a large portion of the DOC substances in wastewater which are generally larger than 3 kDa and can have molecular weights

between 1-10^9 kDa (i.e. alginate, humic substances, and proteins). Thus, it is likely that the DOC in wastewater samples was retained on the ultrafilter.

To assess the accuracy of dissolved silver measured by spICP-MS, 0.4 ppb Ag^+ ions were prepared in various aliquots containing DI water, WW effluent, HAs, FAs and alginate and were analyzed with spICP-MS within few minutes of preparation (Figure 3-5 S1).

The total Ag analysis was performed in standard mode of ICP-MS so as to determine the total Ag mass in all aqueous systems. For the total silver measurements all the samples of nAg were digested by 30-35 % HNO_3 (PlasmaPURE, 67-70% Acid Nitric) for 24 h shaking in the room temperature and then diluted with DI water to 1% acid content prior to analysis with ICP-MS. To ensure all the Ag is dissolved after acid digestion and no particulate Ag has remained in the samples, a few control samples were analyzed with spICP-MS.

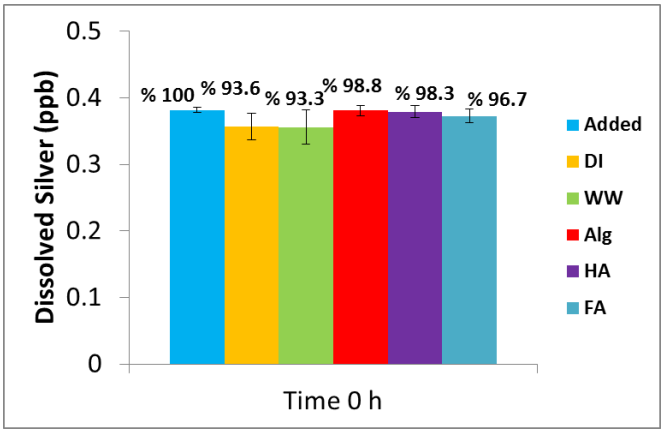

Figure 3-5 S1- spICP-MS measured dissolved silver concentrations for 0.4 ppb Ag^+ added to different test media (WW, DOC, DI water) and analyzed immediately after proper dilutions with DI water. The graph also shows the recovery of the dissolved silver measured with spICP-MS (%) as compared to the total silver mass in the test media. spICP-MS was able to accurately measure more than 93.3% of dissolved silver in all samples.

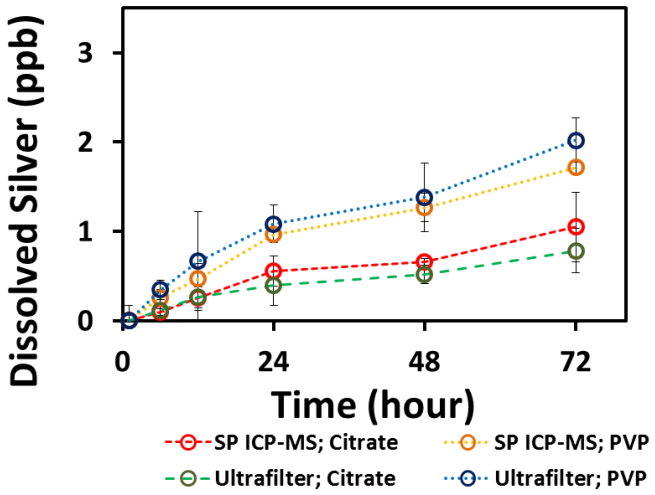

Figure 3-6 S2 The dissolved silver concentrations over time obtained by spICP-MS and centrifugal ultrafiltration-total metal ICP-MS for 80 nm PVP-nAg suspended in DI water.

Table 3-4 S4- Summary of nAg mean size (nm) after 1 and 72 h exposure to DI water, WW effluent and mixed liquor by spICP-MS, and TEM (n=120)

Media	Surface Coating	spICP-MS	TEM
NPs Stock	Citrate	74.8±0.2	74.1±5.3
NPs Stock	PVP	81.7±0.01	79.0±7.5
NPs Mean Size After 72 h Exposure			
DI water	Citrate	55.4±2.4	65.4±9.9
DI water	PVP	57.9±5.5	68.5±7.8
Effluent	Citrate	65.4±1.29	68.6±9.6
Effluent	PVP	64.2±0.5	69.1±7
Mixed Liquor	Citrate	65.9±0.2	66.5±5.7
Mixed Liquor	PVP	65.3±0.2	66.2±7.9

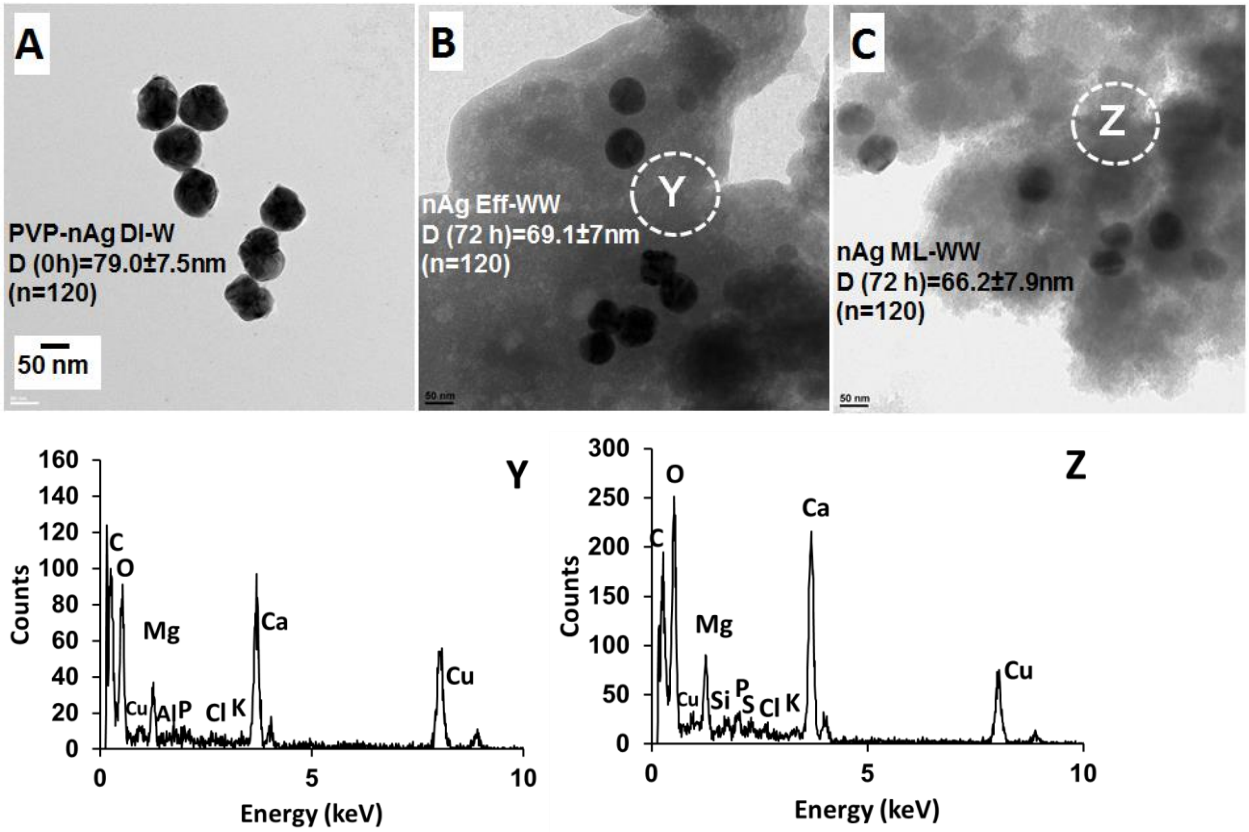

Figure 3-7 S3- (A) TEM image of PVP-nAg at time 0 h contacted with DI water (B) PVP-nAg in WW effluent at 72 h; (C) TEM image of PVP-nAg in WW mixed liquor at 72 h; The scale bar is 50 nm for all images. The EDAX analysis of the nAg in WW effluent; (Y) Analysis of the background WW effluent in panel B; (Z) Analysis of the background WW mixed liquor in panel C.

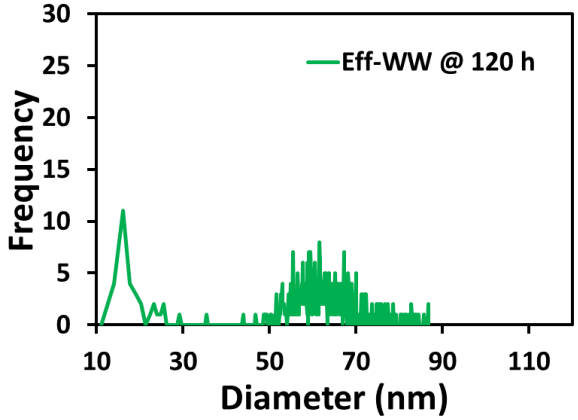

Figure 3-8 S4- Particle size distribution of 1000 ppb nAg in WW effluent at 120 ppb.

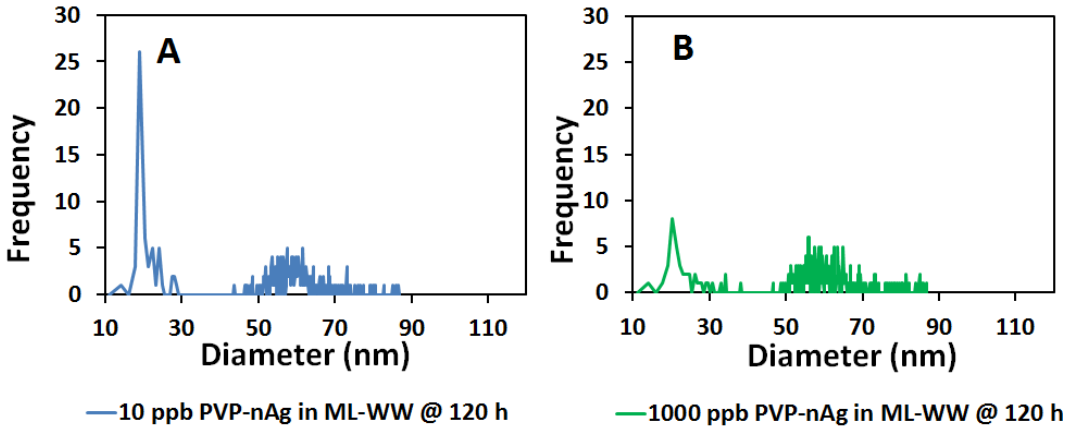

Figure 3-9 S5- Particle size distribution of PVP-nAg in WW mixed liquor in (A) 10 and (B) 1000 ppb at 120 h.

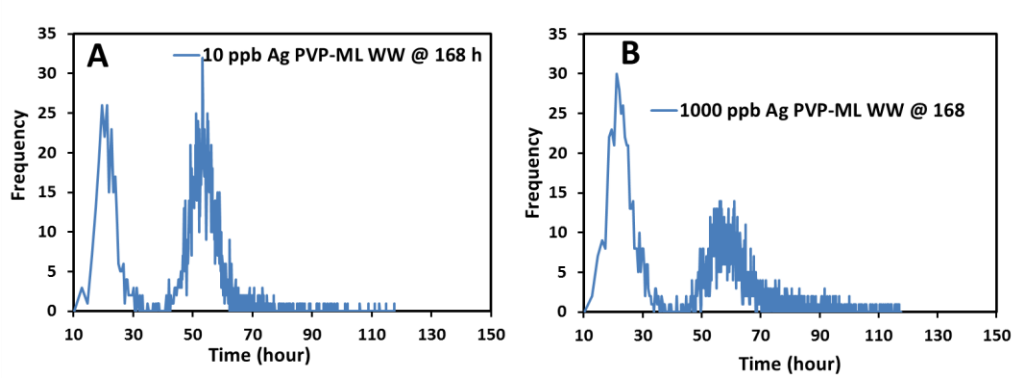

Figure 3-10 S6- Particle size distribution for (A) 10 ppb and (B) 1000 ppb nAg in WW mixed liquor at 168h.

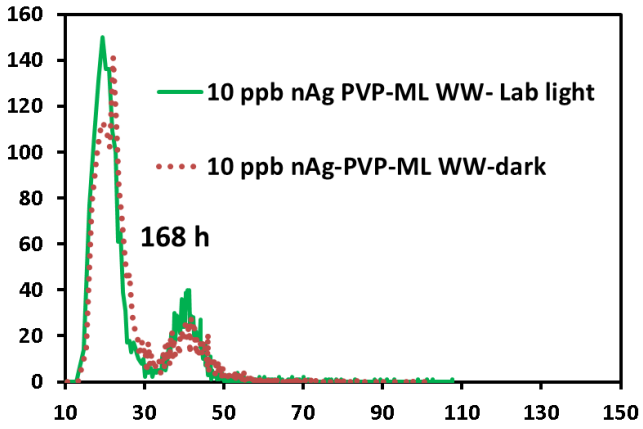

Figure 3-11 S7- The particle size distribution at 168 h for 10 ppb nAg in WW mixed liquor exposed to the laboratory light.

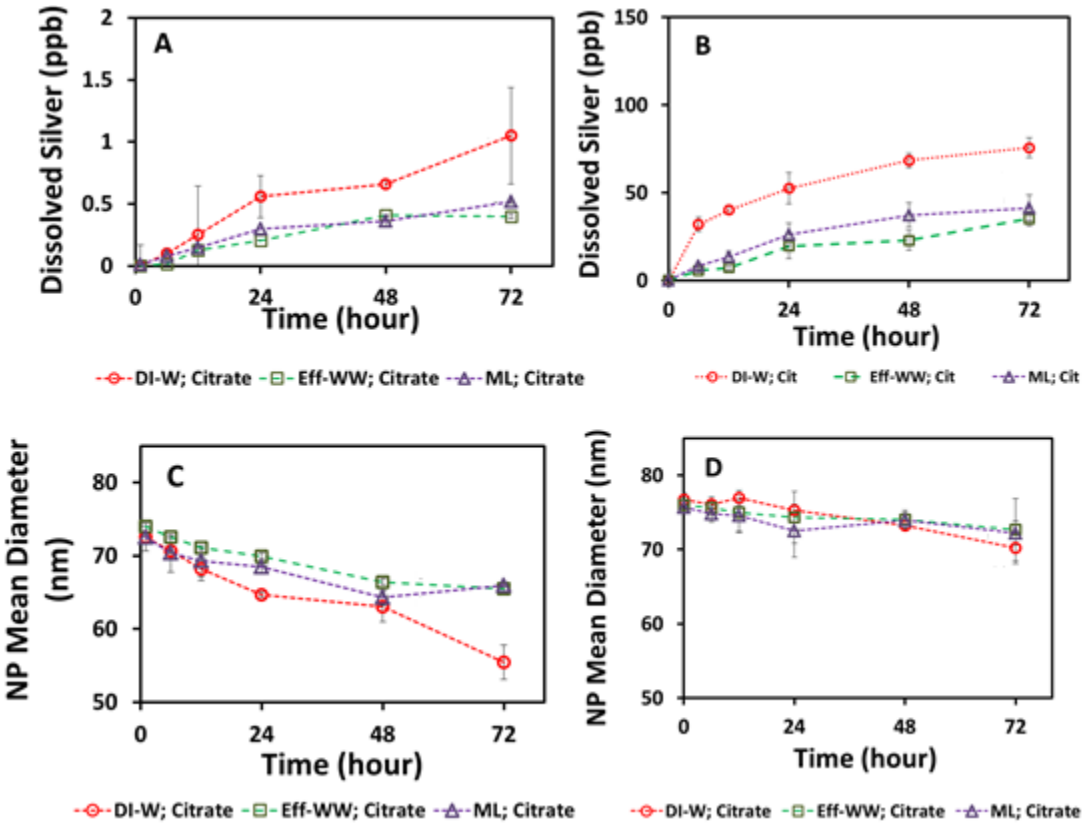

Figure 3-12 S8- The dissolved silver concentration and mean nanoparticle size of citrate-nAg in DI water, WW effluent and mixed liquor. (A & C) the total initial citrate-nAg at 10 ppb (B & D) the total initial citrate-nAg at 1000 ppb.

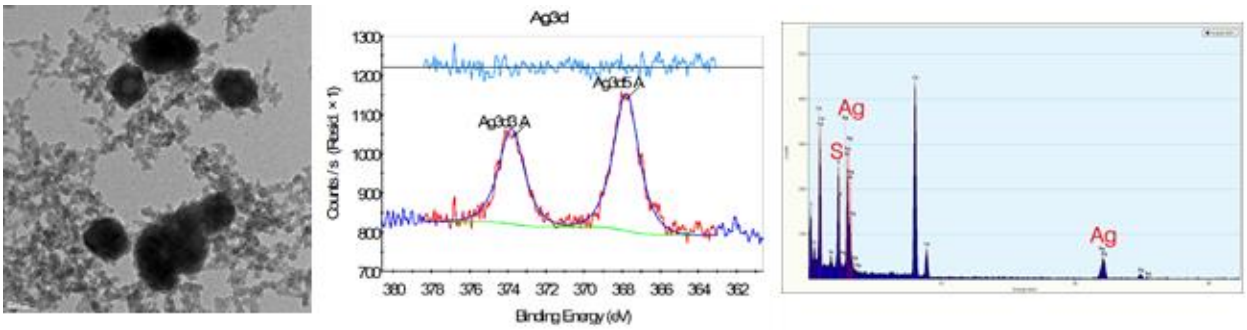

Figure 3-13 S9 XPS analysis of the sulfidated Ag NPs; binding energy of the Ag3d5/2 line at 367.8 eV (A) EDS analysis on the surface of marked Ag NPs (B).

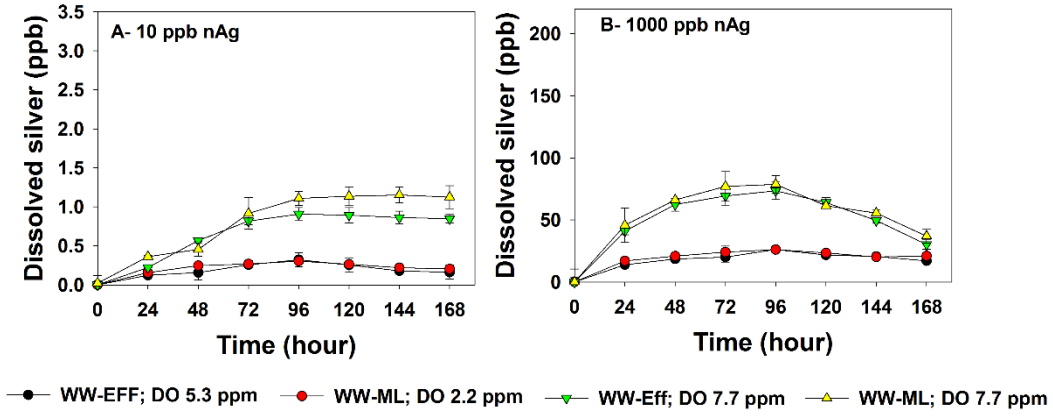

Figure 3-14 S10- The dissolution of PVP-nAg at 10 and 1000 ppb at various degrees of DO concentration in WW effluent and mixed liquor.

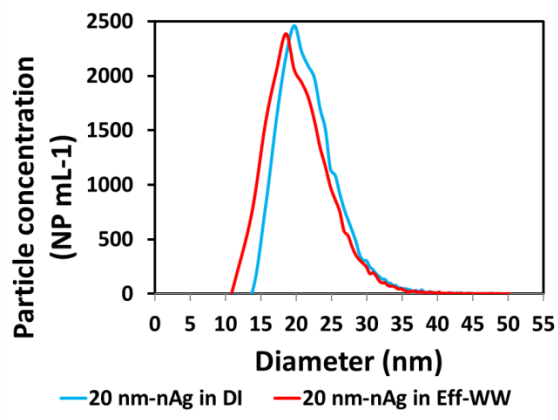

Figure 3-15 S11- NanoXact PVP-nAg (nominal 20 nm) analyzed with spICP-MS at 100 µsec.

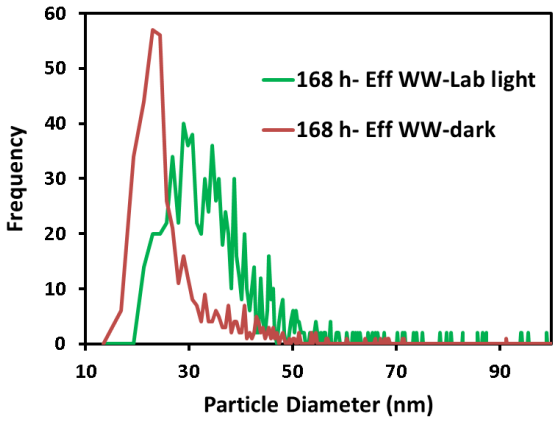

Figure 3-16 S12- Particle size distribution of nAg_xS_y with spICP-MS formed in WW (A) effluent and (B) mixed liquor from free Ag^+ ions at 1000 ppb at 168 h exposed to laboratory light.

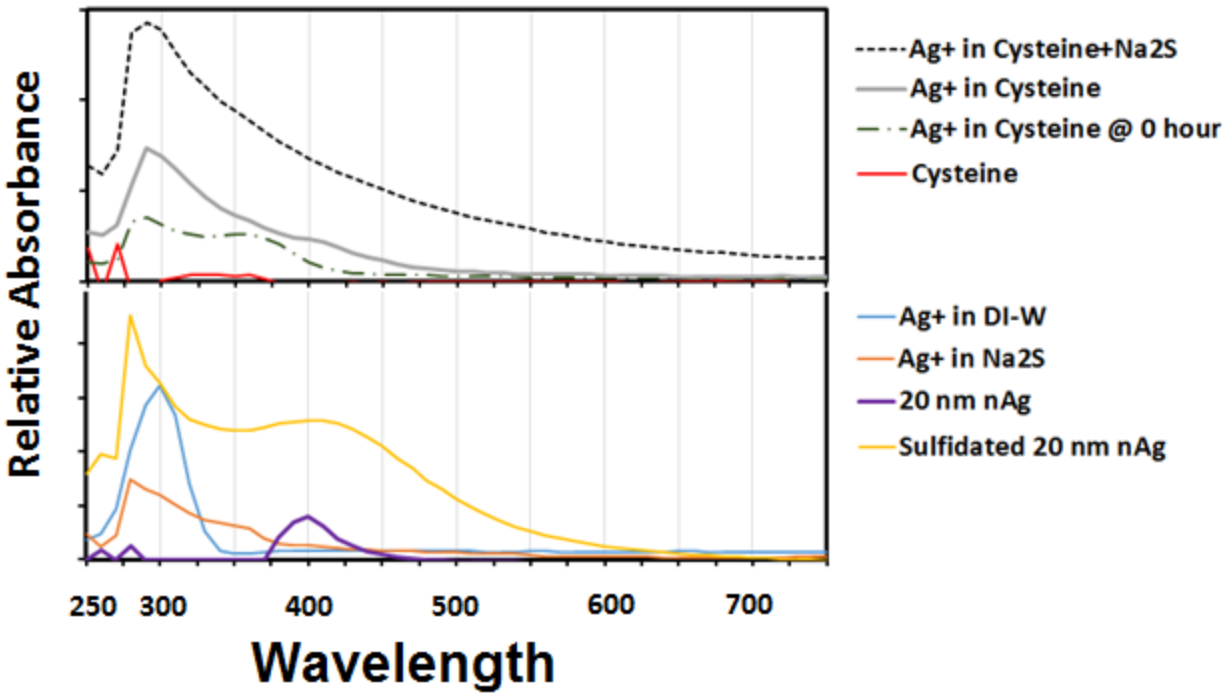

Figure 3-17 S13- UV-visible absorption spectra of Ag_2S NP as a function of initial silver concentration. The initial Ag^+ concentrations added in WW effluent, DI water, and Na_2S were 10 ppm. The mass ratio of cysteine to Ag^+ was 0.5 (100 ppm Ag^+, and 50 ppm cysteine). The spectra for Ag^+ in cysteine were obtained before 1 hour (specified 0 hour in figure) and after one week (specified as Ag^+ in cysteine). The spectra for standard 20 nm PVP-nAg was obtained right out of the NP stock and then after 2 hours reaction with Na_2S (S:Ag:1:1 mole ratio).

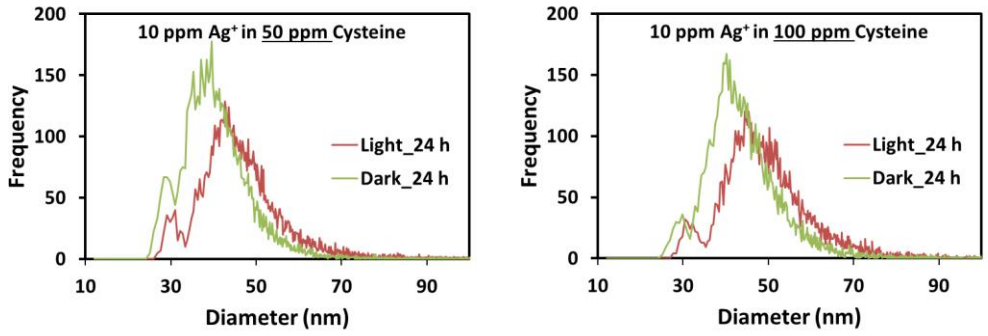

Figure 3-18 S14- Particle size distribution of nAg formed by contacting Ag^+ (10 ppm) in cyteine solution (50 and 100 ppm) for 24 h in both dark and laboratory light.

3.6.4. ToF-SIMS analyses

The pressure in the analysis chamber during the analyses was maintained below 5.0 x 10^{-9} Torr. The spectra were obtained using 25 keV Bi_3^{++} primary ions in bunched mode with a pulse width of 25.0 ns. The ion current at the sample was 0.42 pA and the ion dose was below the static limit of 1×10^{13} ions cm^{-2}.

Ions detected in samples of PVP-nAg suspended in WW effluent are listed below, after subtracting ions (except Ag^-) from analysis of fresh PVP-nAg from the stock solution. Peak intensities in ToF-SIMS are not directly related to the concentration of the identified compounds in the sample because secondary ion yields are strongly affected by matrix effects. Unless otherwise mentioned, 107Ag was analyzed.

Table 3-5 S5- Positive ions detected in ToF-SIMS analysis of nAg suspended in WW effluent.

#	Center Mass (u)	Assignment	Identification	Intensity		
				Raw	Normalized by Ag+	Normalized by total ion intensity
Organosulfur complexes with silver						
1	177.8965	$AgSC_3H_3^+$	Cysteine, methionine	2115	7.84E-01	7.01E-05
2	179.9025	$AgSC_2H_3N^+$	Cysteine	1315	4.88E-01	4.36E-05
3	181.9067	$AgSC_2H_5N^+$	Cysteine	1497	5.55E-01	4.96E-05
4	194.9302	$AgSC_3H_6N^+$	Cysteine	486	1.80E-01	1.61E-05
Silver complexes with amino acids and organics						
5	126.9447	$^{109}AgNH_4$	Amino acids	5138	1.91E+00	1.70E-04
6	203.9158	$AgC_4NO_2H_3^+$	Histidine	1700	6.30E-01	5.63E-05
7	166.9499	$AgC_2H_6NO^+$	Amino acids	1546	5.73E-01	5.12E-05
8	176.9401	$AgC_3H_4NO^+$	Amino acids	987	3.66E-01	3.27E-05
9	177.8993	$AgC_2O_2NH^+$	Histidine	1682	6.24E-01	5.57E-05

Table 3-6 S6- ToF-SIMS analysis of negative ions detected and their attributes for nAg suspended in WW effluent

#	Center Mass (u)	Assignment	Identification	Intensity		
				Raw	Normalized by Ag+	Normalized by total ion intensity
	Silver complexes with thiol and amine containing organics					
1	106.8973	Ag^-	Silver NPs	2700	1.00E+00	6.51E-05
2	165.9015	$C_2H_3SAg^-$	Cysteine	3962	1.47E+00	9.55E-05
3	175.8972	C_3HSAg^-	Cysteine	9881	3.66 E+00	2.38 E-04
4	153.8964	CH_3SAg^-	Cysteine	2134	7.90E-01	5.14E-05
5	206.8772	$C_3SO_2Ag^-$	Cysteine	4955	1.84E+00	1.19E-04
6	179.8856	$C_2H_3SNAg^-$	Cysteine	7946	2.94E+00	1.91E-04
7	180.8925	$C_2H_4SNAg^-$	Cysteine	12686	4.70E+00	3.06E-04
8	189.8867	C_3HSNAg^-	Cysteine	6940	2.57E+00	1.67E-04
9	190.9067	$C_3H_2SNAg^-$	Cysteine	5344	1.98E+00	1.29E-04
10	220.8687	$C_3SNO_2Ag^-$	Cysteine	13241	4.90E+00	3.19E-04
11	221.8726	$C_3HSNO_2Ag^-$	Cysteine	4997	1.85 E+00	1.20E-04
12	222.8697	$C_3H_2SNO_2Ag^-$	Cysteine	13700	5.07E+00	3.30E-04
13	223.8746	$C_3H_3SNO_2Ag^-$	Cysteine	3940	1.46E+00	9.49E-05
	Silver complexes with organics					
15	163.8939	$C_2O_2Ag^-$	Cysteine	6112	2.26E+00	1.47E-04
16	174.8850	$C_3O_2Ag^-$	Histidine, COOH containing amino acids	12481	4.62 E+00	3.0E-04
17	175.8972	$C_3HO_2Ag^-$	Histidine, COOH containing amino acids	9881	3.66 E+00	2.38 E-04
18	240.9029	$C_5N_3O_2Ag^-$	Histidine	1937	7.18E-01	4.67E-05
19	190.9067	$C_3H_2NO_2Ag^-$	Histidine	5344	1.98 E+00	1.29 E-04
20	179.9215	$AgCOOHCNH_2^-$	Histidine,glutathione	2964	1.10E+00	7.14E-05
21	191.9223	$AgCOOHC_2NH_2^-$	Histidine,glutathione	1213	4.49 E-01	2.92 E-05

Table 3-7 S7- Positive and negative ions detected by ToF-SIMS analysis of WW effluent before nAg was spiked.

#	Center Mass (u)	Assignment	Intensity		
			Raw	Normalized by Ag+/ Ag-	Normalized by total ion intensity
Positive Ions					
1	23.98	Mg^+	2.47E+05	4.54E+01	1.39E-02
2	38.96	K^+	2.94E+06	5.39E+02	1.65E-01
3	36.96	Ca^+	1.61E+05	2.95E+01	9.03E-03
4	63.93	Zn^+	1.14E+02	2.09E-02	6.41E-06
5	77.95	Na_2S^+	1315	3.06E+00	9.38E-04
Negative Ions					
6	16.02	NH_2^-	1.12E+03	5.76E-01	8.46E-05
7	30.97	P^-	2.35E+02	1.21E-01	1.78E-05
8	31.97	S^-	3.19E+04	1.65E+01	2.42E-03
9	34.97	Cl^-	7.59E+05	3.92E+02	5.75E-02
10	39.99	C_2O^-	2.47E+04	1.27E+01	1.87E-03
11	40.02	$C_2H_2N^-$	1.06E+04	5.50E+00	8.07E-04
12	42.04	$C_2H_4N^-$	1.04E+04	5.35E+00	7.85E-04
13	44.02	CH_2NO^-	1.56E+03	8.06E-01	1.18E-04
14	44.99	CHO_2^-	3.77E+04	1.95E+01	2.86E-03
15	65.99	C_3NO^-	2.50E+04	1.29E+01	1.89E-03
16	72.00	$C_2H_2NO_2^-$	2.22E+03	1.15E+00	1.68E-04
17	95.95	SO_4^-	2.50E+04	1.29E+01	1.89E-03
18	118.94	$NaSO_4^-$	1.47E+04	7.57E+00	1.11E-03
19	135.92	$CaSO_4^-$	1.71E+04	8.83E00	1.30E-03

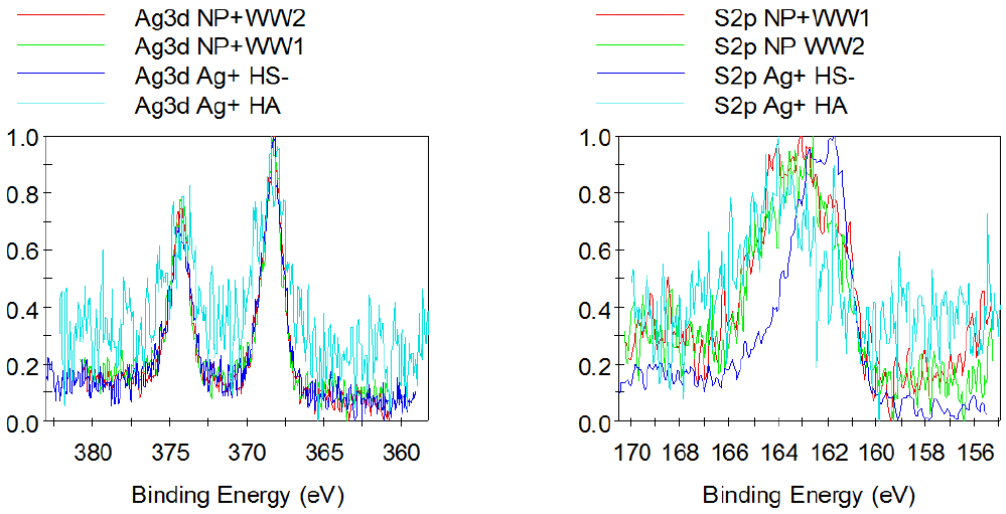

Figure 3-19 S15- XPS analysis of nAg suspended in the WW effluent (two samples WW1 and WW2 from the same treatment plant), and controls comprising free Ag^{+} suspended in Na_2S and HA solutions.

3.6.5. Dissolution of nAg (Citrate and PVP coatings) with time dispersed in DOC solutions

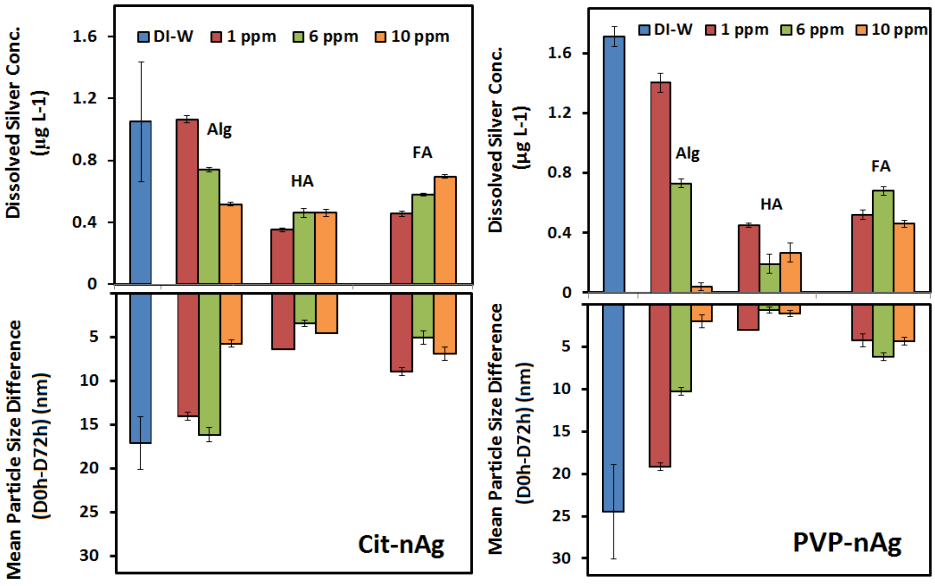

Figure 3-20 S16- Dissolved Ag concentrations and changes in mean particle diameter of 80 nm citrate-nAg and PVP-nAg at 72 h in DI water and alginate, FA, and HA solutions (1 to 10 ppm). The mean particle difference between time point 0 and 72 h are shown against each bar. The bottom panel of the figure shows the difference between the initial nAg diameter and the diameter measured at 72 h.

3.6.6. Mass balances

Two different approaches were taken to evaluate the total mass balance (Table 3-8 S8):

(i) The mean particle size at a certain time point was converted to the mass of silver, then it was subtracted from the initial mass of particles (t=0 h), given the particle density and particle number concentration. This mass change represented the total calculated dissolved silver based on nanoparticle mean size change. The recovery percentage was computed by comparing the dissolved silver values obtained from the software for each sample with the calculated dissolved silver concentrations in a certain volume of test solution (Table 3-8 S8).

(ii) The sum of total measured NPs mass concentration and the dissolved silver mass concentration should yield the total silver mass concentration which must be equal to the total silver mass concentration initially in the test sample (i.e. t=0 h) attained after acid digestion of samples analyzed with standard mode ICP-MS.

The total mass balance consists of the sum of NPs number concentration and the dissolved silver compared with the total silver initially in the test tubes after acid digestion was more than 90% in most of the samples at 72 h. At 168 h the total NPs number concentration dropped to about 50% of the initial NP number concentration which could be due to particle loss by adsorption to the walls of the tube and thus the mass balance decreased accordingly. The overall mass balance for the first several hours is in good agreement with the total silver concentration in each sample which proves the viability of spICP-MS in quantifying the NPs and dissolved metal concentrations with very good precision. Moreover, the silver mass derived by converting the size change of nAg over a time period using the particle density was in very good agreement (>85%) with the dissolved silver concentrations directly attained from spICP-MS by measuring the background dissolved metal.

Mass balance at 168 h- The mass of secondary nAg_xS_y was quantified by calculating the surface area from the particle size distribution of secondary particles. The frequency at each particle mean size was converted to the number of particles by accounting for the sample time, flow rate and transport efficiency for the analysis. The diameter was converted to the mass of silver by calculating the volume and accounting for the nAg density. The total mass of silver representing the secondary particles were then calculated by multiplying the mass of silver for each particle diameter multiplied by the number of particles at that diameter and summing for all the detected particle diameters. The total Ag mass of the secondary nAg_xS_y at 168h was 35.6±3.2 and 37.4±1.7 ppb in effluent and mixed liquor WW samples respectively by taking into account that only 1% of total particles were detected at the mean size of about 20 nm. This percentage was attained by analyzing a standard nAg with mean size of 20 nm and the total number of particles detected was compared with the particle number concentration reported by the manufacturer. The decrease in dissolved Ag between 120 and 168h was 39.85 and 30.41 ppb in WW effluent and mixed liquor. Thus, we maintain that the formation of the secondary particles (~20 nm) was attributable to the decrease in the dissolved Ag concentrations after 120 h because the mass of Ag associated with nAg_xS_y was found to be very close to the decrease in dissolved Ag after 120 h.

Table 3-8 S8 – Total silver mass balance and total dissolved silver mass balance among 3 sample replicates at 72

Water Chemistry	Coating	Dissolved silver mass balance (@t= 72 h)	STD DEV	Total silver mass balance; acid digested (@t= 72 h)	STD DEV
10 ppb Ag NPs					
DI water	Citrate	85%	11%	82%	15%
DI water	PVP	94%	2%	95%	3%
Eff WW	Citrate	89%	14%	90%	5%
Eff WW	PVP	87%	11%	94%	4%
ML WW	Citrate	88.20%	9%	89%	10%
ML WW	PVP	88%	10%	95.5%	4%
1000 ppb Ag NPs					
DI water	Citrate	99.2%	2%	98%	1%
DI water	PVP	94.3%	5%	92%	5%
Eff WW	Citrate	97.0%	3%	88.5%	3%
Eff WW	PVP	95.6%	1%	96%	1%
ML WW	Citrate	89.7%	4%	99%	1%
ML WW	PVP	94.1%	2%	99.1%	1%
Alginate					
0.5 ppm Alg	Citrate	91%	12%	100%	1%
1 ppm Alg	Citrate	85%	5%	99%	2%
5 ppm Alg	Citrate	84%	10%	99.20%	2%
10 ppm Alg	Citrate	88%	9%	99.50%	3%
0.5 ppm Alg	PVP	90.1%	7%	99%	1%
1 ppm Alg	PVP	89%	11%	100%	4%
5 ppm Alg	PVP	88%	13%	100%	5%
10 ppm Alg	PVP	89%	8%	99.80%	1%
Humic Acid (HA)					
0.5 ppm HA	Citrate	95%	11%	87%	11%
1 ppm HA	Citrate	86%	10%	84.80%	7%
5 ppm HA	Citrate	89%	9%	96%	8%
10 ppm HA	Citrate	90%	13%	98.60%	10%
0.5 ppm HA	PVP	94.3%	5%	95%	4%
1 ppm HA	PVP	88.5%	12%	94.80%	8%
5 ppm HA	PVP	89%	13%	99%	3%
10 ppm HA	PVP	89.3%	10%	88.50%	11%
Fulvic Acid (FA)					
0.5 ppm FA	Citrate	96%	3%	99%	2%
1 ppm FA	Citrate	95%	5%	100%	2%
5 ppm FA	Citrate	95.5%	5%	100%	3%
10 ppm FA	Citrate	93%	8%	99.20%	5%
0.5 ppm FA	PVP	88.8%	11%	99.00%	3%
1 ppm FA	PVP	89.7%	10%	98%	1%
5 ppm FA	PVP	89.6%	13%	100%	2%
10 ppm FA	PVP	90.5%	1%	100%	1%
Sulfides (Sulfide:Ag)					
S:Ag:1- DI W	PVP	88.5%	4%	87%	13%
S:Ag:10- DI W	PVP	88.4%	13%	89%	16%
S:Ag:100- DI W	PVP	81%	15%	87.5%	15%
S:Ag:1- Eff W	PVP	85%	9%	87%	11%
S:Ag:10- Eff W	PVP	96%	3%	95%	7%
S:Ag:100- Eff W	PVP	81.7%	9%	86.30%	14%
S:Ag:1- Alg	PVP	89%	5%	88%	11%
S:Ag:10- Alg	PVP	88.7%	12%	87.60%	9%
S:Ag:1- FA	PVP	89.1%	8%	89.20%	11%
S:Ag:10- FA	PVP	90%	6%	85.50%	12%

3.7. References

4. Rai, M., Yadav, A. and Gade, A. (2009) Silver nanoparticles as a new generation of antimicrobials. Biotechnology Advances 27(1), 76-83.
5. Kim, J.S., Kuk, E., Yu, K.N., Kim, J.-H., Park, S.J., Lee, H.J., Kim, S.H., Park, Y.K., Park, Y.H. and Hwang, C.-Y. (2007) Antimicrobial effects of silver nanoparticles. Nanomedicine: Nanotechnology, Biology and Medicine 3(1), 95-101.
6. Misra, S.K., Dybowska, A., Berhanu, D., Luoma, S.N. and Valsami-Jones, E. (2012) The complexity of nanoparticle dissolution and its importance in nanotoxicological studies. Science of the Total Environment 438, 225-232.
7. Morones, J.R., Elechiguerra, J.L., Camacho, A., Holt, K., Kouri, J.B., Ramírez, J.T. and Yacaman, M.J. (2005) The bactericidal effect of silver nanoparticles. Nanotechnology 16(10), 2346.
8. Navarro, E., Piccapietra, F., Wagner, B., Marconi, F., Kaegi, R., Odzak, N., Sigg, L. and Behra, R. (2008) Toxicity of silver nanoparticles to Chlamydomonas reinhardtii. Environmental Science & Technology 42(23), 8959-8964.
9. Jones, A.M., Garg, S., He, D., Pham, A.N. and Waite, T.D. (2011) Superoxide-mediated formation and charging of silver nanoparticles. Environmental Science & Technology 45(4), 1428-1434.
10. Keller, A.A., McFerran, S., Lazareva, A. and Suh, S. (2013) Global life cycle releases of engineered nanomaterials. Journal of Nanoparticle Research 15(6), 1-17.
11. Gottschalk, F., Sonderer, T., Scholz, R.W. and Nowack, B. (2009) Modeled environmental concentrations of engineered nanomaterials (TiO2, ZnO, Ag, CNT, fullerenes) for different regions. Environmental Science & Technology 43(24), 9216-9222.
12. Park, M.V., Neigh, A.M., Vermeulen, J.P., de la Fonteyne, L.J., Verharen, H.W., Briedé, J.J., van Loveren, H. and de Jong, W.H. (2011) The effect of particle size on the cytotoxicity, inflammation, developmental toxicity and genotoxicity of silver nanoparticles. Biomaterials 32(36), 9810-9817.
13. Carlson, C., Hussain, S.M., Schrand, A.M., K. Braydich-Stolle, L., Hess, K.L., Jones, R.L. and Schlager, J.J. (2008) Unique cellular interaction of silver nanoparticles: size-dependent generation of reactive oxygen species. The journal of physical chemistry B 112(43), 13608-13619.
14. Choi, O. and Hu, Z. (2008) Size dependent and reactive oxygen species related nanosilver toxicity to nitrifying bacteria. Environmental Science & Technology 42(12), 4583-4588.
15. Kittler, S., Greulich, C., Diendorf, J., Koller, M. and Epple, M. (2010) Toxicity of silver nanoparticles increases during storage because of slow dissolution under release of silver ions. Chemistry of Materials 22(16), 4548-4554.
16. Zhang, W., Yao, Y., Sullivan, N. and Chen, Y. (2011) Modeling the primary size effects of citrate-coated silver nanoparticles on their ion release kinetics. Environmental Science & Technology 45(10), 4422-4428.
17. Ma, R., Levard, C.m., Marinakos, S.M., Cheng, Y., Liu, J., Michel, F.M., Brown Jr, G.E. and Lowry, G.V. (2011) Size-controlled dissolution of organic-coated silver nanoparticles. Environmental Science & Technology 46(2), 752-759.
18. Liu, J. and Hurt, R.H. (2010) Ion release kinetics and particle persistence in aqueous nano-silver colloids. Environmental Science & Technology 44(6), 2169-2175.
19. Dobias, J. and Bernier-Latmani, R. (2013) Silver release from silver nanoparticles in natural waters. Environmental Science & Technology 47(9), 4140-4146.
20. Li, X., Lenhart, J.J. and Walker, H.W. (2011) Aggregation kinetics and dissolution of coated silver nanoparticles. Langmuir 28(2), 1095-1104.
21. Huynh, K.A. and Chen, K.L. (2011) Aggregation kinetics of citrate and polyvinylpyrrolidone coated silver nanoparticles in monovalent and divalent electrolyte solutions. Environmental Science & Technology 45(13), 5564-5571.

22. Chappell, M.A., Miller, L.F., George, A.J., Pettway, B.A., Price, C.L., Porter, B.E., Bednar, A.J., Seiter, J.M., Kennedy, A.J. and Steevens, J.A. (2011) Simultaneous dispersion–dissolution behavior of concentrated silver nanoparticle suspensions in the presence of model organic solutes. Chemosphere 84(8), 1108-1116.
23. Ostermeyer, A.-K., Kostigen Mumuper, C., Semprini, L. and Radniecki, T. (2013) Influence of Bovine Serum Albumin and Alginate on Silver Nanoparticle Dissolution and Toxicity to Nitrosomonas europaea. Environmental Science & Technology 47(24), 14403-14410.
24. Levard, C., Reinsch, B.C., Michel, F.M., Oumahi, C., Lowry, G.V. and Brown Jr, G.E. (2011) Sulfidation processes of PVP-coated silver nanoparticles in aqueous solution: impact on dissolution rate. Environmental Science & Technology 45(12), 5260-5266.
25. Liu, J., Pennell, K.G. and Hurt, R.H. (2011) Kinetics and mechanisms of nanosilver oxysulfidation. Environmental Science & Technology 45(17), 7345-7353.
26. Levard, C., Mitra, S., Yang, T., Jew, A.D., Badireddy, A.R., Lowry, G.V. and Brown Jr, G.E. (2013) Effect of chloride on the dissolution rate of silver nanoparticles and toxicity to E. coli. Environmental Science & Technology 47(11), 5738-5745.
27. Fujiwara, K., Sotiriou, G.A. and Pratsinis, S.E. (2015) Enhanced Ag+ Ion Release from Aqueous Nanosilver Suspensions by Absorption of Ambient CO2. Langmuir 31(19), 5284-5290.
28. Ma, H., Allen, H.E. and Yin, Y. (2001) Characterization of isolated fractions of dissolved organic matter from natural waters and a wastewater effluent. Water Research 35(4), 985-996.
29. Imai, A., Fukushima, T., Matsushige, K., Kim, Y.-H. and Choi, K. (2002) Characterization of dissolved organic matter in effluents from wastewater treatment plants. Water Research 36(4), 859-870.
30. Drewes, J. and Croue, J. (2002) New approaches for structural characterization of organic matter in drinking water and wastewater effluents. WATER SCIENCE AND TECHNOLOGY-WATER SUPPLY- 2(2), 1-10.
31. Du, W. and Parker, W. (2013) Characterization of Sulfur in Raw and Anaerobically Digested Municipal Wastewater Treatment Sludges. Water Environment Research 85(2), 124-132.
32. Kaegi, R., Voegelin, A., Ort, C., Sinnet, B., Thalmann, B., Krismer, J., Hagendorfer, H., Elumelu, M. and Mueller, E. (2013) Fate and transformation of silver nanoparticles in urban wastewater systems. Water Research.
33. Ma, R., Levard, C., Judy, J.D., Unrine, J.M., Durenkamp, M., Martin, B., Jefferson, B. and Lowry, G.V. (2013) Fate of zinc oxide and silver nanoparticles in a pilot wastewater treatment plant and in processed biosolids. Environmental Science & Technology 48(1), 104-112.
34. Kent, R.D. and Vikesland, P.J. (2012) Controlled evaluation of silver nanoparticle dissolution using atomic force microscopy. Environmental Science & Technology 46(13), 6977-6984.
35. Baalousha, M., Arkill, K., Romer, I., Palmer, R. and Lead, J. (2015) Transformations of citrate and Tween coated silver nanoparticles reacted with Na 2 S. Science of the Total Environment 502, 344-353.
36. Gondikas, A.P., Morris, A., Reinsch, B.C., Marinakos, S.M., Lowry, G.V. and Hsu-Kim, H. (2012) Cysteine-induced modifications of zero-valent silver nanomaterials: implications for particle surface chemistry, aggregation, dissolution, and silver speciation. Environmental Science & Technology 46(13), 7037-7045.
37. Miller, R.J., Lenihan, H.S., Muller, E.B., Tseng, N., Hanna, S.K. and Keller, A.A. (2010) Impacts of metal oxide nanoparticles on marine phytoplankton. Environmental Science & Technology 44(19), 7329-7334.
38. Mitrano, D., Ranville, J., Bednar, A., Kazor, K., Hering, A. and Higgins, C. (2014) Tracking dissolution of silver nanoparticles at environmentally relevant concentrations in laboratory, natural, and processed waters using single particle ICP-MS (spICP-MS). Environmental Science: Nano 1(3), 248-259.

39. Mitrano, D.M., Barber, A., Bednar, A., Westerhoff, P., Higgins, C.P. and Ranville, J.F. (2012a) Silver nanoparticle characterization using single particle ICP-MS (SP-ICP-MS) and asymmetrical flow field flow fractionation ICP-MS (AF4-ICP-MS). Journal of Analytical Atomic Spectrometry 27(7), 1131-1142.
40. Mitrano, D.M., Lesher, E.K., Bednar, A., Monserud, J., Higgins, C.P. and Ranville, J.F. (2012b) Detecting nanoparticulate silver using single-particle inductively coupled plasma–mass spectrometry. Environmental Toxicology and Chemistry 31(1), 115-121.
41. Degueldre, C. and Favarger, P.-Y. (2003) Colloid analysis by single particle inductively coupled plasma-mass spectroscopy: a feasibility study. Colloids and Surfaces A: Physicochemical and Engineering Aspects 217(1), 137-142.
42. Laborda, F., Jiménez-Lamana, J., Bolea, E. and Castillo, J.R. (2011) Selective identification, characterization and determination of dissolved silver (I) and silver nanoparticles based on single particle detection by inductively coupled plasma mass spectrometry. Journal of Analytical Atomic Spectrometry 26(7), 1362-1371.
43. Hadioui, M., Leclerc, S. and Wilkinson, K. (2012) Multimethod quantification of Ag< sup>+</sup> release from nanosilver. Talanta.
44. Yang, Y., Long, C.-L., Li, H.-P., Wang, Q. and Yang, Z.-G. (2016) Analysis of silver and gold nanoparticles in environmental water using single particle-inductively coupled plasma-mass spectrometry. Science of the total environment.
45. Hadioui, M., Merdzan, V. and Wilkinson, K.J. (2015) Detection and characterization of ZnO nanoparticles in surface and waste waters using single particle ICPMS. Environmental Science & Technology 49(10), 6141-6148.
46. Peters, R., Herrera-Rivera, Z., Undas, A., van der Lee, M., Marvin, H., Bouwmeester, H. and Weigel, S. (2015) Single particle ICP-MS combined with a data evaluation tool as a routine technique for the analysis of nanoparticles in complex matrices. Journal of Analytical Atomic Spectrometry 30(6), 1274-1285.
47. Donovan, A.R., Adams, C.D., Ma, Y., Stephan, C., Eichholz, T. and Shi, H. (2016) Single particle ICP-MS characterization of titanium dioxide, silver, and gold nanoparticles during drinking water treatment. Chemosphere 144, 148-153.
48. Metcalf, E. (2003) Wastewater Engineering: Treatment, Disposal, Reuse, Metcalf & Eddy. Inc., McGraw-Hill, New York.
49. Courrol, L.C., de Oliveira Silva, F.R. and Gomes, L. (2007) A simple method to synthesize silver nanoparticles by photo-reduction. Colloids and Surfaces A: Physicochemical and Engineering Aspects 305(1), 54-57.
50. Akamatsu, K., Takei, S., Mizuhata, M., Kajinami, A., Deki, S., Takeoka, S., Fujii, M., Hayashi, S. and Yamamoto, K. (2000) Preparation and characterization of polymer thin films containing silver and silver sulfide nanoparticles. Thin Solid Films 359(1), 55-60.
51. León-Velázquez, M.S., Irizarry, R. and Castro-Rosario, M.E. (2010) Nucleation and growth of silver sulfide nanoparticles. The Journal of Physical Chemistry C 114(13), 5839-5849.
52. Litvin, V.A., Galagan, R.L. and Minaev, B.F. (2012) Kinetic and mechanism formation of silver nanoparticles coated by synthetic humic substances. Colloids and Surfaces A: Physicochemical and Engineering Aspects 414, 234-243.
53. Thalmann, B., Voegelin, A., Sinnet, B., Morgenroth, E. and Kaegi, R. (2014) Sulfidation kinetics of silver nanoparticles reacted with metal sulfides. Environmental Science & Technology 48(9), 4885-4892.
54. Akaighe, N., MacCuspie, R.I., Navarro, D.A., Aga, D.S., Banerjee, S., Sohn, M. and Sharma, V.K. (2011) Humic acid-induced silver nanoparticle formation under environmentally relevant conditions. Environmental Science & Technology 45(9), 3895-3901.

55. Adegboyega, N.F., Sharma, V.K., Siskova, K., Zbořil, R., Sohn, M., Schultz, B.J. and Banerjee, S. (2012) Interactions of aqueous Ag+ with fulvic acids: Mechanisms of silver nanoparticle formation and investigation of stability. Environmental Science & Technology 47(2), 757-764.
56. Siriwardana, K., Suwandaratne, N., Perera, G.S., Collier, W.E., Perez, F. and Zhang, D. (2015) Contradictory Dual Effects: Organothiols Can Induce Both Silver Nanoparticle Disintegration and Formation under Ambient Conditions. The Journal of Physical Chemistry C 119(36), 20975-20984.
57. Khan, Z. and Talib, A. (2010) Growth of different morphologies (quantum dots to nanorod) of Ag-nanoparticles: role of cysteine concentrations. Colloids and Surfaces B: Biointerfaces 76(1), 164-169.
58. Goh, S.W., Buckley, A.N., Lamb, R.N. and Woods, R. (2006) The ability of static secondary ion mass spectrometry to discriminate submonolayer from multilayer adsorption of thiol collectors. Minerals Engineering 19(6), 571-581.
59. Advanced Powder TechnologyGoh, S.W., Buckley, A.N., Gong, B., Woods, R., Lamb, R.N., Fan, L.-J. and Yang, Y.-w. (2008) Thiolate layers on metal sulfides characterised by XPS, ToF-SIMS and NEXAFS spectroscopy. Minerals Engineering 21(12), 1026-1037.
60. Gades, H. and Urbassek, H.M. (1995) Dimer emission in alloy sputtering and the concept of the “clustering probability”. Nuclear Instruments and Methods in Physics Research Section B: Beam Interactions with Materials and Atoms 103(2), 131-138.
61. Adams, N.W. and Kramer, J.R. (1999) Silver speciation in wastewater effluent, surface waters, and pore waters. Environmental Toxicology and Chemistry 18(12), 2667-2673.
62. Stumm, W. and Morgan, J.J. (1981) Aquatic chemistry: an introduction emphasizing chemical equilibria in natural waters, John Wiley.
63. Cotton, F.A., Wilkinson, G., Murillo, C.A., Bochmann, M. and Grimes, R. (1999) Advanced inorganic chemistry, Wiley New York.
64. Morf, W.E., Kahr, G. and Simon, W. (1974) Theoretical treatment of the selectivity and detection limit of silver compound membrane electrodes. Analytical Chemistry 46(11), 1538-1543.
65. Furman, O., Usenko, S. and Lau, B.L. (2013) Relative importance of the humic and fulvic fractions of natural organic matter in the aggregation and deposition of silver nanoparticles. Environmental Science & Technology 47(3), 1349-1356.
66. Delay, M., Dolt, T., Woellhaf, A., Sembritzki, R. and Frimmel, F.H. (2011) Interactions and stability of silver nanoparticles in the aqueous phase: Influence of natural organic matter (NOM) and ionic strength. Journal of Chromatography A 1218(27), 4206-4212.
67. Aiken, G.R., Hsu-Kim, H. and Ryan, J.N. (2011) Influence of dissolved organic matter on the environmental fate of metals, nanoparticles, and colloids. Environmental Science & Technology 45(8), 3196-3201.
68. Gunsolus, I.L., Mousavi, M.P., Hussein, K., Buhlmann, P. and Haynes, C.L. (2015) Effects of Humic and Fulvic Acids on Silver Nanoparticle Stability, Dissolution, and Toxicity. Environmental Science & Technology.
69. Sal’nikov, D., Pogorelova, A., Makarov, S. and Vashurina, I.Y. (2009) Silver ion reduction with peat fulvic acids. Russian Journal of Applied Chemistry 82(4), 545-548.

Chapter 4 DISSOLUTION BEHAVIOR OF SILVER NANOPARTICLES IN THE PRESENCE OF INORGANIC SULFIDES AND DISSOLVED ORGANICS CARBON

Connecting text: In Chapter 3, the presence of inorganic sulfides and dissolved organic carbon (DOC) compounds in municipal WW specimen resulted in lower dissolution rates and extents over 72 h. DOC compounds containing thiol and amine functional groups were abundantly bound or otherwise associated with the surface of nAg as confirmed by XPS and ToF-SIMs analysis. Inorganic sulfides were stable in the aerobic WW, likely in the form of metal sulfides, and reacted with nAg resulted in the formation of Ag_2S with little solubility. Experiments suggested that dissolution inhibition extent by inorganic sulfides strongly depends on the S:Ag mole ratio. In this chapter, dissolution of nAg coated with PVP in the presence of inorganic sulfides (at two S:Ag ratio) and various DOC compounds in long-term (27 d) is studied. The effect of the presence of DOC compounds on the sulfidation reaction of PVP coated nAg in three different exposure scenarios is investigated; simultaneous exposure to sulfides and DOC, post- and pre-sulfidation of nAg.

The Chapter will be submitted to the journal Environmental Science and Technology as:

Azodi, M. and Ghoshal, S. (2017) "Dissolved Organic Carbon Enhances Dissolution of Sulfidated Silver Nanoparticles." **Environmental Science and Technology**.

4.1. Introduction

Silver nanoparticles (nAg) are amongst the most commonly used engineered nanomaterials in commercial products (Benn et al. 2010). The environmental fate of nAg after release is of great importance for assessment of its risk to environment and human health (Gottschalk and Nowack 2011, Keller et al. 2013). The solubility, size and surface chemistry of nAg in aquatic and terrestrial environments are closely associated with their toxicity (Navarro et al. 2008, Kittler et al. 2010, Greulich et al. 2012). Dissolution (ion release) is an important transformation process for nAg as it not only influences the Ag speciation in environmental systems, but also the size and composition of any residual nAg (Liu et al. 2012, Azodi et al. 2016). The rates and extents of dissolution are influenced by the composition of the aqueous media (pH, concentrations of dissolved O_2, Cl^-, HS^-, and organic matter) as well as the size, structural characteristics and concentrations of nAg (Ma et al. 2011, Misra et al. 2012, Zhang et al. 2011).

Sulfidation has been suggested to detoxify nAg by limiting its dissolution (Levard et al. 2013). However, recent studies have demonstrated that in case of incomplete sulfidation, nAg is prone to oxidation of unexposed surface and ion release to various extents (Kent and Vikesland 2012, Baalousha et al. 2015). Ag^+ reacts rapidly with sulfide ions (HS^-, S^{2-}) (Levard et al. 2011, Liu et al. 2011) and metal sulfides (e.g., ZnS, CuS) (Thalmann et al. 2014, Adams and Kramer 1998) to form insoluble Ag_2S. Sulfidation of nAg results in formation of Ag_2S NPs or core-shell Ag-Ag_2S NPs through oxysulfidation reactions or by precipitation of dissolved Ag, depending on the relative abundance of sulfides (Levard et al. 2011, Liu et al. 2011). Thiols (-SH) containing organic compounds can also bind to nAg surfaces, limiting its dissolution (Liu et al. 2010). nAg has been shown to generate smaller, daughter NPs as a result of dissolution-reprecipitation

reactions in municipal wastewater (WW) (Azodi et al. 2016) due to reactions with inorganic sulfides and organosulfur compounds, as well as in the presence of thiols (Liu et al. 2012).

In natural waters, sulfidation of nAg is likely to occur in the presence of DOC (dissolved organic carbon). DOC is abundant in aquatic environment; such as WW (Imai et al. 2002), natural waters (Ma et al. 2001), sediments and groundwater (McArthur et al. 2004, Accardi-Dey and Gschwend 2002), and sea water (Kepkay 1994) and includes primarily humic substances, carboxylic acids, polysaccharides, and amino acids. DOC molecules contain metal-binding functional groups (i.e. carboxylates, phenols, amines, thiols) are shown to interact strongly with nAg and Ag^{+} , and impact their speciation, solubility (Kramer et al. 2007, Delay et al. 2011, Furman et al. 2013, Pokhrel et al. 2014, Wirth et al. 2012, Shafer et al. 1998) and sulfidation (Zhu et al. 2016, Zhang et al. 2016).

Only a few recent studies have investigated the effect of presence of DOC and sulfides together on nAg transformation. Zhang *et al.* showed that the presence of humic acids (HA) decreased the sulfidation rate of Ag nanowires up to 36% (Zhang et al. 2016) and Collin *et al.* observed 5 times higher dissolution for sulfidated nAg in Pony Lake Fulvic Acid (FA) solution as compared to FA-free systems (Collin et al. 2016). Thalmann *et al.* (Thalmann et al. 2016) reported faster sulfidation rates of nAg in the presence of HA as compared to nAg in systems containing solely the bisulfides (HS^{-}), however, those experiments were conducted at significantly higher HA and sulfide concentrations. Liu *et al.*, also observed slightly faster sulfidation rates of nAg in the presence of SFRA (Liu et al. 2011). Both these studies attributed the faster sulfidation to binding of HS^{-} to DOC, but the impact of the higher sulfidation rate on dissolution of nAg was not assessed. Zhu *et al.* (Zhu et al. 2016) and Baalousha *et al.* (Baalousha et al. 2015) found that nAg sulfidated in the presence of HA had higher colloidal stability

compared to HA-free systems. The impact of other types of DOC compounds rather than HA and FA, such as amino acids, and polysaccharides on the sulfidation of nAg are unknown. In addition, these studies only considered simultaneous exposure to humic substances and sulfides and other sequence of exposure and other DOC compounds are not explored.

The aim of this study was to investigate how DOC compounds can affect the sulfidation of nAg and dissolution behavior and extent of sulfidated and pristine nAg. In this paper, monodisperse nAg of three different sizes (30, 50, and 100 nm) coated with PVP were exposed to sulfides and DOC solutions in three exposure systems. In first system, nAg was dispersed in solutions already containing the sulfides and DOC. In second system, nAg was first contacted with DOC solutions for 24 h and then were reacted with sulfides. In the third system, nAg was first sulfidated for 24 h then suspended in DOC solutions. The DOC solutions used were a mixture of (i) HA and FA; (ii) cysteine and methionine, and alginate alone.

Experiments were conducted with 1 ppb nAg and 1ppm DOC as these concentrations are environmentally relevant. In addition, CuS and ZnS were chosen as the source of sulfides instead of sodium sulfides. Metal sulfides are observed to be more stable in aerobic condition as was shown in our previous study (Azodi et al. 2016) and have half-life times longer than 35 days in oxygenated waters in contrast to unstable HS^- in aerobic conditions (Thalmann et al. 2014). Furthermore, metal sulfides are a more realistic source of sulfides and better capture the complexity of natural waters (Kramer et al. 2007). Recently few studies have used metal sulfides such as CuS and ZnS to study sulfidation of nAg. Ag_2S ($2Ag^+ + S^{2-} = Ag_2S, logK = 50.1$) has a higher stability constant than CuS ($2Cu^{2+} + S^{2-} = CuS, logK = 22.3$) and ZnS ($2Zn^{2+} + S^{2-} = ZnS, logK = 25.1$), therefore sulfides migrate to nAg with an accompanying release of Cu and Zn ions (Thalmann et al. 2014, Ma et al. 2014).

nAg of three various sizes were chosen for this study because nAg dissolution rates and extents and the surface areas available for reactions and binding of molecules changes with the surface area. Furthermore, nAg in natural waters are likely to be polydisperse.

spICP-MS, which can simultaneously analyse NP mean size, particle and dissolved Ag concentration with excellent precision was used to study the dissolution of nAg, was used. The extent of sulfides associated with nAg and the amount of DOC sorbed onto the nAg was evaluated in the different systems examined. The sulfide to silver ratio of 0.4 was chosen to be in the range of the metal sulfide concentration in the oxic waters and WWTPs where the concentration of ZnS can be as low as 1.5 nM (0.14 ppb) (Priadi et al. 2012). In addition, a significantly higher sulfide to silver ratio of 10 was chosen to study the waters with sulfide in excess of nAg (i.e. sewage sludge) (Stover et al. 1976).

4.2. Material and Method

4.2.1. Chemicals

Nanoparticles- PVP-coated NanoXact nAg (NanoComposix) of three nominal sizes of 30, 50 and 100 nm, at a nominal stock concentration of 20 ppm was chosen were diluted as appropriate in various experiments. The nAg was close to spherical and the mean diameter was estimated by sizing more than 100 individual particles with TEM which were 26.9±4.2 (n=125), 49.5±4.6 (n=120), 100.5±11.5 nm (n=100). These values were consistent with the manufacturer-reported values (Figure 4-7 S 1A, C, E). spICP-MS analysis of the nAg dispersed in DI water provided consistent mean diameter with TEM images. The mean size obtained with spICP-MS was 28.6±1.8, 50.1±5.9, 102±2.8 nm (Figure 4-7 S 1B, D, F). The nAg of three mean sizes was well dispersed in the suspension without aggregation. The dissolution kinetics of nAg in DI

water is studied (Figure 4-8 S2, 4-9 S3). Dissolution kinetic parameter (k, h^{-1}) for nAg with nominal mean sizes of 30, 50, and 100 nm suspended at 1 ppb in DI water was determined (Table 4-1 S1) and a comparison with previous literature is provided (Table 4-2 S2).

Dissolved Organic Carbon- Cysteine ($C_3H_7NO_2S$, Sigma-Aldrich) is a low molecular weight hydrophilic amino acid (M.W. 121 g mol^{-1}). Methionine ($C_5H_{11}NO_2S$, Sigma-Aldrich) is also an amino acid (M.W. 149.21 g mol^{-1}). Alginate (Sigma, sodium salt of alginic acid from brown algae), FAs (Suwannee River Fulvic Acids standard II, International Humic Substances Society) and HAs (Suwannee River Humic Acids standard II) were purchased. Suwannee river HA used in this research was reported to contain 1.19 and 0.58 %(w/w) (of a dry, ash free sample) of N and S and Suwannee river FA contains 0.72 and 0.44 %(w/w) N and S respectively according to the manufacturer, International Humic Substances Society (IHSS). The DOC solutions prepared for this study were a mix of HA and FA, a mix of cysteine and methionine at equal concentrations of 1 ppm each and alginate solution prepared at 1 ppm in DI water.

Metal Sulfides- A sulfide solution of 1 mM Na_2S (Sigma Aldrich) solution in 0.5 mM $NaNO_3$ was prepared in an anaerobic chamber according to methods reported elsewhere (Levard et al. 2011). The DI water used for sample preparation was purged with N_2 gas to ensure anaerobic conditions. Standard metal solutions of Cu^{2+} and Zn^{2+} (PlasmaCAL standard solution of 1000 ppm copper or zinc in HNO3, SCP Science) were contacted with the sulfide solution in an anaerobic chamber and left on an end-over-end shaker for 24 h. Metal sulfides were separated from any unreacted sulfide by centrifugal ultrafiltration at 4600g for 40 min. The nAg was then suspended in the metal sulfides solution to attain S:Ag=0.4 and 10 mole ratio so as to have two very different sulfide to silver mole ratio. In one system the sulfide is less than required for

complete sulfidation of nAg (S:Ag=0.4) and in the other system the sulfides is highly in excess of nAg (S:Ag=10).

Dissolution Experiments- PVP-nAg were exposed to metal sulfides and DOC in three different exposure scenarios. In one set of experiments (System C/S), nAg was introduced into the systems simultaneously with the CuS and ZnS mixture and the DOC solution. In a parallel system (System C-S) nAg was first contacted with DOC solutions and then reacted with the sulfides. In the third set (System S-C), the nAg was first contacted with the sulfides for 24 h and then DOC was added. DOC-free control systems were maintained, one in which only nAg was contacted with DI water (System DI), and the other contained nAg and the sulfides in DI water (System S). Another control only contained nAg in all the three DOC solutions (System C) of humic substances, alginate and the mixture of cysteine and methionine. Each system was set up in triplicate and analyzed frequently for dissolved silver concentrations, and at selected time points for sulfides and total organic carbon associated with nAg. The error bars on all graphs represents the standard deviation of three replicate samples analyzed.

4.2.2. Instrumentation

spICP-MS- A Perkin Elmer NexION 300X ICP-MS supported by Syngistix software (ver1.1.) was used in single particle mode for nAg characterization. The operating principles of spICP MS have been reported previously (Degueldre and Favarger 2003). The integration dwell time of 100 µs was generally used. The daily optimization included optimizing the torch alignment and nebulizer gas flow of spICP-MS for the highest sensitivity to Ag. A total data collection time of 100 s was set for all other samples. The data collection time was increased to

150-200 s for sample analysis after time point 168 h to 648 h. Other instrumental parameters are presented in Table 4-3 S3.

Two calibrations were performed before the analysis. First, the transport efficiency of the system in order to determine the percentage of particles reached the plasma, and second, the dissolved Ag calibration to compute the silver concentration in the samples. The standard reference gold nanoparticles (nAu) was purchased from National Institute of Standards and Technology (NIST), with a nominal 60 nm diameter and a stock particle concentration of 2.38×10^{10} particles/mL. nAu was sonicated for 3 minutes, then suspended in DI water at a concentration of 207 ppt (9.5×10^{4} particles/mL) to determine the transport efficiency of the spICP-MS. The transport efficiency of spICP-MS was evaluated on a day-to-day basis with freshly prepared nAu suspension and attained values between 7-9% at dwell time of 100 µs.

A dissolved Ag standard solution of 1001±4 ppm in 4% HNO_3 (PlasmaCAL) was used for preparing the ICP-MS dissolved calibration curve including one blank and 6 dissolved Ag solutions (0-2 ppb) in 1% HNO_3 in both standard and single particle modes. Moreover, every 10-15 samples, one quality control sample containing 100 ppt dissolved Ag in 1% HNO_3 was analyzed from the stock of 100 ppm dissolved Ag solution (PlasmaCAL, Q.C. Standard 4, in 5% HNO_3). Every 3-4 analyses, a sample of 1% HNO_3 in DI water was analyzed in order to indicate any drift (>20%) in intensity of counts by the instrument and in case of any contamination occurred.

The total Ag analysis was performed in standard mode of ICP-MS to determine the total Ag mass in all aqueous systems. For the total silver measurements all the samples of nAg were digested by 30-35 % HNO_3 (PlasmaPURE, 67-70% Acid Nitric) for 24 h shaking in the room temperature and then diluted with DI water to 1% acid content prior to analysis with ICP-MS.

The detection limit of spICP-MS is 30 ppt for the dissolved silver and nAg. The total Ag analysis was done by ICP-MS (Perkin Elmer NexION 300X) after acid digestion of the WW samples.

ICP-OES- Total sulfur analysis was performed using ICP-OES (Perkin Elmer Optima 8300). A blank DI water and nine dissolved sulfur standard samples (25-5000 ppb) were used to perform the calibration curve for sulfur analysis. 4 mL of each sample was transferred to Amicon ultrafilter tubes (Amicon, NMWL 3 kDa) and were centrifuged at 4600g for 30 min. The centrifugation was repeated two more times with the same settings by adding 3 mL DI water each time to each ultrafilter tube in order to ensure that any unreacted sulfides passed through the filter. Total sulfur in the WW samples was analyzed after acid digestion with aqua regia (HNO_3:HCl=1:3) in a microwave at 90 ^oC for 75 min. The samples were then diluted using DI water to reduce the acid concentration to below 4%. Samples were triplicated and each sample replicate was analyzed three times by ICP-OES. The error bars in each graph represents the standard deviation among the sample replicates. Every two to four samples, one sample of acidified DI water was analyzed for any cross contamination from one sample to the other.

Transmission Electron Microscopy (TEM)- TEM analysis was performed using a FEI Tecnai G2 F20 S/TEM equipped with Gatan Ultrascan 4000 4k x 4k CCD Camera System (Model 895) and EDAX Octane T Ultra W /Apollo XLT2 SDD Analysis System for energy dispersive X-ray spectroscopy (EDS) measurements. nAg out of stock NP dispersion was deposited on the copper TEM substrates (Electron Microscopy Sciences, Carbon film 200 mesh copper grids) were air dried in dark.

Total organic carbon (TOC) Analyzer- The mass of organic molecules (DOC) adsorbed to the 30 nm PVP-nAg (1 ppm) in three exposure System to DOC and sulfides (S:Ag=0.4) (pre-sulfidation, post-sulfidation and simultaneous approach) was estimated by the

solution depletion method. The nAg was separated by centrifugation (6500g, 90 min) and the supernatant containing the unadsorbed organic molecules was gently removed living the sedimented nAg and adsorbed organics undisturbed at the bottom of the tube. The supernatant was then analyzed with a TOC analyzer.

UV-vis spectroscopy- The optical absorption spectra of Ag were measured in a wavelength range of 200-800 nm by a SpectraMax M5 Multimode Plate Reader. PVP-nAg (30 nm) was analyzed for UV-visible absorbance suspended in several solutions containing DI water, sulfides, DOC solutions, as described earlier, after 24 h and one week.

4.3. Results and Discussion

4.3.1. Dissolution of nAg in the presence and absence of sulfides

Figure 4-1 shows that PVP-nAg (hereafter referred to as nAg) dissolution extent in equilibrated systems was influenced by the type of DOC (HA/FA, Alginate or Cysteine/Methionine), the sequence in which DOC and sulfides were introduced into the batch systems, and by the primary size of the nAg. Equilibrium was attained at ~144 h (Figures 4-10 S4 to 4-12 S6) and each of the boxes in the box plots in Figure 4-1 show the range of equilibrium concentrations between 144 and 648 h.

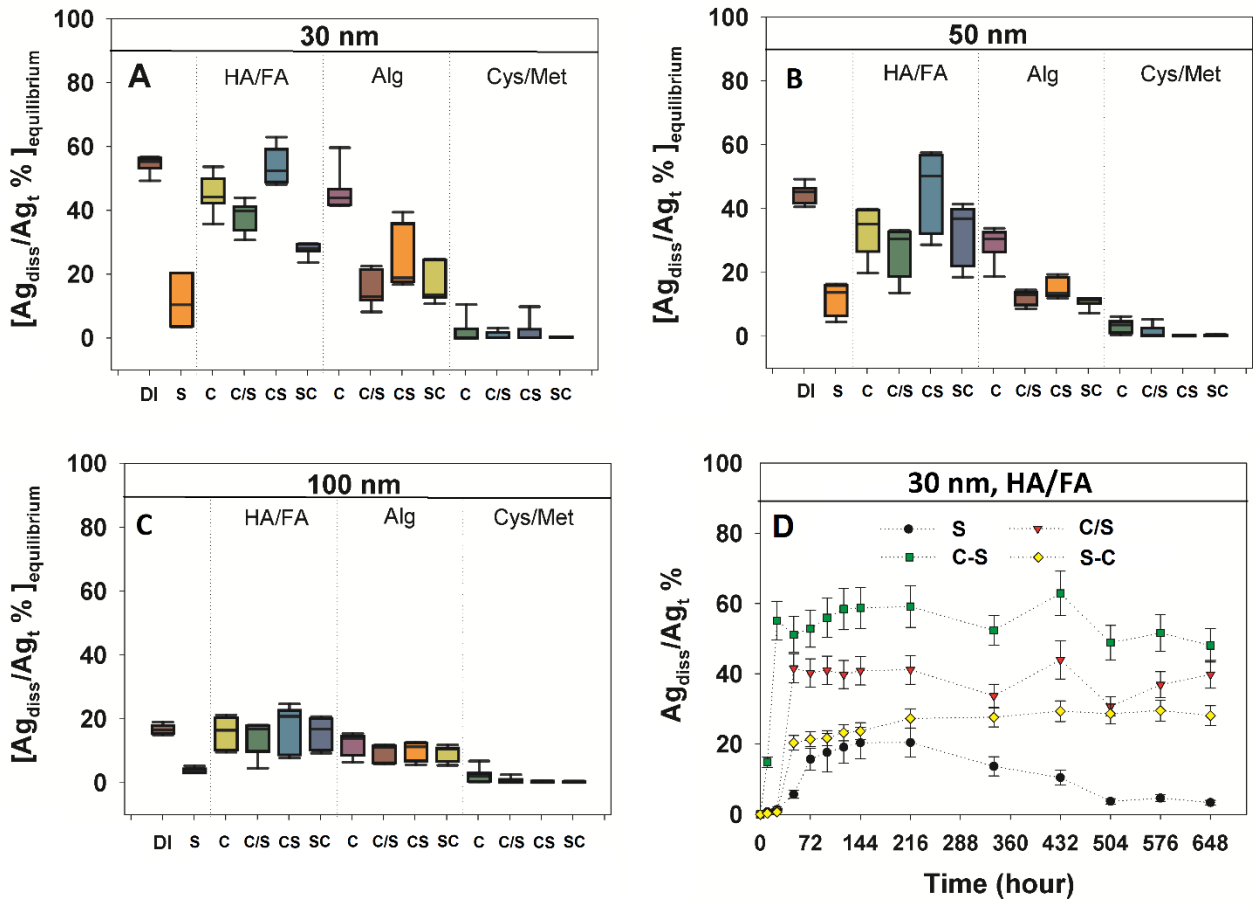

Figure 4-1-Boxplots of the equilibrium dissolved Ag concentrations (>144 to 648 h) normalized to initial total silver concentration (1ppb) added to the systems as nAg of (A) 30, (B) 50 and (C) 100 nm. DI represent systems with nAg suspended in DI water only; S for nAg suspended in DI water containing sulfides; and C/S, C-S, and S-C represent systems where the sequence of exposure to nAg to sulfides and DOC was varied. In System C/S, nAg was suspended in a solution of DOC and sulfides; in System C-S, nAg was contacted with DOC for 24 h and then sulfides were added (post-sulfidation); in System S-C, nAg was contacted sulfides for 24 h and then DOC was added (pre-sulfidation). Each box plot presents, minimum, first quartile, median, third quartile, and maximum. The central rectangle spans the first quartile to the third quartile. A segment inside the rectangle shows the median and "whiskers" above and below the box show the minimum and maximum of dissolved silver for each respective system. (D) The dissolved Ag concentrations (648 h) normalized to initial total silver concentration (1ppb) for 30 nm nAg in Systems S, C/S, C-S, and S-C in HA/FA over 648 h. Each system was set up in triplicate and the error bars represents the standard deviation among three sample measurements.

In System S, nAg dissolved considerably less after reaction with sulfides than in System DI (Figure 4-1). The dissolved concentrations for nAg in sulfides slowly increased with time to a

maximum of 10.9±7.5, 11.2±5.1 and 3.8±0.8 % of the total Ag added as 30, 50 and 100 nm nAg, respectively, up to 5 times lower concentrations than in System DI. However, between 216 and 360 h, it suddenly decreased (Figure 4-1D and 4-12 S 6D). At 648 h, the dissolved Ag was 3.3±0.7, 6.6±0.6, and 3±0.5 % of total silver concentration for 30, 50 and 100 nm nAg respectively. Some of the released Ag ions were either be re-adsorbed onto the sulfidated nAg (Liu and Hurt 2010) or reacted with available sulfides and form Ag_2S nuclei and precipitated out of solution as they aggregated and grew larger over time.

The equilibrium dissolved Ag concentration relative to the total Ag added in System DI was 54.4±2.5, 44.4±3, 16.6±1.4 % for 30, 50 and 100 nm nAg respectively (Figure 4-1 and 4-8 S2). Although the total Ag (as nAg) added to each system was 1 ppb, the equilibrium dissolved Ag concentration changed with particle size. According to the modified form of Kelvin equation (Ostwald-Freundlich relation) metal solubility is related to NP radius (Dokoumetzidis and Macheras 2006). The smaller NPs also have higher ion release rates due to higher specific surface area and smaller radius (Tables 4-1 S1and 4-2 S2) (Zhang et al. 2011).

Ag_2S has extremely low solubility (log K_{sp}=50.1) (Choi et al. 2009), and even under partial sulfidation conditions (S:Ag=0.4), a significant decrease in equilibrium concentrations was observed. Our results are in qualitative agreement with Levard *et al.* (Levard et al. 2011), but a direct quantitative comparison is not possible given significant system differences such as the nAg concentrations (1000 ppm versus 1 ppb) and the source of the sulfides (Na_2S versus CuS/ZnS). The amount of sulfides reacted with nAg was quantified by separating the NPs from solution by centrifugal ultrafiltration and analyzing the filtered NPs by ICP-OES after acid digestion. Figure 4-2A shows that 64.5±2.5% of total sulfides available in metal solution reacted with 30 nm nAg over 24 h. This indicates an effective S:Ag= 0.257 (mole) in System S.

Whereas, in system containing Na_2S, 91±11 % of sulfides reacted with 30 nm nAg over 24 h. Oxidative dissolution of Cu_xS_y clusters from precipitation reaction of CuO with sodium sulfide and formation of soluble copper sulfate hydroxides particularly at sulfides to copper ratio of less than one is shown to have affected the sulfidation rate of nAg by copper sulfides crystals (Thalmann et al. 2014, Ma et al. 2014).

It should be noted that although dissolution experiments were conducted with 1 ppb nAg, the results in Figure 4-2 are derived from systems dosed with 1 ppm nAg and proportionately higher amounts of other amendments, to provide sufficient sulfide for detection by ICP-OES. Our previous study on the dissolution of 1 ppm of nAg did not show any aggregation of NPs at this elevated concentration (Azodi et al. 2016). The limit of detection for sulfur is about 25 ppb using ICP-OES, and the TOC analyzer has a detection limit of >1 ppm for TOC.

4.3.2. Dissolution of nAg in the presence of sulfides and DOC

Figure 4-3 shows that with increasing contact time, the differences in dissolved Ag concentrations in HA/FA and alginate systems and DI water systems decreased. Figure 4-3A shows that the dissolved silver in HA/FA and alginate system reached an equilibrium concentration similar to DI water, unlike in cysteine/methionine. HA and FA have been generally shown to decrease dissolution of nAg by binding to their surface (Delay et al. 2011, Liu and Hurt 2010, Mitrano et al. 2014, Gunsolus et al. 2015, Gao et al. 2012) within the first several hours of study. In addition, it was observed that the surface coating of nAg interacts with humic substances and is partially replaced with these DOC molecules (Zhu et al. 2016, Lau et al. 2013). The decreases in the extents of nAg are attributed to the complexation of dissolved Ag to the bound DOC (Liu and Hurt 2010, Gao et al. 2012, Sikora and Stevenson 1988, Dubas and

Pimpan 2008) and reversible reactions (Dubas and Pimpan 2008, Litvin et al. 2012, Akaighe et al. 2012). Decreases in dissolution extents observed in this study for 30 nm nAg (Figure 4-1 and 4-13 S7, System OC) at equilibrium, are smaller than in previous studies which conducted the experiment for only 24 h (Liu and Hurt 2010). The equilibration time in this study is significantly higher than in previous studies, and likely provided sufficient time for Ag^+ to overcome diffusional limitations. In our previous study we also observed 50% lower dissolution in the presence of HA/FA and 10% lower dissolution in the presence of alginate, compared to DI water in the first 72 h exposure, using 10 ppb 80 nm nAg and spICP-MS analyses. Moreover, the decreases are in agreement for larger nAg (50, and 100 nm) as compared to 80 nm nAg in our previous study (Figure 4-13 S7, and 4-14 S8).

This observation is made for the first time as previous studies conducted dissolution experiments in alginate and humic substances only for a few hours (Ostermeyer et al. 2013). Previous literature suggested that alginate inhibited the dissolution within the first several hours by either preventing the release of Ag ions from the surface of nAg or by blocking the active sites for further oxidation of nAg surface (Ostermeyer et al. 2013). Alginate is a polysaccharide with hydroxyl and carboxylic functional groups, which can sorb onto nAg and due to its polymeric structure, may increase the colloidal stability through steric repulsion within the first several hours. Thus, it is unlikely that alginate simply blocked the oxidation sites for nAg due to which the dissolved Ag concentration should not have increased to close to values in DI water at equilibrium as observed in this study (Figure 4-3A, and 4-14 S8).

Figure 4-1 show that in the presence of HA/FA, dissolved Ag equilibrium concentrations were higher compared to alginate and cysteine/methionine systems, irrespective of the sequence of exposure of HA/FA and the sulfides to nAg. In particular, when sulfidation

occurred after contact of HA/FA with nAg (System C-S), dissolved Ag equilibrium concentrations were comparable to System DI, and the fraction of dissolved Ag to total Ag reached 54.6±5.7 and 45.5±12.3 % for 30 and 50 nm nAg, respectively. To summarize, in the presence of HA/FA, nAg dissolved in DI water>S-C>S/C>S-C. Similar patterns but lower extents of dissolution were observed with alginate, and negligible dissolution occurred in the presence of cysteine/methionine.

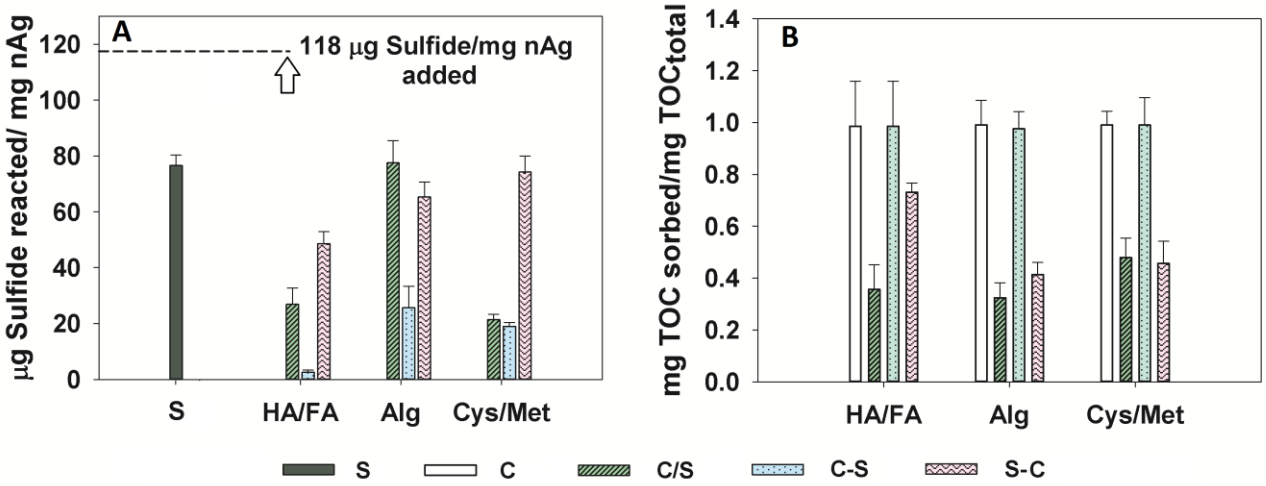

Figure 4-2 The amount of sulfides (A) and TOC (B) adsorbed onto 30 nm PVP-nAg in sulfides and in each DOC solution and in three exposure Systems to DOC and sulfides. Total initial Ag concentration as nAg was 1 ppm.

Dissolution was limited under all conditions for 100 nm nAg, and there were no significant differences between simultaneous or sequenced addition of DOC and sulfides. Overall, the results show that with smaller nAg (up to 50 nm) the extents of dissolution vary greatly depending on the sequence of exposure of DOC and sulfides, for partial sulfidation of nAg. Furthermore, the extents of nAg dissolution varied significantly depending on the type of DOC. The underlying causes of the differences in dissolution are explained in the following paragraphs.

4.3.3. Sulfidation extent of nAg in the absence and presence of DOC

The inhibited sulfidation reaction of nAg with sulfides in the presence of HA/FA can be explained in two ways. First, HA/FA molecules have been shown to chelate reduced sulfur (Ferdelman et al. 1991, Francois 1987) and thus the free metal sulfides were sorbed by HA/FA molecules and not available to subsequently react with nAg. Second, HA/FA adsorbed onto the nAg surface during the 24 h before sulfidation was commenced, and reduced the available sites for sulfides to react with nAg. To assess these processes several experiments were conducted where the amount of sulfides and TOC sorbed onto nAg in each exposure System was determined.

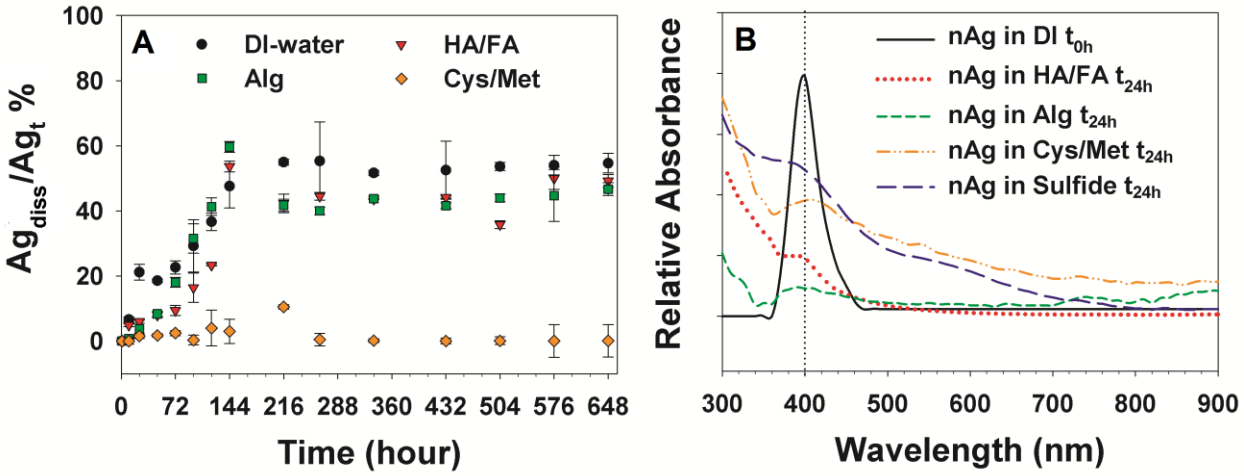

Figure 4-3 (A) The dissolved 30 nm PVP-nAg normalized to total silver in each solution in 4 different media in three different Systems. Sulfides concentration was 300 ppt (S/Ag=2 mole base) and DOC concentration were 1 ppm in all the systems. (B) UV visible absorbance of nAg suspended in DOC solutions and the sulfides mixture at 24 h.

The TOC analysis showed that in System C/S, HA/FA sorbed less on nAg as compared to Systems 2 and 3 with only 0.36±0.1 mg TOC/mg TOC_{tot} compared to 0.98±0.2 and 0.73±0.03 mg TOC/mg TOC_{tot} for Systems 2 and 3, respectively (Figure 4-2B). In System C/S, it was hypothesized that HA/FA was bound by sulfide in solution and thus HA/FA did not deposit as

much as in System C-S. To examine this hypothesis, in a set of control experiments, sulfides were mixed with DOC solutions for 3 hour and then the samples were filtered at 3 kDa (centrifugal ultrafiltration at 4600 g for 45 min). 50.9±7% of HA/FA (1 ppm total concentration) and 35.6±3.3% of the alginate was retained on the filter as determined by TOC measurements of the whole DOC and the filtrate. The filtered phase and filtrate were both analyzed for total sulfur. The results showed that there was a 68.7±3.4 % fraction of sulfides (S total=1187.4 ppb) associated with the 50.9% of HA/FA that was retained on the filter whereas in case of alginate at least 1.2±0.9% of the sulfide was found in the filtrate similar to control systems (Table 4-10 S4). Therefore, these results qualitatively confirmed that HA/FA in solution bound sulfides but not alginate.

In System C-S, HA/FA extensively (0.98±0.2 mg TOC/mg TOC_{tot}) bound to nAg (Figure 4-2B) and inhibited sulfide deposition resulting in only 2.5±0.8 μg sulfides/mg nAg (Figure 4-2A). These process are explained in the schematic in Figure 4-4, and explains why the nAg dissolution extent was limited in System C/S (38.2±4.6 %) compared to System C-S (54.6±5.7 %) for 30 nm nAg (Figure 4-1). Sulfide sorbed onto nAg in various degrees depending on sequence of exposure to HA/FA solution and sulfides. In System C/S and S-C, more sulfides were reacted with 30 nm nAg; 26.8±5.8 and 48.6±4.3 μg sulfides/mg nAg in HA/FA solution respectively. Consequently, the TOC associated with nAg in System C/S and S-C was 0.36±0.1 and 0.73±0.03 mg TOC/mg TOC_{tot} respectively. HA/FA was associated with nAg more in System S-C than C/S. In System S-C, HA/FA is likely sorbed on the sulfidated nAg whereas in System C/S, HA/FA is partially associated with free sulfides in solution and not nAg. Zhu *et al.* similarly showed that HA was sorbed onto the sulfidated nAg during the simultaneous exposure of nAg to HA and sulfides (Zhu et al. 2016).

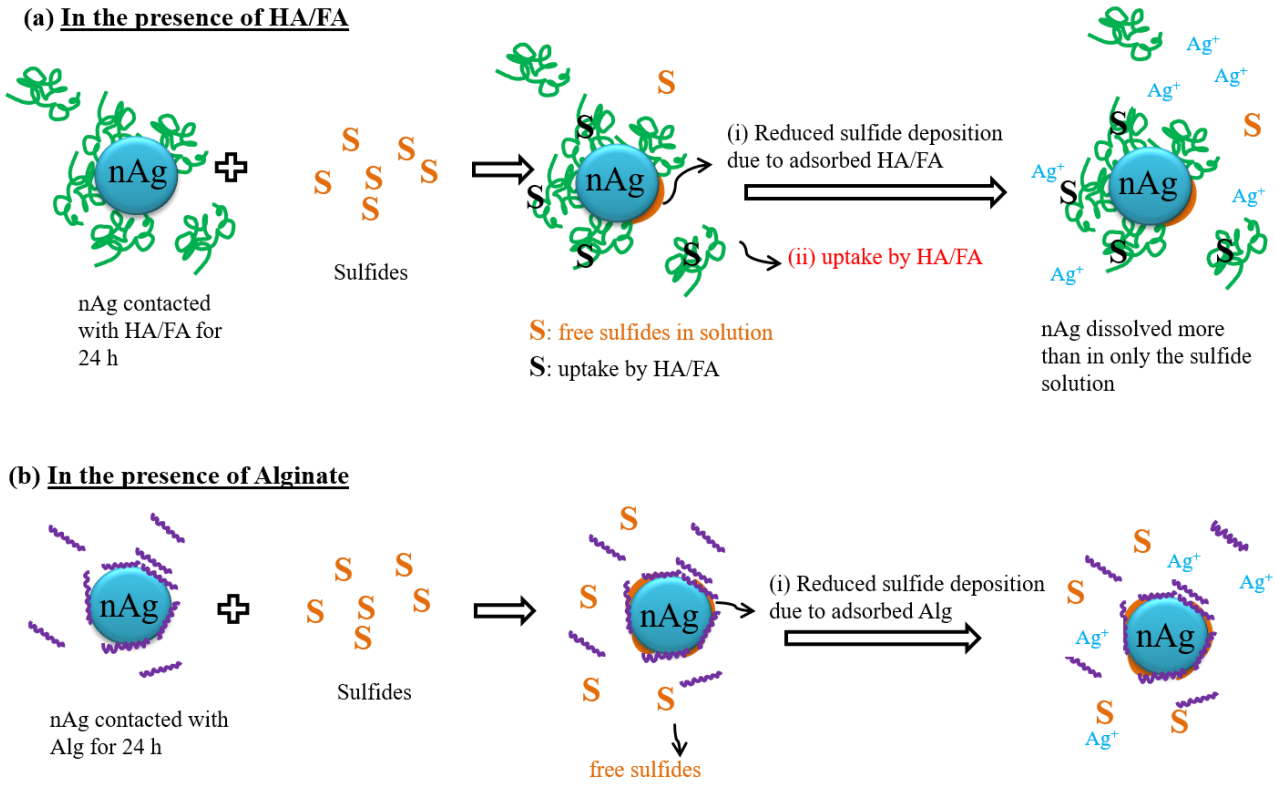

Figure 4-4- The schematic illustrating the effect of DOC on the sulfidation reaction of nAg in System C-S (post-sulfidation) in the presence of (A) HA/FA and (B) alginate solutions.

Zhang *et al.* also observed supressed sulfidation of Ag nanowires to various extents in the presence of SRHA at S:Ag=0.5 (Zhang et al. 2016). They similarly attributed the reduced sulfidation of nAg to limited available site for sulfidation reaction due to adsorption of SRHA on the nAg. The binding capacity of humic substances to silver is closely related to the availability of amine functional groups. Ag-humic substances stability constants range between 3.08 to 4.51 (Sikora and Stevenson 1988), much lower than that of Ag-sulfide stability constants. Therefore, once nAg is reacted with sulfide, the dissolution of Ag by complexation with humic substances is thermodynamically not favorable. In System S-C, that dissolved silver concentration was larger than in System S, it cannot be due to complexation and oxidation of silver sulfide. The dissolved

silver is attributable to oxidation of un-sulfidated fractions of the NPs which was likely complexed by HA/FA in the solution and stabilized due to steric repulsion and therefore did not precipitate out similar to what was observed earlier in System S. Several studies have shown that complete sulfidation of nAg did not occur when sulfides were stoichiometrically not significantly in excess of Ag, and nAg oxidation and Ag ion release occurred from partially sulfidated nAg under aerobic conditions (Azodi et al. 2016, Baalousha et al. 2015, Thalmann et al. 2014, Kent et al. 2014). In a separate set of experiments where the sulfide concentration was elevated to S:Ag=10, lower, but measurable of 11.3±2.2, 13.3±2.7, and 3.6±0.72 was observed in System C/S, C-S and S-C respectively containing HA/FA (Figure 4-15 S9). Similarly, Collin *et al.* observed that dissolved Ag concentration from nAg sulfidated at a dose of S:Ag=2, increased to 0.47 % in the presence of Pony Lake Fulvic Acid suspended in moderately hard reconstituted water from 0.1% in the absence of FA (Collin et al. 2016).

The equilibrium dissolved Ag concentration normalized to the total silver concentration for System C-S in alginate solution were 23.2±10.1 and 11.9±1.8% for 30 and 50 nm nAg, respectively (Figure 4-1). The concentrations in Systems S/C and S-C were lower and similar in magnitude. The TOC analysis for 30 nm nAg showed that for nAg in System C/S, 0.32±0.06 mg TOC/mg TOC_{tot} was associated with nAg, whereas 0.97±0.07 and 0.41±0.05 mg TOC/mg TOC_{tot} was associated with nAg in System C-S and S-C (Figure 4-2B). The lower extent of association of alginate to nAg in Systems C/S and S-C is likely because of the preferential binding of sulfides to nAg and a lack of affinity of alginate and sulfides.

Similar to HA/FA, once alginate was added before the sulfides in System C-S, the sulfidation was inhibited to a great extent with only 25.6±7.7 μg sulfides/mg nAg reacted

compared to 77.6±7.0 and 65.3±5.4 µg sulfides/mg nAg for System C/S and S-C respectively (Figure 4-2A).

nAg suspended in cysteine and methionine in all systems showed very limited dissolution over 648 h. The thiol chain in cysteine has high affinity to nAg and Ag ions (Leung et al. 2013), which likely inhibited sulfidation in particular in Systems C/S and C-S to 18.9±1.5 and 21.3±1.9 µg sulfides/mg nAg respectively (Figure 4-2A). Moreover, cysteine/methionine had similar association extents with nAg and trends with HA/FA and alginate (Figure 4-2B). Nevertheless, no changes in dissolved Ag concentration over time were observed in any of the systems including the sulfide-free cysteine/methionine system.

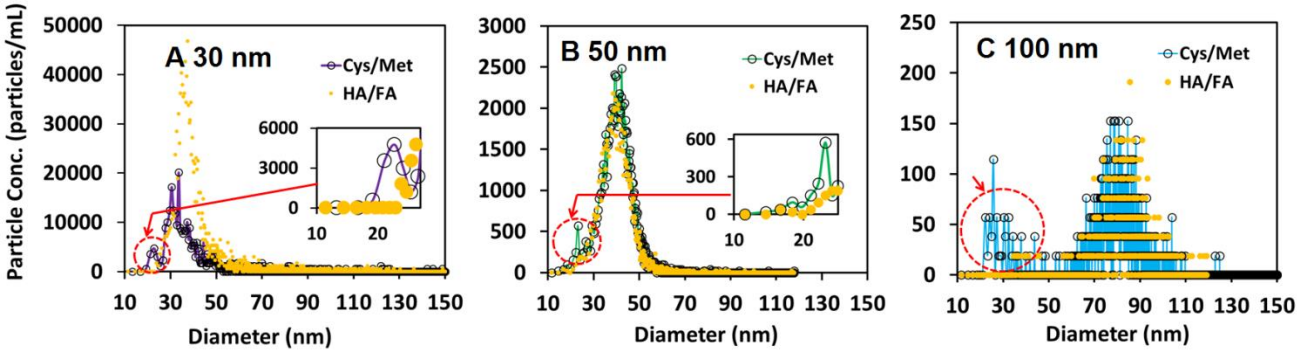

Figure 4-5- Particle size distribution of 30, 50 and 100 nm nAg in exposure to cysteine-methionine solution compared with the particle size distribution of nAg at similar time point in the solution of HA/FA; Particle size distribution for 50 and 100 nm nAg at 48 h and for 30 nm nAg at 144 h was obtained.

One noteworthy feature was the change in particle size distribution of nAg suspended in cysteine/methionine solution over time. A secondary peak appeared with a mean size centered 27.4 nm and 22.7 were first observed at 48 h for 50 and 100 nm nAg respectively (Figure 4-5 B, C). The first sign of a secondary peak for 30 nm nAg was only observed in a form of small shoulder at 23.2 nm at 144 h (Figure 4-5A). This secondary peak could be attributed to reformation of particulate Ag from the dissolved Ag. As the mean size of the secondary particles

is smaller than 20 nm it could have overlapped with the particle distribution of nAg itself and therefore appeared only as small shoulder. In a few studies, Ag ions in the presence of cysteine reformed into plasmon-active nAg via reduction of Ag ions to particulate silver (Azodi et al. 2016, Khan and Talib 2010). Therefore, in this study, it is hypothesized that as the Ag ions were complexed with cysteine/methionine and released from the surface of nAg, they were chemically reduced to Ag-cysteine/methionine particles. As a result, no increase in dissolved Ag concentration was registered whereas a small secondary peak appeared after several hours in the solutions containing amino acids, but not in HA/FA or alginate solutions.

4.3.4. Changes in particle concentrations and sizes of nAg in the presence of sulfides and DOC

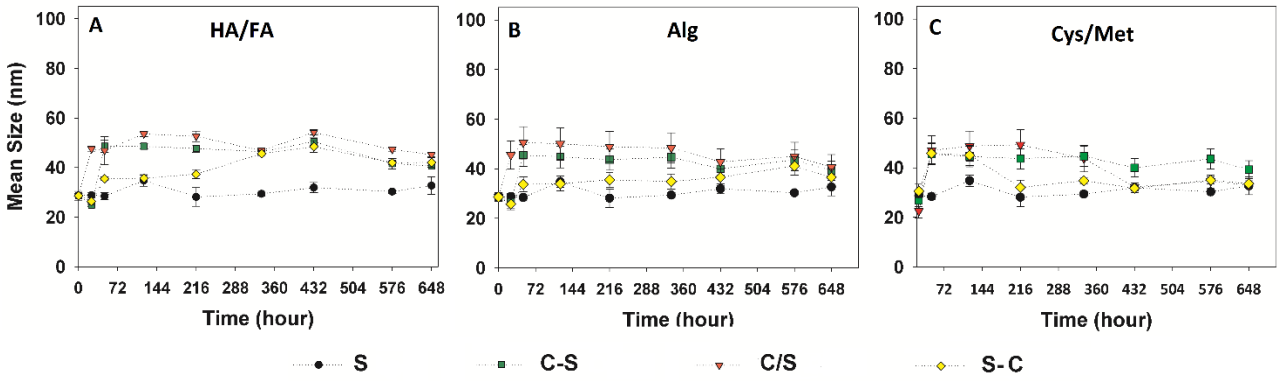

Figure 4-6- The mean size of 30 nm PVP-nAg contacted with (A) HA/FA, (B) Alginate, (C) Cysteine and methionine, and sulfide in exposure Systems S, C/S, C-S, and S-C.

Figures 4-6A, B, C show the mean size of 30 nm nAg suspended in sulfides and cysteine/methionine solutions in three exposure Systems. The mean size of nAg in Systems S/C, C-S and S-C increased in the first 24 h, whereas the mean size of 50 and 100 nm nAg slowly decreased over 648 h (Figure 4-16 S10, S11). The particle number concentration is much higher for 30 nm (6×10^6 particles/mL) as compared to the particle concentration for 50 nm (1.95×10^6

particles/mL) and 100 nm (0.2×10^6 particles/mL) at 1 ppb total silver concentration. Therefore, the higher the particle concentration, causes a greater likelihood of particle-particle collision which can result in aggregation of 30 nAg (Kruis et al. 2000, Raychoudhury et al. 2012). Overall, the particle mean sizes were stable over time.

4.4. Conclusions

This study for the first time showed that dissolution of PVP-coated nAg (30, 50 and 100 nm) in HA/FA and alginate resulted in equilibrium dissolved silver concentration, which was very close to that obtained in DI. Other studies, reported lower dissolved Ag compared to DI in humic substances and alginate solution over significantly shorter contact times. In addition, sequence of addition of DOC and sulfides affected DOC association extents with nAg and the sulfidation extents of nAg. HA/FA or alginate greatly influenced the dissolution behavior of nAg under aerobic conditions where stoichiometrically-limited amounts of sulfides were present. These sulfide loads however were sufficient to decrease nAg dissolution extents in HA/FA or alginate free systems. The sulfidation extents are reduced when nAg is pre-exposed to HA/FA, and as a result the extent of dissolution of nAg is similar to those in DI water, and sulfide-free systems. Humic substances interfered with the sulfidation of nAg by binding the free sulfides in the solution or by associating with nAg and therefore inhibiting the sulfidation reaction. Alginate molecules also sorbed onto nAg before addition of sulfides and therefore decreased the extent of nAg sulfidation. Furthermore, it was observed that amino acids such as cysteine and methionine strongly bound to nAg and as a result, the dissolved Ag concentrations were much smaller than in the other DOC solutions. The small increase in the dissolved silver concentration is attributed to the formation of secondary NPs in cysteine and methionine solution which was observed after

several hours in this systems with spICP-MS and not in other DOC solutions (i.e. HA/FA or alginate).

4.5. Acknowledgement

We thank David Liu, McGill, for TEM analysis of nAg, Andrew Golsztajn, McGill, for TOC analysis, and Mariana Umpieretz with assisting with ICP-OES analysis. Funding from Natural Sciences and Engineering Research Council, Canada (Grants STPGP 430659 – 12), Environment and Climate Change Canada, Perkin Elmer Health Sciences Canada, and SNC Lavalin Environnment, is gratefully acknowledged.

4.6. Supplementary Data

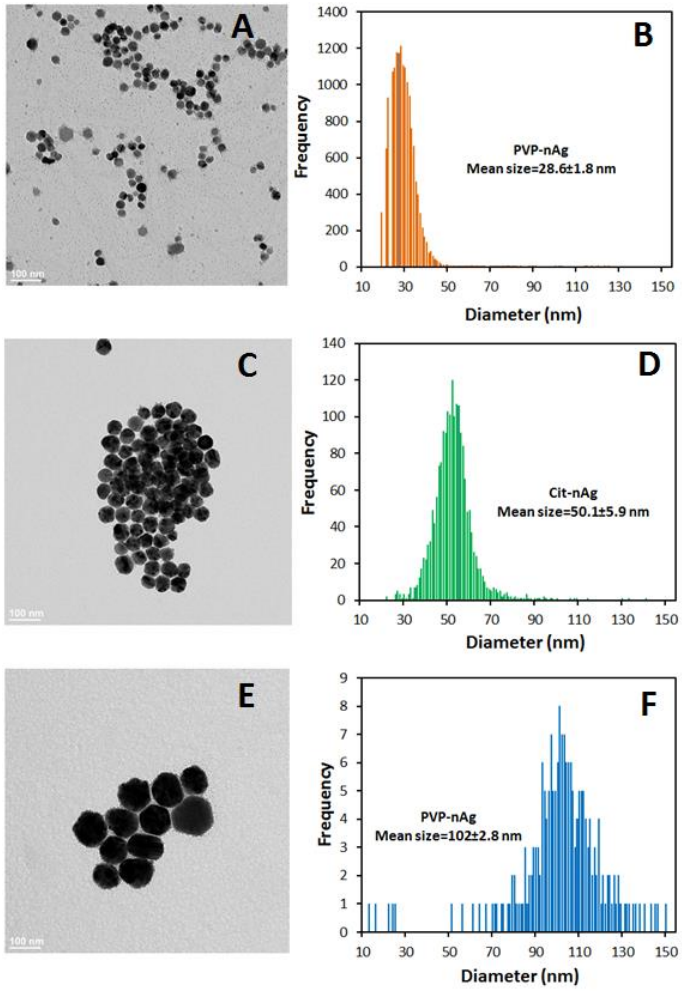

Figure 4-7 S1- (A, C, E) TEM images of 30, 50 and 100 nm nAg on a copper grid. The white bar on the left equals 100 nm. (B, D, F) The particle size distribution of nAg freshly dispersed in DI water and analyzed with spICP-MS.

4.6.1. Dissolution kinetic of nAg (30, 50, 100 nm) in DI water

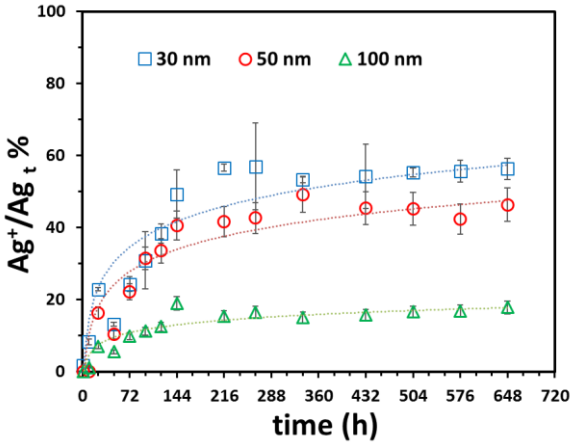

Figure 4-8 S2- The dissolution of nAg (30, 50 and 100 nm) in DI water over time (for 648 h) using spICP-MS. The dissolved Ag concentrations are normalized to the total Ag concentration in each system.

The nAg with three nominal mean size of 30, 50 and 100 nm were dispersed in DI water at a total concentration of 1 ppb. Figure 4-8 S2 shows the dissolved Ag concentrations normalized to the total silver concentration in each sample over time. The dissolved Ag concentrations reached 0.56±0.03, 0.46±0.05, 0.18±0.02 ppb for 30, 50 and 100 nm nAg respectively at 648 h. The initial dissolved Ag concentrations (t=0 h) were obtained 30-60 min after the sample preparations and attained values very close to zero and similar to background Ag measured in DI water (0.003-0.005 ppb) which is well below the detection limit of spICP-MS and therefore assumed as zero for all the three nAg samples.

The small nAg, 30 and 50 nm, took longer (approximately time point 336 h) to reach equilibrium, whereas large nAg, 100 nm, reached equilibrium after 144 h. After 468 h, nAg did not dissolve completely which was similarly observed in previous studies (Liu and Hurt 2010, Zhang et al. 2011).

Furthermore, the equilibrium dissolved Ag concentration depend on the primary particle size even though the initial Ag concentration was equal for the three nAg (1 ppb). According to a modified form of Kelvin equation (Ostwald-Freundlich relation) particle solubility is related to its radius (Ma et al. 2011). Thus the smaller NPs have a higher ion release rates and have higher solubility than the larger NPs (Liu et al. 2009b).

The first order kinetic model based on hard sphere theory using the Arrhenius equation developed by Zhang *et al* (Zhang et al. 2011) was applied to the experimental data obtained in this study (Figure 4-9 S3). The model fitted the experimental data well with correlation coefficients of 0.97, 0.98, and 0.96 for 30, 50 and 100 nm nAg respectively.

The kinetic parameter, k, was determined for the nAg and was compared with previous studies for similar size nAg (Table 4-2 S2).

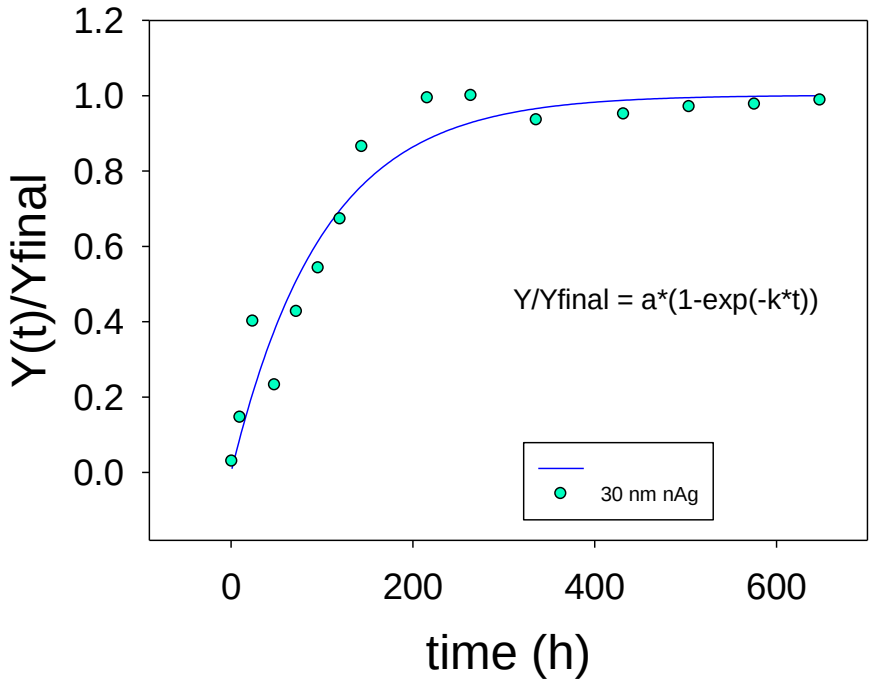

Figure 4-9 S3- First order kinetic model applied on dissolved Ag concentration over time.

Table 4-1 S1- Kinetic parameter (k, h^{-1}) for nAg with nominal mean sizes of 30, 50, and 100 nm suspended in DI water.

Nanoparticles	k (h^{-1})	Std. Error	R^2
30 nm PVP-nAg	**0.0099**	0.0014	0.97
50 nm Cit-nAg	**0.0106**	0.0013	0.98
100 nm PVP-nAg	**0.0134**	0.0022	0.96

Table 4-2 S2- Kinetic parameter for nAg from the literature

Author	Cit-nAg	k (h-1)
Kittler et al.	50±20 nm, 140 mg/L	0.0017
Liu et al.	4.8±1.6 nm, 0.05 mg/L	0.0252
Zhang et al.	20 nm, 0.3 mg/L	0.0147
	40 nm, 0.3 mg/L	0.0258
	80 nm, 0.3 mg/L	0.0555

Table 4-3 S3- Single Particle ICP-MS Instrumental Parameters

Parameter	Value
Sample Uptake Rate	0.295 mL/min
Nebulizer	Glass Concentric
Spray Chamber	Glass Cyclonic
RF Power	1600 W
Analyte	Ag107
Analysis time	100-200 sec
Dwell time	100 µsec
Transport Efficiency	9.1-10.1%
Daily optimization	1 ppb Ag+ in 1% HNO3 For torch alignment and nebulizer gas flow

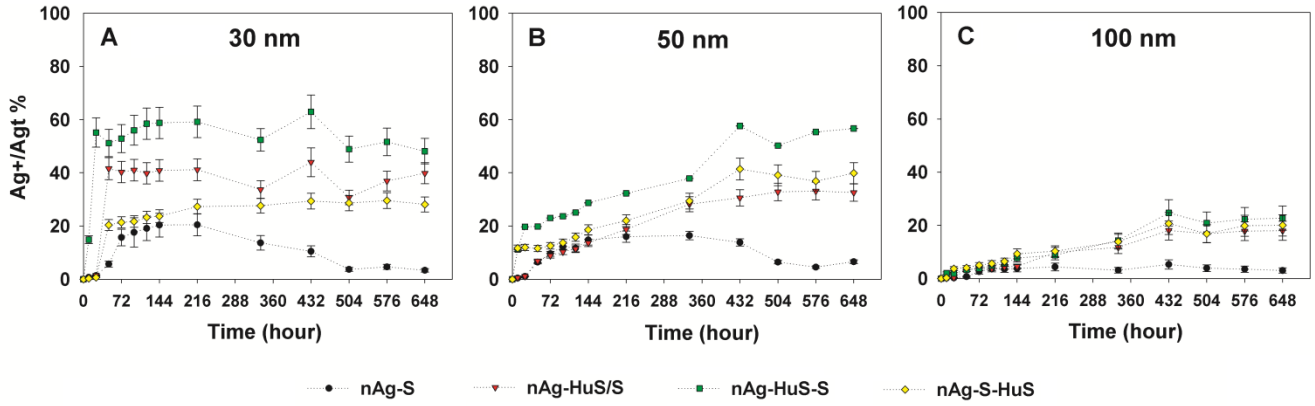

Figure 4-10 S4- The dissolved Ag concentrations normalized to initial total silver concentration for nAg of 30, 50, and 100 nm mean size in solutions containing sulfides, and equal mass mixture of HA and FA in 3 different exposure Systems. nAg-S, samples contained only Sulfides; nAg-Hu/S, nAg was added to solution containing Sulfides, HA and FA (HuS); nAg-Hu-S, nAg was equilibrated with the mixture of HA and FA for 24 h, then Sulfides was added; nAg-S-HuS, nAg was equilibrated with Sulfides first for 24 h, then the mixture of HA and FA was added.

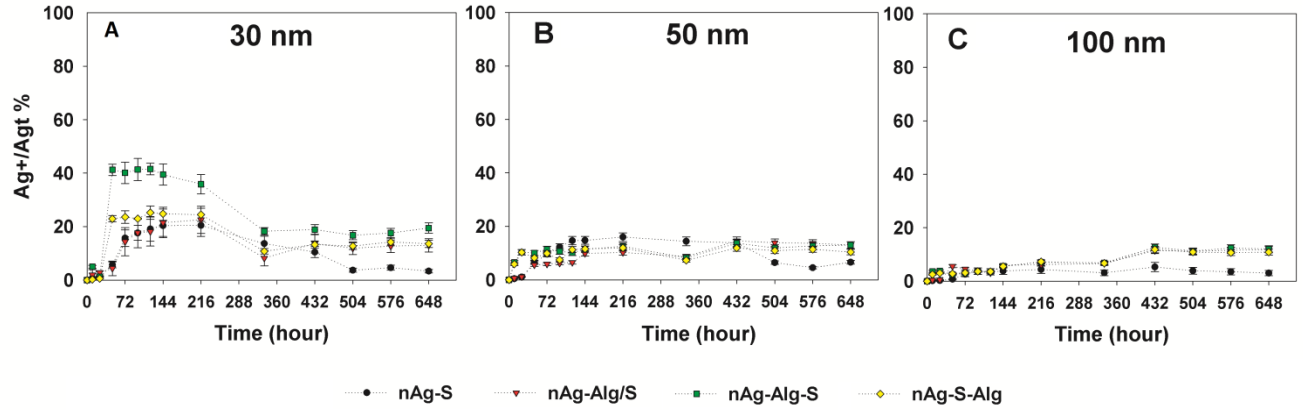

Figure 4-11 S5- The dissolved Ag concentrations normalized to initial total silver concentration for nAg of 30, 50, and 100 nm mean size in solutions containing sulfides, and alginate in 3 different exposure Systems. nAg-S, samples contained only Sulfides; nAg-Alg/S, nAg was added to solution containing Sulfides, Alginate (Alg); nAg-Alg-S, nAg was equilibrated with the alginate for 24 h, then Sulfides was added; nAg-S-Alg, nAg was equilibrated with Sulfides first for 24 h, then the alginate was added.

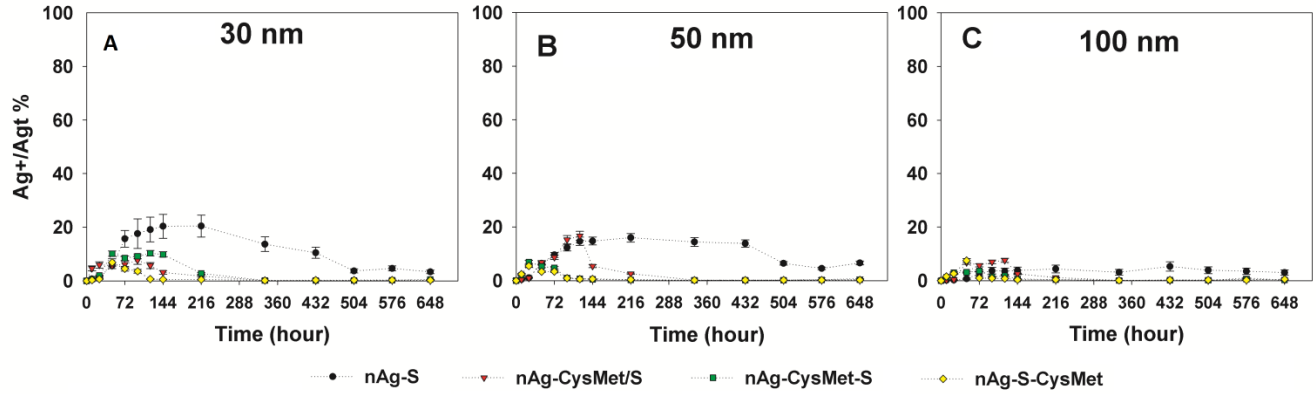

Figure 4-12 S6- The dissolved Ag concentrations normalized to initial total silver concentration for nAg of 30, 50, and 100 nm mean size in solutions containing sulfides, and equal mass mixture of cysteine and methionine in 3 different exposure Systems. nAg-S, samples contained only sulfides; nAg-CysMet/S, nAg was added to solution containing Sulfides, cysteine and methionine (CysMet); nAg-CysMet-S, nAg was equilibrated with the mixture of cysteine/methionine for 24 h, then Sulfides was added; nAg-S-CysMet, nAg was equilibrated with Sulfides first for 24 h, then the mixture of cysteine/methionine was added.

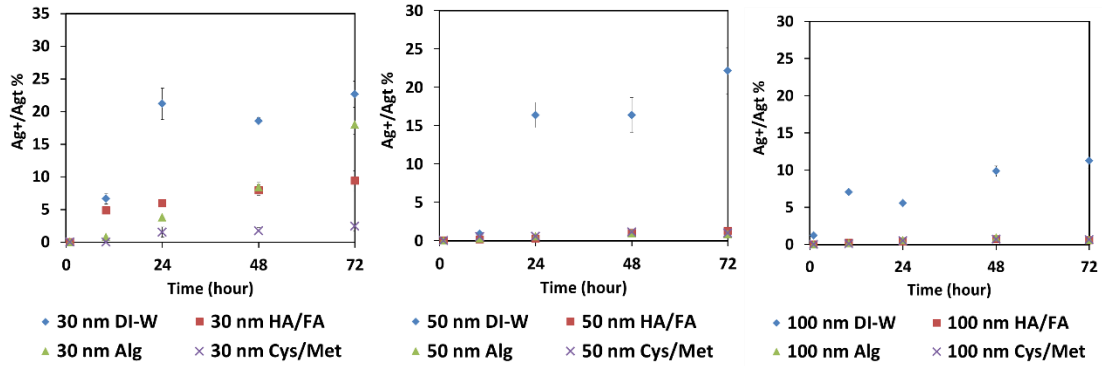

Figure 4-13 S7- The dissolved Ag concentration normalized to total silver in solution over the first 72 h of exposure to DI water, alginate, mixture of HA and FA, and mixture of cysteine and methionine.

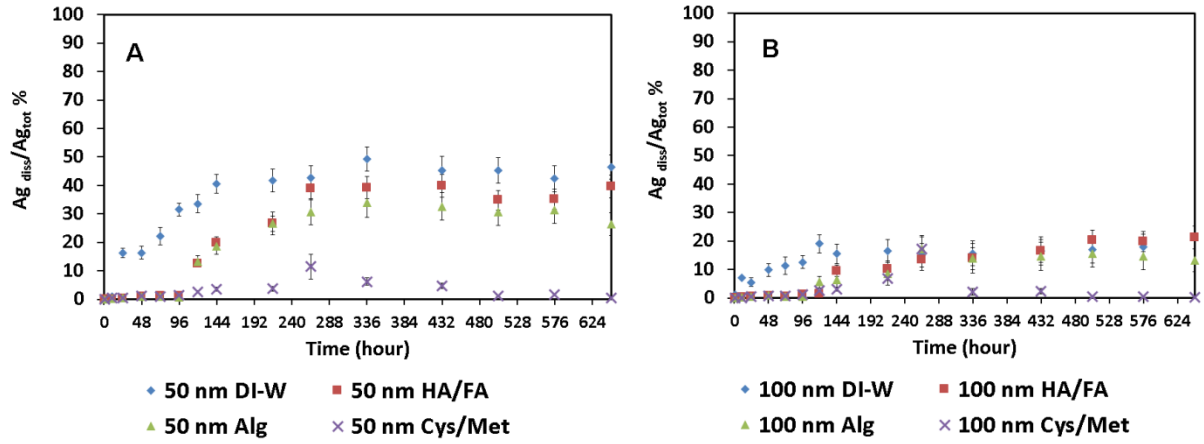

Figure 4-14 S8– The dissolved Ag normalized to total silver in each solution for 50 and 100 nm nAg in DI water and three DOC solutions.

Table 4-4 S4- The percentage of sulfides (% S) on the filter and in the filtrate for the three sulfides solutions (1187.4, 593.7, and 296.8 ppb) mixed with alginate or HA/FA solution, then filtered at 3 kDa at 4600 g.

Ctrl: Only sulfides; Alginate or HA/FA at 1 ppm mixed with sulfides		Total Sulfides at various conc. (ppb) filtered at 3 kDa		
		S=1187.4	**S=593.7**	**S=296.8**
% S on the filter	***Ctrl***	1.7±0.2	n/a	n/a
	Alginate	1.2±0.9	2.2±0.5	2.5±0.4
	HA/FA	68.7±3.4	78±4.1	99.5±1.3
% S in the filtrate	***Ctrl***	98.2±12.3	n/a	n/a
	Alginate	94.2±8.9	96.3±11.1	97.3±13.6
	HA/FA	34±10.3	23.9±5.7	2±1.5

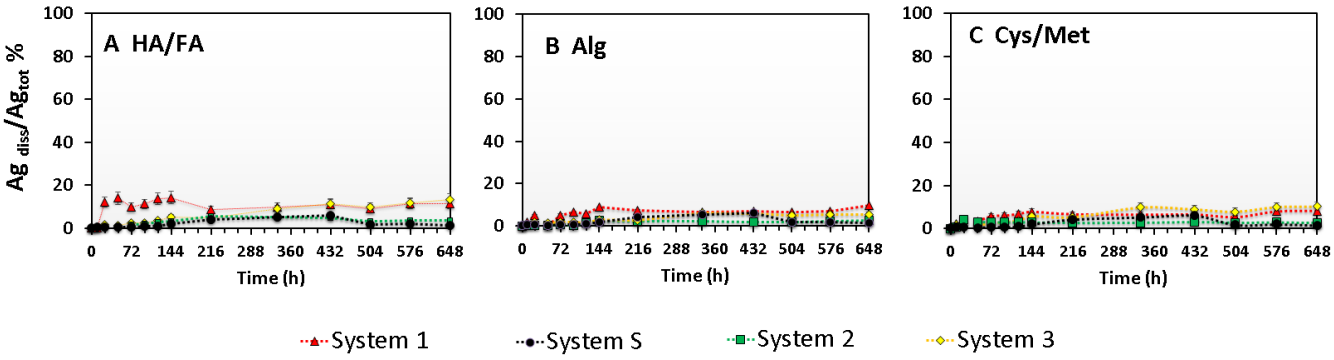

Figure 4-15 S9- The dissolution of 30 nm PVP-Ag NPs in Systems 1, 2, and 3 in (A) HA/FA and sulfides (B) Alginate and sulfides (C) Cysteine/methionine. Sulfides to silver mole ratio of 10 was prepared and DOC concentration was 1 ppm in all the systems. System 1: nAg was added to sulfides and DOC simultaneously; System 2: nAg was contacted with DOC for the first 24 h; System 3: nAg was contacted with sulfides for the first 24 h.

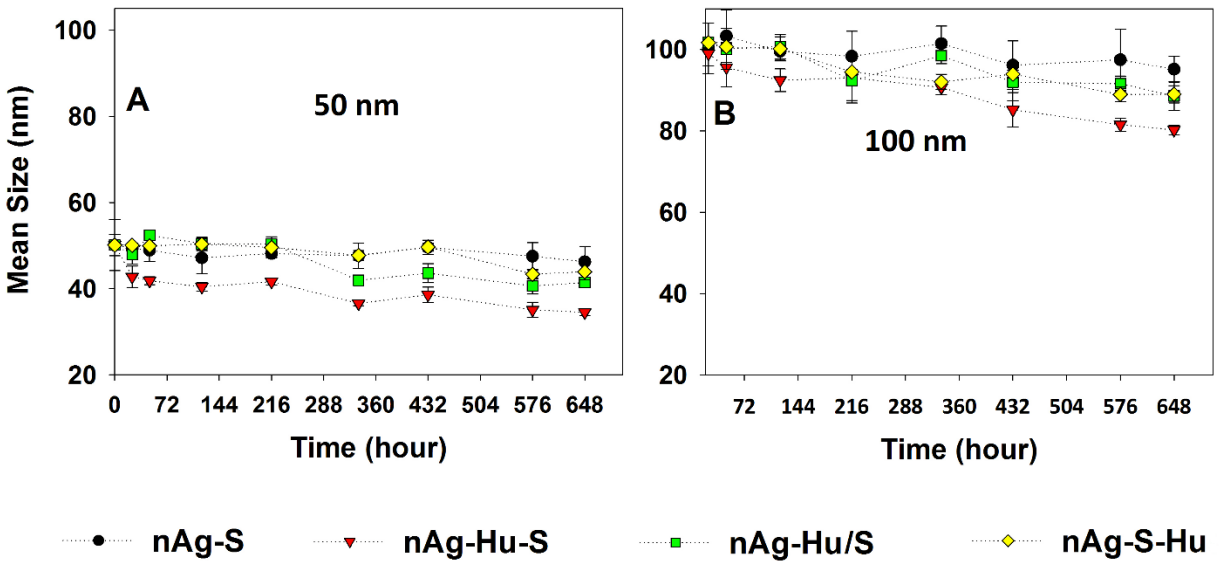

Figure 4-16 S10- Mean size of 30 nm PVP-nAg in various exposure Systems to HA/FA and sulfides.

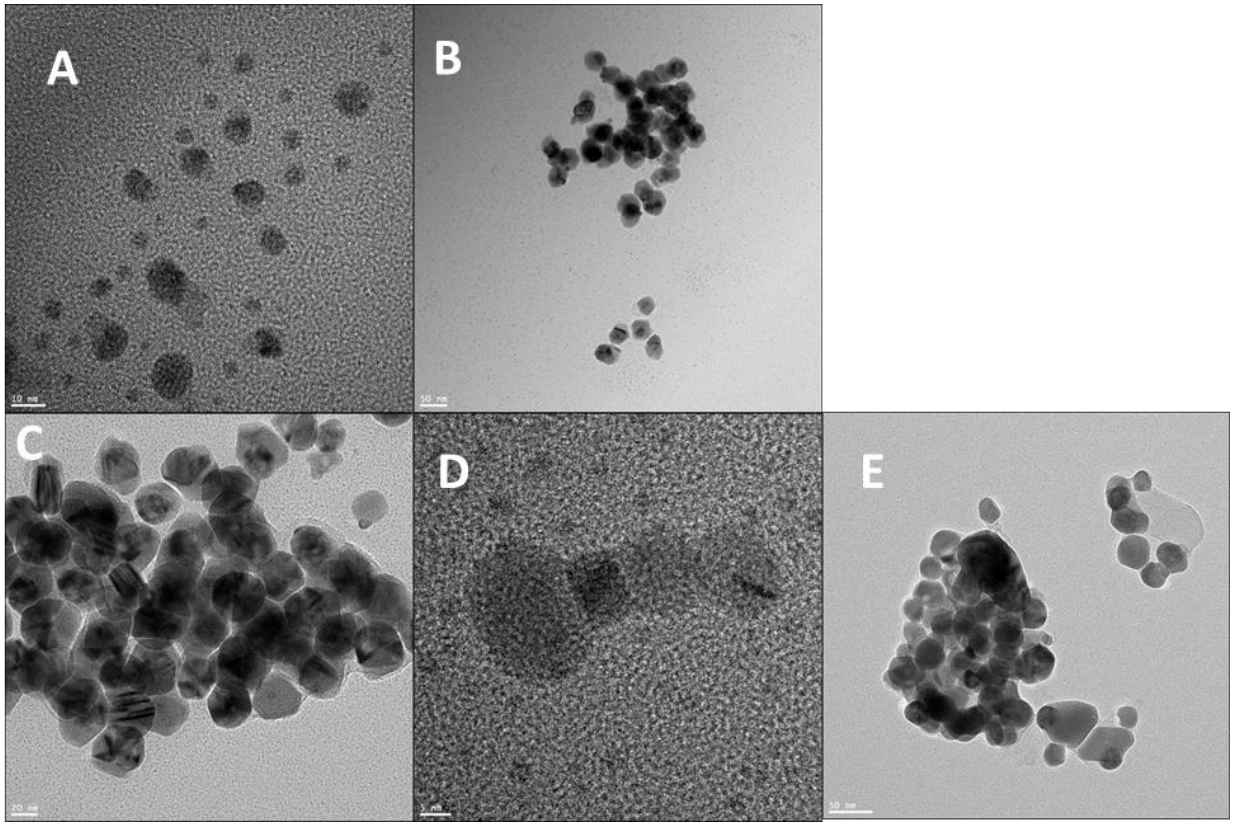

Figure 4-17 S11- TEM of 30 nm nAg in DI water (A), sulfides (B), simultaneous exposure System to HA/FA and sufides, (D) post-sulfidation and (E) pre-sulfidation of nAg after 72 h.

4.7. References

1. Benn, T., Cavanagh, B., Hristovski, K., Posner, J.D. and Westerhoff, P. (2010) The release of nanosilver from consumer products used in the home. Journal of environmental quality 39(6), 1875-1882.
2. Gottschalk, F. and Nowack, B. (2011) The release of engineered nanomaterials to the environment. Journal of Environmental Monitoring 13(5), 1145-1155.
3. Keller, A.A., McFerran, S., Lazareva, A. and Suh, S. (2013) Global life cycle releases of engineered nanomaterials. Journal of Nanoparticle Research 15(6), 1-17.
4. Navarro, E., Piccapietra, F., Wagner, B., Marconi, F., Kaegi, R., Odzak, N., Sigg, L. and Behra, R. (2008) Toxicity of silver nanoparticles to Chlamydomonas reinhardtii. Environmental Science & Technology 42(23), 8959-8964.
5. Kittler, S., Greulich, C., Diendorf, J., Koller, M. and Epple, M. (2010) Toxicity of silver nanoparticles increases during storage because of slow dissolution under release of silver ions. Chemistry of Materials 22(16), 4548-4554.
6. Greulich, C., Braun, D., Peetsch, A., Diendorf, J., Siebers, B., Epple, M. and Köller, M. (2012) The toxic effect of silver ions and silver nanoparticles towards bacteria and human cells occurs in the same concentration range. RSC Advances 2(17), 6981-6987.
7. Liu, J., Wang, Z., Liu, F.D., Kane, A.B. and Hurt, R.H. (2012) Chemical transformations of nanosilver in biological environments. ACS nano 6(11), 9887.
8. Azodi, M., Sultan, Y. and Ghoshal, S. (2016) Dissolution Behavior of Silver Nanoparticles and Formation of Secondary Silver Nanoparticles in Municipal Wastewater by Single-Particle ICP-MS. Environmental Science & Technology 50(24), 13318-13327.
9. Ma, R., Levard, C.m., Marinakos, S.M., Cheng, Y., Liu, J., Michel, F.M., Brown Jr, G.E. and Lowry, G.V. (2011) Size-controlled dissolution of organic-coated silver nanoparticles. Environmental Science & Technology 46(2), 752-759.
10. Misra, S.K., Dybowska, A., Berhanu, D., Luoma, S.N. and Valsami-Jones, E. (2012) The complexity of nanoparticle dissolution and its importance in nanotoxicological studies. Science of the Total Environment 438, 225-232.
11. Zhang, W., Yao, Y., Sullivan, N. and Chen, Y. (2011) Modeling the primary size effects of citrate-coated silver nanoparticles on their ion release kinetics. Environmental Science & Technology 45(10), 4422-4428.
12. Levard, C., Hotze, E.M., Colman, B.P., Dale, A.L., Truong, L., Yang, X., Bone, A.J., Brown Jr, G.E., Tanguay, R.L. and Di Giulio, R.T. (2013) Sulfidation of silver nanoparticles: natural antidote to their toxicity. Environmental Science & Technology 47(23), 13440-13448.
13. Kent, R.D. and Vikesland, P.J. (2012) Controlled evaluation of silver nanoparticle dissolution using atomic force microscopy. Environmental Science & Technology 46(13), 6977-6984.
14. Baalousha, M., Arkill, K., Romer, I., Palmer, R. and Lead, J. (2015) Transformations of citrate and Tween coated silver nanoparticles reacted with Na 2 S. Science of the Total Environment 502, 344-353.
15. Levard, C., Reinsch, B.C., Michel, F.M., Oumahi, C., Lowry, G.V. and Brown Jr, G.E. (2011) Sulfidation processes of PVP-coated silver nanoparticles in aqueous solution: impact on dissolution rate. Environmental Science & Technology 45(12), 5260-5266.
16. Liu, J., Pennell, K.G. and Hurt, R.H. (2011) Kinetics and mechanisms of nanosilver oxysulfidation. Environmental Science & Technology 45(17), 7345-7353.
17. Thalmann, B., Voegelin, A., Sinnet, B., Morgenroth, E. and Kaegi, R. (2014) Sulfidation kinetics of silver nanoparticles reacted with metal sulfides. Environmental Science & Technology 48(9), 4885-4892.

18. Adams, N.W. and Kramer, J.R. (1998) Reactivity of Ag+ ion with thiol ligands in the presence of iron sulfide. Environmental Toxicology and Chemistry 17(4), 625-629.
19. Liu, J., Sonshine, D.A., Shervani, S. and Hurt, R.H. (2010) Controlled release of biologically active silver from nanosilver surfaces. ACS nano 4(11), 6903-6913.
20. Imai, A., Fukushima, T., Matsushige, K., Kim, Y.-H. and Choi, K. (2002) Characterization of dissolved organic matter in effluents from wastewater treatment plants. Water Research 36(4), 859-870.
21. Ma, H., Allen, H.E. and Yin, Y. (2001) Characterization of isolated fractions of dissolved organic matter from natural waters and a wastewater effluent. Water Research 35(4), 985-996.
22. McArthur, J., Banerjee, D., Hudson-Edwards, K., Mishra, R., Purohit, R., Ravenscroft, P., Cronin, A., Howarth, R., Chatterjee, A. and Talukder, T. (2004) Natural organic matter in sedimentary basins and its relation to arsenic in anoxic ground water: the example of West Bengal and its worldwide implications. Applied Geochemistry 19(8), 1255-1293.
23. Accardi-Dey, A. and Gschwend, P.M. (2002) Assessing the combined roles of natural organic matter and black carbon as sorbents in sediments. Environmental Science & Technology 36(1), 21-29.
24. Kepkay, P.E. (1994) Particle aggregation and the biological reactivity of colloids. Marine Ecology-Progress Series 109, 293-293.
25. Kramer, J.R., Bell, R.A. and Smith, D.S. (2007) Determination of sulfide ligands and association with natural organic matter. Applied Geochemistry 22(8), 1606-1611.
26. Delay, M., Dolt, T., Woellhaf, A., Sembritzki, R. and Frimmel, F.H. (2011) Interactions and stability of silver nanoparticles in the aqueous phase: Influence of natural organic matter (NOM) and ionic strength. Journal of Chromatography A 1218(27), 4206-4212.
27. Furman, O., Usenko, S. and Lau, B.L. (2013) Relative importance of the humic and fulvic fractions of natural organic matter in the aggregation and deposition of silver nanoparticles. Environmental Science & Technology 47(3), 1349-1356.
28. Pokhrel, L.R., Dubey, B. and Scheuerman, P.R. (2014) Natural water chemistry (dissolved organic carbon, pH, and hardness) modulates colloidal stability, dissolution, and antimicrobial activity of citrate functionalized silver nanoparticles. Environmental Science: Nano 1(1), 45-54.
29. Wirth, S.M., Lowry, G.V. and Tilton, R.D. (2012) Natural organic matter alters biofilm tolerance to silver nanoparticles and dissolved silver. Environmental Science & Technology 46(22), 12687-12696.
30. Shafer, M.M., Overdier, J.T. and Armstong, D.E. (1998) Removal, partitioning, and fate of silver and other metals in wastewater treatment plants and effluent-receiving streams. Environmental Toxicology and Chemistry 17(4), 630-641.
31. Zhu, T., Lawler, D.F., Chen, Y. and Lau, B.L. (2016) Effects of natural organic matter and sulfidation on the flocculation and filtration of silver nanoparticles. Environmental Science: Nano 3(6), 1436-1446.
32. Zhang, Y., Xia, J., Liu, Y., Qiang, L. and Zhu, L. (2016) Impacts of Morphology, Natural Organic Matter, Cations, and Ionic Strength on Sulfidation of Silver Nanowires. Environmental Science & Technology 50(24), 13283-13290.
33. Collin, B., Tsyusko, O.V., Starnes, D.L. and Unrine, J.M. (2016) Effect of natural organic matter on dissolution and toxicity of sulfidized silver nanoparticles to Caenorhabditis elegans. Environmental Science: Nano.
34. Thalmann, B., Voegelin, A., Morgenroth, E. and Kaegi, R. (2016) Effect of humic acid on the kinetics of silver nanoparticle sulfidation. Environmental Science: Nano 3(1), 203-212.

35. Ma, R., Stegemeier, J., Levard, C., Dale, J.G., Noack, C.W., Yang, T., Brown, G.E. and Lowry, G.V. (2014) Sulfidation of copper oxide nanoparticles and properties of resulting copper sulfide. Environmental Science: Nano 1(4), 347-357.
36. Priadi, C., Le Pape, P., Morin, G., Ayrault, S., Maillot, F., Juillot, F., Hochreutener, R., Llorens, I., Testemale, D. and Proux, O. (2012) X-ray absorption fine structure evidence for amorphous zinc sulfide as a major zinc species in suspended matter from the Seine River downstream of Paris, Ile-de-France, France. Environmental Science & Technology 46(7), 3712-3720.
37. Stover, R., Sommers, L. and Silviera, D. (1976) Evaluation of metals in wastewater sludge. Journal (Water Pollution Control Federation), 2165-2175.
38. Degueldre, C. and Favarger, P.-Y. (2003) Colloid analysis by single particle inductively coupled plasma-mass spectroscopy: a feasibility study. Colloids and Surfaces A: Physicochemical and Engineering Aspects 217(1), 137-142.
39. Liu, J. and Hurt, R.H. (2010) Ion release kinetics and particle persistence in aqueous nano-silver colloids. Environmental Science & Technology 44(6), 2169-2175.
40. Dokoumetzidis, A. and Macheras, P. (2006) A century of dissolution research: from Noyes and Whitney to the biopharmaceutics classification system. International Journal of Pharmaceutics 321(1), 1-11.
41. Choi, O., Clevenger, T.E., Deng, B., Surampalli, R.Y., Ross, L. and Hu, Z. (2009) Role of sulfide and ligand strength in controlling nanosilver toxicity. Water Research 43(7), 1879-1886.
42. Mitrano, D., Ranville, J., Bednar, A., Kazor, K., Hering, A. and Higgins, C. (2014) Tracking dissolution of silver nanoparticles at environmentally relevant concentrations in laboratory, natural, and processed waters using single particle ICP-MS (spICP-MS). Environmental Science: Nano 1(3), 248-259.
43. Gunsolus, I.L., Mousavi, M.P., Hussein, K., Buhlmann, P. and Haynes, C.L. (2015) Effects of Humic and Fulvic Acids on Silver Nanoparticle Stability, Dissolution, and Toxicity. Environmental Science & Technology.
44. Gao, J., Powers, K., Wang, Y., Zhou, H., Roberts, S.M., Moudgil, B.M., Koopman, B. and Barber, D.S. (2012) Influence of Suwannee River humic acid on particle properties and toxicity of silver nanoparticles. Chemosphere 89(1), 96-101.
45. Lau, B.L., Hockaday, W.C., Ikuma, K., Furman, O. and Decho, A.W. (2013) A preliminary assessment of the interactions between the capping agents of silver nanoparticles and environmental organics. Colloids and Surfaces A: Physicochemical and Engineering Aspects 435, 22-27.
46. Sikora, F. and Stevenson, F. (1988) Silver complexation by humic substances: conditional stability constants and nature of reactive sites. Geoderma 42(3), 353-363.
47. Dubas, S.T. and Pimpan, V. (2008) Humic acid assisted synthesis of silver nanoparticles and its application to herbicide detection. Materials Letters 62(17), 2661-2663.
48. Litvin, V.A., Galagan, R.L. and Minaev, B.F. (2012) Kinetic and mechanism formation of silver nanoparticles coated by synthetic humic substances. Colloids and Surfaces A: Physicochemical and Engineering Aspects 414, 234-243.
49. Akaighe, N., Depner, S.W., Banerjee, S., Sharma, V.K. and Sohn, M. (2012) The effects of monovalent and divalent cations on the stability of silver nanoparticles formed from direct reduction of silver ions by Suwannee River humic acid/natural organic matter. Science of the Total Environment 441, 277-289.
50. Ostermeyer, A.-K., Kostigen Mumuper, C., Semprini, L. and Radniecki, T. (2013) Influence of Bovine Serum Albumin and Alginate on Silver Nanoparticle Dissolution and Toxicity to Nitrosomonas europaea. Environmental Science & Technology 47(24), 14403-14410.

51. Ferdelman, T.G., Church, T.M. and Luther, G.W. (1991) Sulfur enrichment of humic substances in a Delaware salt marsh sediment core. Geochimica et Cosmochimica Acta 55(4), 979-988.
52. Francois, R. (1987) A study of sulphur enrichment in the humic fraction of marine sediments during early diagenesis. Geochimica et Cosmochimica Acta 51(1), 17-27.
53. Kent, R., Oser, J. and Vikesland, P.J. (2014) Controlled Evaluation of Silver Nanoparticle Sulfidation in a Full-Scale Wastewater Treatment Plant. Environmental Science & Technology.
54. Leung, B.O., Jalilehvand, F., Mah, V., Parvez, M. and Wu, Q. (2013) Silver (I) complex formation with cysteine, penicillamine, and glutathione. Inorganic Chemistry 52(8), 4593-4602.
55. Khan, Z. and Talib, A. (2010) Growth of different morphologies (quantum dots to nanorod) of Ag-nanoparticles: role of cysteine concentrations. Colloids and Surfaces B: Biointerfaces 76(1), 164-169.
56. Kruis, F.E., Maisels, A. and Fissan, H. (2000) Direct simulation Monte Carlo method for particle coagulation and aggregation. AIChE Journal 46(9), 1735-1742.
57. Raychoudhury, T., Tufenkji, N. and Ghoshal, S. (2012) Aggregation and deposition kinetics of carboxymethyl cellulose-modified zero-valent iron nanoparticles in porous media. Water Research 46(6), 1735-1744.
58. Liu, J., Aruguete, D.M., Murayama, M. and Hochella Jr, M.F. (2009) Influence of size and aggregation on the reactivity of an environmentally and industrially relevant nanomaterial (PbS). Environmental Science & Technology 43(21), 8178-8183.

Chapter 5 IMPROVEMENTS TO THE DETECTION OF SIZE AND PARTICLE CONCENTRATION OF SILVER NANOPARTICLES WITH SINGLE PARTICLE ICP-MS.

Connecting text: In earlier chapters, we demonstrated that spICP-MS is capable of quantifying the dissolution and characterizing nAg in complex environmental samples. The results suggested that as nAg dissolved, the silver ions were reformed into secondary particles, nAg_xS_y, due to interactions with inorganic sulfides and organosulfur compounds such as cysteine. Thus, a secondary peak appeared in the nAg size distribution at a mean size smaller than 30 nm due to reformation of particulate silver from Ag^+ ions. Moreover, we observed that nAg in the presence of inorganic sulfides, and DOC compounds such as cysteine and methionine aggregated. As a result, the mean size of nAg increased and particle number concentration in the samples decreased due to aggregation. Therefore, in this chapter the methods and procedures to improve the characterization of various diameters of nAg, from 10 to 200 nm, representative of small and large particles, are developed. Furthermore, the impact of WW matrix on the quality of data by spICP-MS is investigated.

The results of this research will be submitted to the Journal of Analytical Atomic Spectrometry as:

Azodi, M. and Ghoshal, S. **(2017)**, "Characterization of 10 and 200 nm Ag nanoparticles in environmental samples with spICP-MS", **Journal of Analytical Atomic Spectrometry.**

5.1. Introduction

In the past two decades, significant quantities of many engineered nanoparticles (ENPs) have been introduced commercially thanks to their novel properties. There are numerous benefits of nanotechnology, but the rapid growth is associated with an inevitable release of the ENPs in the environment at the end or during their life-cycle (Dunphy Guzman et al. 2006). There has been a growing concern over the potential risk and hazards of the ENPs to the environmental receptors (Nowack and Bucheli 2007, Mueller and Nowack 2008). There is a need to improve the knowledge on the fate and concentration of ENPs in the environment. However, it is essential to first develop reliable analytical methods that are capable of rapid detection of ENPs in environmental matrices.

Some of the most commonly used characterization techniques for measuring the size of metal NPs include electron microscopy, transmission (TEM) (Mock et al. 2002) and scanning (SEM), light scattering techniques, dynamic light scattering (DLS) and nanoparticle tracking analysis (NTA) (Liu et al. 2008), and field flow fractionation (FFF) (Kammer et al. 2011, Fedlheim and Foss 2001). Electron and atomic force microscopy are also widely used for the characterization of NPs. Nevertheless, the presence of background colloids and particles in the environmental matrices can interfere with the data quality obtained from microscopy techniques (Montaño et al. 2016). Light scattering techniques obtain useful information on particle size distribution, but are challenged with environmental samples which often contain trace levels of polydisperse NPs and numerous background particles and colloids which can disrupt the particle size distribution (Pace et al. 2012).

Single particle ICP-MS is a rapid and sensitive elemental analysis technique which is able to detect NPs at mass concentration levels down to part per trillion. spICP-MS provides

information about size distribution, and number concentration, and measures the dissolved analyte which makes it feasible methodology for characterization of ENPs (Tuoriniemi et al. 2012, Telgmann et al. 2014, Olesik and Gray 2012).

spICP-MS has been used to characterize the size of metal NPs (e.g., Ag, Au, TiO2) spiked in various matrices, such as biological tissues (Gray et al. 2013), plant tissues (Dan et al. 2015), fruit juices (Witzler et al. 2016), lake water (Furtado et al. 2014) and sea water (António et al. 2015). This technique is also used to study the release of Ag and TiO_2 from consumer products such as textiles, and food packaging (Mitrano et al. 2014b, Mitrano et al. 2015, Verleysen et al. 2015). Furthermore, development of spICP-MS methods for the detection of ENPs in complex environmental samples has received increasing attention recently (Tuoriniemi et al. 2012, Peters et al. 2015). For example, spICP-MS has been used for the detection of various NPs (i.e. Ag, Au, ZnO) in WW matrices, yet the impact of WW matrix on the quality of data has not been investigated (Mitrano et al. 2012a, Proulx et al. 2016, Yang et al. 2016a, Hadioui et al. 2015). In one study by Telgmann *et al.*, an internal calibration of spICP-MS by the isotope dilution of ^{109}Ag was proposed to compensate for the matrix effect of WW on the particle size of nAg (Telgmann et al. 2014).

The basic methodology of spICP-MS as it is known today was established initially by Degueldre *et al*. for the analysis of colloids (Degueldre et al. 2006, Degueldre and Favarger 2003, 2004). Liquid samples are introduced to spICP-MS for the analysis of NPs on a particle-by-particle basis assuming that a single particle generates a discrete transient pulse whereas the dissolved species generate a continuous baseline signal. The liquid sample is aspirated through a nebulization system that produces an aerosol of droplets. The droplets are then desolvated, atomized and ionized by passing through the plasma. Then they are sorted according to their

mass–to-charge ratio (m/z) in a mass spectrometer. Certain calibration and optimization steps are needed in order to analyze NPs in aqueous matrices accurately (Laborda et al. 2016).

In the early stages of development of this technique, the dwell time was in a range of 3 to 20 ms which caused multiple particle coincidences in a single detection response if the sample was not adequately diluted (Lee et al. 2014, Mitrano et al. 2012a, Montaño et al. 2016, Tuoriniemi et al. 2012). The cloud of ions from a single NP is about 400 to 500 μs. Once the dwell time is longer than the NP event (≥1000 μs), more than one particle can occur within a millisecond dwell time and if the NP suspension is not diluted enough, large dwell time results in particle coincidence and eventually particle events form a continuum response and cannot be detected. At shorter dwell time (≤100 μs), the NP event is larger than the length of dwell time and thus the number of detected points per each single particle event increases from which the signal profile for each NP event is reconstructed (Abad-Álvaro et al.). In addition, spICP-MS system in most of the literature to date have invoked a settling time during data acquisition due to which events are missed or partial events are captured (Mitrano et al. 2012b). New generation of spICP-MS allows for measurements at microsecond dwell times by which relatively higher particle number concentrations can be analyzed and partial particle event integration are eliminated (Hineman and Stephan 2014, Montano et al. 2014, Tuoriniemi et al. 2015, Liu et al. 2014). Nevertheless, this technique requires sufficiently diluted samples to ensure only one particle is measured during each reading period (i.e. dwell time) (Laborda et al. 2013).

Theory. spICP-MS determines the size of particles by correlating the intensity of an event signal directly to the number of atoms of the element in that particle event. Therefore, the mass of the element is then converted to the particle diameter assuming that the particle has a spherical shape, and the density and the mass fraction of the element in the particle are known.

Early in the development of spICP-MS, calibration curves would be prepared by using different NPs of standard size, preferably the same element as the test analyte, so as to relate the signal intensity to the particle mass (or diameter) (Laborda et al. 2011, Olesik and Gray 2012).

When standard particles are not available, an easier calibration route is to relate the intensity of dissolved standards to the mass of the particle suggested first by Pace *et al.* (Pace et al. 2011) This procedure has become the preferred calibration technique, likely because of the costs of obtaining different-sized reference NPs. Those authors proposed that if each detected signal pulse represented one single particle, then the number of events counted during an acquisition time provides the number of particles per unit volume of solution aspirated. However, only a fraction of particles delivered to the nebulizer enters the plasma, and this fraction was defined as the transport efficiency. Pace *et al.* (Pace et al. 2011) calculated the transport efficiency from the signal intensity obtained from aspirating 60 nm gold reference nanoparticles and the total (known) mass of gold in the sample. Thus the transport efficiency (η_n) is then found using the pulse frequency of 60 nm gold NPs at a certain particle concentration, $f(I_P)(no.of\ pulses/ms)$, flow rate, $q_{liq}\ (mL/ms)$, and particle number concentration, N_P, by following equation (Pace et al. 2011);

$$\eta_n = \frac{f(I_P)}{q_{liq}N_P} \qquad (5\text{-}1)$$

Another method of calculation of the transport efficiency involve determining the analyte mass reaching the plasma by comparing the waste volume to the sample uptake volume (Smith and Browner 1982, Olson et al. 1977, Gustavsson 1984).

For the determination of particle size in samples, first the signal intensity, (I_p), obtained is correlated to the concentration of the analyte, C (µg/mL), using a dissolved standard

calibration curve (Figure 5-6 S1). Then, the total mass of each event, W (µg/event), transported as:

$$W = \left[\eta_n q_{liq} t_{dt} C\right] \quad (5\text{-}2)$$

where, $t_{dt}, (ms/event)$, is the dwell time. Dwell time is the time spent by the quadrupole to analyze each mass-to-charge ratio (m/z) (Hineman and Stephan 2014). The intensity of each individual pulse is converted to particle mass, m_P, and particle diameter, d, using the slope, m, and y-intercept, b, by following equations;

$$m_P = f_a^{-1}\left[\frac{\left((I_P - I_{Bgd})\varepsilon_i\right) - b}{m}\right] \quad (5\text{-}3)$$

$$d = \sqrt[3]{\left[\frac{6m_P}{\pi\rho}\right]} \quad (5\text{-}4)$$

Where $\varepsilon_i$is the particle ionization efficiency; shown to be 100% for nAg (80 nm) and nAu (60 nm) in the study by Pace *et al.* (Pace et al. 2011), where f_a is the mass fraction of the analyzed element, and ρ is the particle density.

In this study, we propose that the analysis approach described above that can be improved in two ways. First, we propose a range of dwell times to be employed depending on particle sizes and concentrations, and particularly a shorter than usual dwell time of 10 µs to improve the detection of small NPs. Secondly, we propose the use of particle size-appropriate transport efficiencies. To the best of our knowledge, all spICP-MS studies in the literature have employed 60 or 100 nm gold reference NPs for determining the transport efficiency (Lee et al. 2014, Pace et al. 2011), irrespective of the target particle sizes analyzed. We hypothesize that the fraction of ions from a gold nanoparticle that reaches the detector will change with particle diameter, and thus a 60 nm gold reference particle may not be as suitable for use in analyses of

NPs of significantly different diameter as gold reference particles closer to the sizes being analyzed.

Previous studies have calculated a size detection limit between 13-20 nm for nAg analyzed with spICP-MS at millisecond dwell times (Lee et al. 2014, Tuoriniemi et al. 2012). Very few studies have reported on the improvement to the resolution of spICP-MS for the detection of small sized nAg (Tuoriniemi et al. 2015). Cornelis and Hasselöv demonstrated an efficient deconvolution data analysis method for detection of small nAg (<30 nm) by using a Polygaussian probability mass function to described the background signal and therefore discriminate the particle signal at millisecond dwell times (Cornelis and Hassellöv 2014). To the best of our knowledge, no study by far has analyzed nAg as small as 10 nm neither as large as 200 nm using spICP-MS and obtained accurate mean particle size.

In this study, standard nAg of a very wide size range, 10, 20, 80, 200 nm, was analyzed using spICP-MS at different concentrations (10 ppt to 2000 ppt) in DI water and WW. Signal intensities obtained were used to derive particle dimeters using the transport efficiencies obtained from the commonly used 60 nm gold reference NPs and with gold reference NPs with a comparable size to the test nAg. Furthermore, the results obtained from spICP-MS are compared with the mean size of nAg attained from TEM.

The effectiveness of the use of different-sized gold reference NPs and short (10 and 100 µs) dwell times was verified with samples of nAg spiked in DI water and in WW (mixed liquor). WW samples were used to assess the impact of WW matrix on the detection of size and NP number concentrations. nAg was the target analyte because of their common use in many consumer products (e.g. textiles) (Nogi 2012) and its toxicity to aquatic organisms (Kim et al. 2007). When analyzing environmental (water) samples for NPs, it is important to optimize

spICMS methods to account for the possible presence of NPs of a large range of sizes. Environmental processes may result in greater polydispersity of NPs and enabling analytical techniques need to be able to characterize such polydispersivity. For example, agglomeration of NPs can result in the formation of large aggregates in the environment (Hotze et al. 2010). On the other hand, nAg is shown to dissolve under aerobic condition and the dissolved Ag^+ ions can form secondary NPs which have diameter between 2 to 20 nm (Pal et al. 1997).

5.2. Material and Method

5.2.1. Instrumentation

SPICP-MS A Perkin Elmer NexION 300X ICP-MS supported by Syngistix software (ver1.1.) was used in single particle mode for nAg characterization. The torch alignment and nebulizer gas flow of spICP-MS were optimized for the highest sensitivity to Ag for daily optimization of the instrument. The integration dwell time of 10, 50, 100, 1000, and 3000 µs were used depending on the analysis. A total data acquisition time of 100 s was set for samples in general and for the aged samples and the samples in WW, the sample time was increased up to 180 s. Other instrumental parameters are presented in Table 5-2 S1. Three calibrations were prepared before analysis in single particle. The first was the dissolved calibration curve was performed by preparing the dissolved Ag standard solution of 1001±4 ppm in 4% HNO_3 (PlasmaCAL) in 4-5 dissolved Ag solutions (0-5 ppb) and including one blank in 1% HNO_3. The second calibration was performed using the standard reference Au NPs (NIST), with a nominal 20, 60 and 100 nm diameter at a concentration of 207 ppt (9.5×10^4 particles/mL) in DI water in order to estimate the transport efficiency of NPs and therefore the particle number concentration in the test samples. The third calibration was performed by aspirating three sizes of standard nAg

(30, 50, 100 nm) to relate the signal intensity by each particle to the mass/mean size of nAg. The transport efficiencies obtained at each dwell time are presented in Table 5-1.

TEM- TEM was used for sizing and characterization of nAg was Philips CM200 TEM, operated at 200kv and the CCD camera was AMTv600 Camera. To prepare nAg for TEM anlaysis, 10 µL of nAg at 200 ppb, for 10, 20, and 80 nm, and 1 ppm for 200 nm, was deposited on the copper TEM substrates (Electron Microscopy Sciences, Carbon film 200 mesh copper grids). The grids were kept in dark and were air-dried.

5.2.2. Samples and sample processing

Silver nanoparticles- Citrate-coated NanoXact nAg (NanoComposix) with nominal size of 10, 50, 200 nm and a stock concentration of 20 ppm (5.1×10^{12} particles/mL), 22 ppm (2.5×10^{10} particles/mL), 22 ppm (5.5×10^{8} particles/mL) respectively were purchased. PVP-coated NanoXact nAg (NanoComposix) with nominal size of 30, 80, 100 nm at a stock concentration of 22 ppm (1.5×10^{11} particles/mL), 23 ppm (8.4×10^{9} particles/mL), 21 ppm (3.2×10^{9} particles/mL) were purchased. TEM analysis of 10, 20, 80 and 200 nm nAg yielded a mean size of 8.2±3.5 nm (n=150), 8.1±2.1 nm (n=150), 76.1±9.7 nm (n=110), and 189±33 (n=110) respectively (Figure 5-7, S2).

Gold nanoparticles- 20 nm PELCO Tannic NanoXact gold (TedPella) at stock concentration of 50 ppm (6.81×10^{11} particles/mL), 60 nm NIST standard gold at stock concentration of 2.38×10^{10} particles/mL, and 100 nm PELCO Tannic NanoXact gold (TedPella) at stock concentration of 50 ppm (4.94×10^{9} particles/mL) were purchased to estimate the transport efficiency of spICP-MS after dilutions down to 207 ppt.

Samples of WW and sulfides- Experiments were conducted in 15 mL polypropylene conical tubes (Falcon™). The WW mixed liquor samples collected from the activated sludge

basin at the WW treatment facility near Montreal. The WW specimens were first filtered using 0.45-micron cellulose acetate filters (Corning) and transferred to the tubes. PVP-nAg of various sizes was suspended in the WW specimens in a range of concentrations depending on the experiment. nAg was also exposed to Na_2S solution prepared in DI water at S:Ag=0.5 to 1.

5.3. Results and Discussion

5.3.1. Optimization of dwell time and transport efficiency for analyses of 10 nm nAg

Comparison of measured transport efficiency. The transport efficiency was calculated at two dwell times, 10 and 100 μs, using three standard nAu (20, 60, 100 nm). The results in Table 5-1 show that the transport efficiency varied as the dwell time changed, because the pulse intensity of the reference nAu changes with the dwell time, consistent with Equation 1 (Figure 5-8 S3). In addition, the transport efficiency decreased with smaller standard nAu due to a decrease in the pulse intensity of the particle in response to the smaller mass of the particle. The transport efficiency decreased significantly with nAu of 20 nm, compared to that typically derived using 60 nm nAu (Table 5-1). Therefore using the transport efficiency of standard 60 nm nAu for analysis of nAg that have a diameter considerably smaller than 60 nm may not be appropriate which is discussed in the next section.

Table 5-1- Transport efficiency gold reference NPs at different dwell times

Dwell time (μs)	Transport Efficiency 20 nm nAu%	Transport Efficiency 60 nm nAu %	Transport Efficiency 100 nm nAu%	Sample time (s)
10	4.2±0.2	17.9±2.3	7.6±1.6	50
100	1.1±0.3	9.9±1.4	7.1±1.1	100

Mean size of 10 nm nAg at two different transport efficiencies. The 10 nm nAg was aspirated at two dwell times; 10 and 100 µs. spICP-MS estimated a mean size equal to 13±0.9 and 19.6±0.2 nm respectively at silver mass concertation of 50 ppt at dwell time 10 and 100 µs respectively using the transport efficiency of 60 nm nAu and a dissolved standard silver calibration (Figure 5-1A). The dwell time, and the transport efficiency can greatly affect the measurement accuracy of NP size by spICP-MS. Millisecond dwell time (i.e. 1000 µs) was not adequately short for the analysis of 10 nm nAg, and resulted in counting of multiple NPs as one event (particle) in such a long dwell time, which overestimated the particle mean size. Analysis of 10 nm nAg at 100 µs dwell time and transport efficiency of 60 nm obtained a wide size distribution between 15 to larger than 30 nm which confirmed the multiple counting of events (Figure 5-9 S4). In addition, the continuous background signal increases with an increase in dwell time while the signal from a single particle does not (Hineman and Stephan 2014) and detection of 10 nm nAg becomes less accurate. Tuoriniemi *et al.* that found a mean size of about 30 to 40 nm for the analysis of nAg with nominal size of 20 nm at dwell time 5000 µs. In this study, at long dwell time of 1000 µs, even though 20 nm nAg particle events were detected, the mean size was severely overestimated by up to 100% (Figure 5-10 S5A).

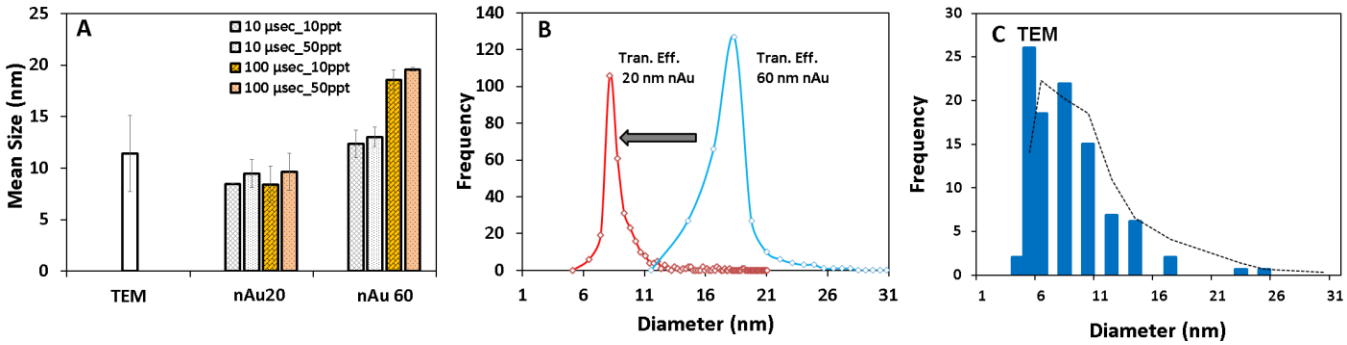

Figure 5-1- 10 nm PVP- nAg characterized with spICP-MS in DI water; (A) The impact of two dwell times and two silver mass concentrations on particle mean size at two different transport efficiencies. (B) Particle size distribution of nAg at two different transport efficiencies, first with

standard NIST 60 nm nAu and second with 20 nm nAu at dwell time 100 µs and an initial concentration of 10 ppt; (C) Particle size distribution of 10 nm nAg with TEM

TEM analyses of 10 nm nAg obtained a mean size of 8.2±3.5 nm (n=150) (Figure 5-1C and 5-7 S2). The particle size distribution (Figure 5-1) showed that 78.8 % of total number of particles sized with TEM were equal or below 10 nm whereas spICP-MS detected no particle with diameter smaller than 10 nm at either of 10 or 100 µs dwell time, using the 60 nm nAu derived transport efficiency.

The 10 nm nAg suspension was reanalyzed by repeating the standard dissolved calibration curve using the transport efficiency of 20 nm nAu, instead of NIST 60 nm nAu and the dissolved standard silver calibration. The mean size obtained by the modified transport efficiency was 8.4±0.5 and 9.5±0.7 nm at dwell time 10 µs and was 8.4±0.9 and 9.6±0.8 nm at dwell time 100 µs for 10 and 50 ppt nAg mass concentration respectively (Figure 5-1A). The particle size distribution obtained after application of the modified transport efficiency with 20 nm nAu (Figure 5-1B) clearly shows a more comparable particle sizing to that of TEM analysis. It was observed that the transport efficiency derived from 60 nm nAu is significantly larger than those derived from nAu of similar size to that of the nAg target sample, which resulted in overestimation of the size of nAg according to Equation 2. The transport efficiency of 20 nm nAu was also applied for analysis of 20 nm nAg and attained a mean size of 8.5±0.7 nm which was in agreement with the mean size by TEM (8.2±3.5 nm) (Figure 5-10 S5 B) and could be due dissolution of nAg in the stock solution over several months storage. This study for the first time demonstrates the significance of the size of the reference nAu for determination of transport efficiency.

Different approaches have been reported for addressing the inconsistencies in particle size measurements at long dwell times. In the study by Cornelis and Hassellöv they developed a

signal deconvolution method, which helped in the detection of nAg smaller than 30 nm at 3-5 µs dwell time that otherwise were not detected at such long dwell times (Cornelis and Hassellöv 2014). Nevertheless, they applied 60 nm reference gold NP for transport efficiency determination and the NP size distribution obtained for nAg (10, 15 and 30 nm) was wider than the size distribution attained from TEM analysis. In addition, Lee *et al.* calculated the detection limit of spICP-MS as 13 nm for nAg by considering 3 times above the standard deviation of background signal obtained for silver in DI water, as well as knowing the NP density, the mass fraction of analyzed metallic element in the nanoparticle and sensitivity of detector for silver (Lee et al. 2014). The particle limit of detection for nAg was determined at 18 nm at 5000 µs dwell time and the analysis of 10 nm nAg only resulted in distorted Poisson profile characteristic of dissolved silver which indirectly provided an evidence of the presence of NP (Laborda et al. 2011). In contrast, in our study, we improved the detection for target nAg with nominal size of 10 and 20 nm by using more relevant dwell times and nAu sizes to derive a reliable transport efficiency.

5.3.2. Optimization of dwell time and calibration method for analyses of 200 nm nAg

To evaluate the impact of transport efficiency on the means size measured by spICP-MS, a separate set of experiments were conducted using 100 nm standard nAu to calculate the transport efficiency. The transport efficiency of 100 nm nAu was 7.63 and 7.11 % at 10 and 100 µs dwell times respectively (Table 5-1). The NP suspension of 200 nAg at three silver mass concentration (100, 500 and 1000 ppt) was re-analyzed using the modified transport efficiency aspirated at two dwell times, 10 and 100 µs. spICP-MS measured the mean size of 138.8±15.6 nm and 131.3±14.7 nm for 200 nm nAg suspension (500 ppt) analyzed at dwell time 10 and 100

μs respectively with the modified transport efficiency of 100 nAu. Transport efficiency using 100 nm nAu was not considerably different from that of 60 nm nAu at dwell time 100 μs and likely, due to which the mean size did not change significantly. The mean size was recalculated using the NP calibration and this time the mean sizes were measured at 185.9±15.3 nm and 178.8±15.7 nm.

spICP-MS analysis of 200 nm nAg at 500 ppt suspended in DI water at dwell time 10 and 100 μs attained a mean size of 175.2±16.3 and 140.6±13.1 nm using a dissolved silver calibration and the transport efficiency of 60 nm reference nAu (Figure 5-2A). The 200 nm nAg suspension was analyzed also at longer dwell times (1000 and 3000 μs) and at larger silver mass concentration (up to 2000 ppt) with the same calibration. There was a significant decrease in mean size of 200 nm nAg to 109.4±1.4 nm once the analysis was repeated at 3000 μs instead of 10 μs dwell time (Figure 5-11 S6) at 500 ppt silver mass concentration. The TEM analysis of the same nAg suspension attained a mean size of 189±33 nm (Figure 5-2C, and 5-7 S2). The results suggested that the longer the dwell time, the smaller the mean size obtained. The transit time through the detector for 200 nm nAg is longer than the dwell time (i.e. 10 μs). Thus, the more accurate assessment of the mean size of nAg at 10 μs dwell time is attributed to the larger number of points per peak for a single particle at shorter dwell time.

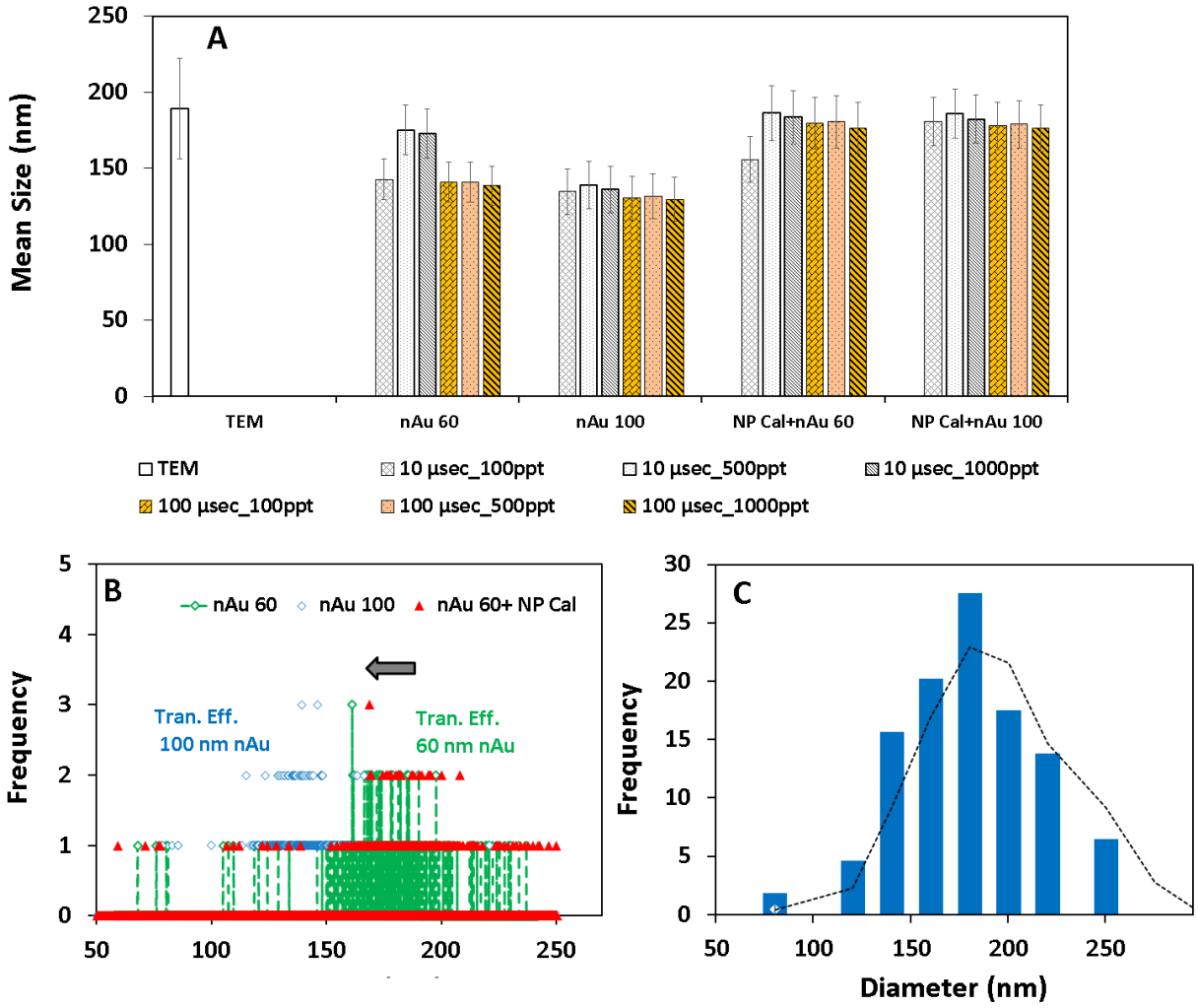

Figure 5-2- The impact of dwell time, transport efficiency and NP calibration on (A) the mean size of 200 nm nAg suspension; (B) the particle size distribution. (C) The particle size distribution of 200 nm nAg with TEM.

An increase in total nAg mass concentration from 100 to 1000 ppt, resulted in the increase in mean size from 142.7±13.3 nm to 172.6±16.1 nm respectively. It was noted that the number of peaks detected for 200 nm nAg at 100 ppt silver mass concentration was 72±12 at 10 µs dwell time whereas for a reliable detectability a minimum of 200 peaks is required. Detectability of adequate number of peaks is directly related to the sample time, and due to instrument limitations it could not be increased to longer than 50 s at 10 µs dwell time. The particle number concentration of nAg at 100 ppt silver mass concentration with a diameter equal

to or larger than 200 nm was calculated at 82.4 particles/mL at 100 µs dwell time. However, by increasing the silver mass concentration to 1000 ppt, the particle number concentration with diameter equal or larger than 200 nm increased to 1071.9 particles/mL. This is consistent with TEM analyses, which provided a mean size of 189±33 nm (n=120) of which 34.9 % of particles had a diameter of 200 nm or larger (Figure 5-2C).

Dissolved standard silver calibration is a common method to correlate the signal intensity to the silver mass and then NP diameter (Equation 2 and 3). This method first developed by Pace *et al.* assumes that if the transport efficiency of the system is known it can account for the differences in the mass delivery of dissolved *versus* a single NP (Pace et al. 2011). Whereas, before the dissolved calibration was used, a standard NP calibration had to be made which plots the pulse intensity *versus* the NP diameter of reference standards of specific particle sizes. The standard NP calibration was used to determine the diameter and the size distribution of nAg in an unknown sample (Laborda et al. 2011, Olesik and Gray 2012). The difference between the two calibration curves is that the dissolved standard assumes that ions from a dissolved standard solution and ions from a nanoparticle (the same analyte) once past the plasma will behave comparably. However, in Equation 2 to 4 described it is assumed that the ionization efficiency, η_i, is the same for the analyte of both dissolved and NP form and therefore η_i is equal to one. Therefore, the relationship described by following equation can be used to determine the diameter and size distribution of nAg where r_{NP} is the signal corresponding to a single NP and K is the slope of the NP calibration curve which is constant for a specific set of instrumental conditions (Laborda et al. 2011);

$$r_{NP} = Kd^3 \qquad (5\text{-}5)$$

In a second set of experiments, the NP calibration curve using monodisperse standard nAg (30, 50 and 100 nm) was plotted (Figure 5-12 S7) besides the standard dissolved Ag calibration in order to evaluate the mean particle size determined for large nAg using the two different calibrations. In this study, the mean size of 200 nm nAg increased to 186.2±17.8 nm from 175.2±16.3 by applying the standard NP calibration at dwell time 10 μs (Figure 5-2A). The difference in mean size attained from the two calibration curves suggested that the earlier assumption about the ionization efficiency was not applicable for 200 nm nAg. Pace *et al.* also suggested a variation in ionization efficiency is likely with increasing particle size (Pace et al. 2011). Our results demonstrate that applying the NP calibration can help improve the determination of the mean size for larger nAg.

Similarly a suspension containing 80 nm nAg at five total silver mass concentrations (50-1000 ppt) by serial dilutions of the stock of at 20 ppm (nominal 10^{11} particles/mL) was prepared. Then the samples were continuously aspirated as the dwell time varied from 10 to 3000 μs, once using the standard dissolved silver calibration and another time using the NP calibration (Figure 5-13 S8). The results showed that NP calibration improved the mean size measured for 80 nm nAg (81.5±1.5 nm) at 100 ppt silver mass concentration and at 100 μs dwell time which was in closer agreement with the mean size attained by TEM (76.1±9.9 nm, n=100) (Figure 5-13 S8 C).

5.3.3. Characterization of nAg in WW

Environmental samples often contain soluble and particulate background compounds such as DOC, ions, colloids, etc. which makes the detection of any occurring NP (i.e. nAg) challenging due to the considerable levels of background organic and inorganic compounds as compared to clean aqueous samples, which can increase the noise or continuous background signal which is called the matrix effect. To investigate the impact of matrix of municipal WW on

the characterization of nAg (10 and 200 nm), an initial mass concentration of 100 ppt of nAg were suspended in a specimen of WW mixed liquor (0.45 micron filtered), and DI water. Moreover, the same concentration of NPs was suspended in the samples containing 1, 10, 20, 50% WW mixed liquor prepared by diluting the WW mixed liquor by DI water. The WW mixed liquor specimen were first analyzed for any significant background dissolved or particulate silver before it was spiked with nAg. The background dissolved silver was very small and measured at 0.006±0.001 ppt and there was no detectable particles.

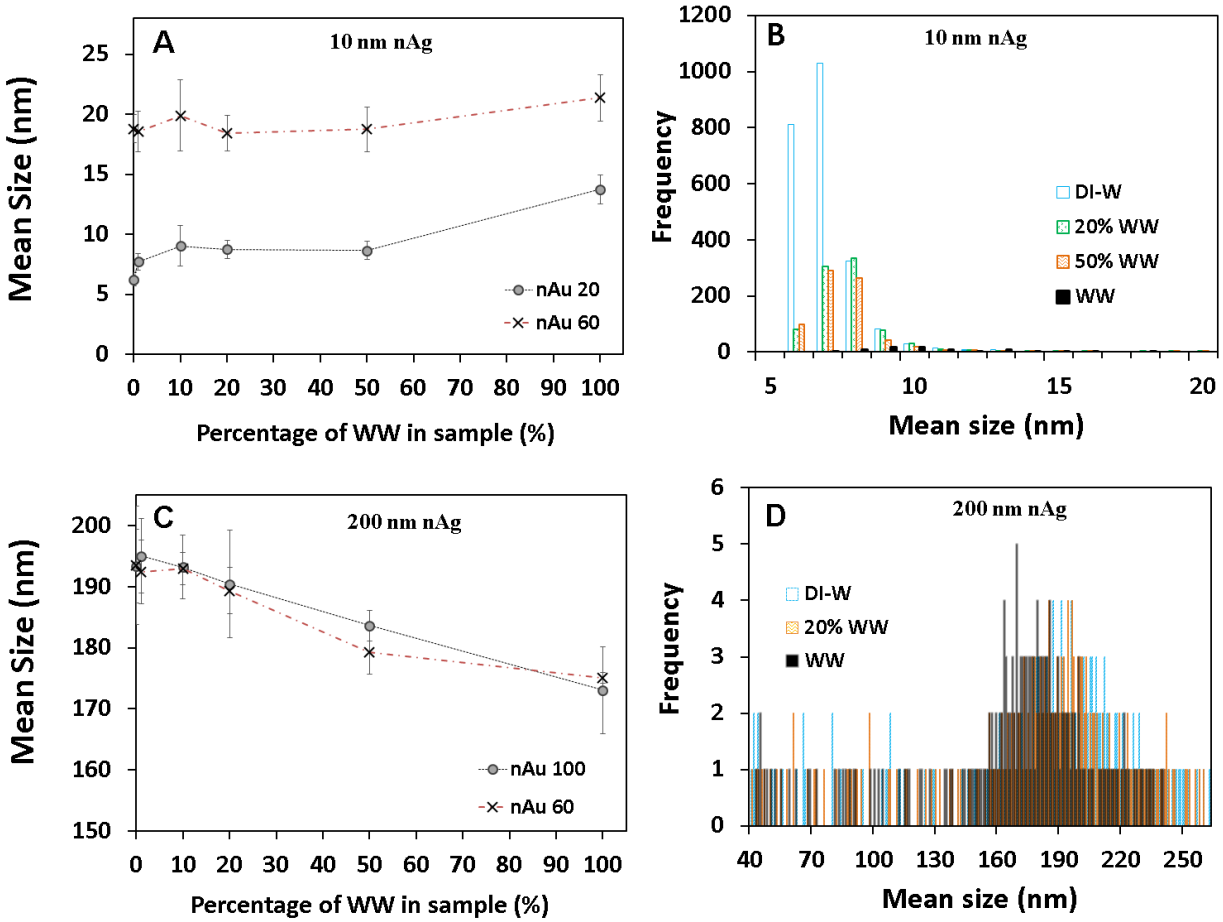

Figure 5-3- The impact of WW matrix on the particle mean size (A) 10 nm; (B) 200 nm nAg, and on the NP size distribution (C) 10 nm; and (D) 200 nm nAg.

The result showed that the particle size distributions and mean size were both affected as the fraction of WW in the medium increased (Figure 5-3A-D). The mean size of 10 nm nAg was

6.2±0.5 nm and 13.7±1.2 nm in DI water and undiluted WW mixed liquor. The WW mixed liquor was diluted 100 times with DI water and the mean size for this sample measured at 7.7±0.7 nm (Figure 5-3A). The particle histogram shifted considerably to larger particle diameters as the fraction of WW in solution increased. For an undiluted WW sample, the frequency of peaks decreased and fewer particle events were detected (Figure 5-14 S9 A). As a result, the particle counting decreased and the particle number concentration measured was 2.9×10^4 particles/mL in undiluted WW *versus* 7×10^6 particles/mL that was measured in DI water. Detectability of small particles, such as 10 nm nAg in this study, are likely to be more affected in as such complex, high background samples. As the WW fraction in the sample increased, the background signal also continuously increased, whereas the signal generated by a single particle remained the same. Thus, it became more difficult to differentiate between the background and the particle signal. It was concluded that the ion plume generated by the ionization of 10 nm nAg was small enough to be affected by the background signal and was not detected as a particle event. Moreover, most of the particle events detected in undiluted WW were larger than 10 nm (Figure 5-3B).

However, an opposite trend for the mean size of 200 nm nAg in WW specimen was observed (Figure 5-3C&D). The mean size of 200 nm nAg was measured at 193.3±6 and 173.1±7 nm in DI water and undiluted WW respectively. The result showed that as the WW was diluted less the spICP-MS measured a smaller mean size for nAg (Figure 5-3C). The particle size histogram also slowly moved to smaller particle diameters. The particle number concentration did not change considerably and remained relatively stable in all systems. Similar experiments were conducted with 80 nm nAg in DI water and various dilutions of WW mixed liquor.

Although mean size decreased as the fraction of WW in solution increased, the particle number concentration was not affected (Figure 5-15 S10).

The matrix of WW mixed liquor, once it was larger than 20% of total volume of the solution, posed a significant effect on sizing accuracy of the spICP-MS. The result of this study suggests that adequate dilution of environmental samples such as WW before analysis helped to eliminate the matrix effect. Nevertheless, the environmental samples often contain trace levels of nAg (ppt-ppb) (Gottschalk et al. 2009, Keller et al. 2013) and therefore further dilutions can result in low counting statistics. One strategy to alleviate the low counting statistics is to increase the sample time which is typically chosen between 60 to 100 s for the analysis of a commercial nAg but can be increased to 180 to 200 s at dwell time larger than 100 µs (Figure 5-16 S11). In addition, increasing the sample time can also help to eliminate the arbitrary peaks.

5.3.4. Particle counting efficiency

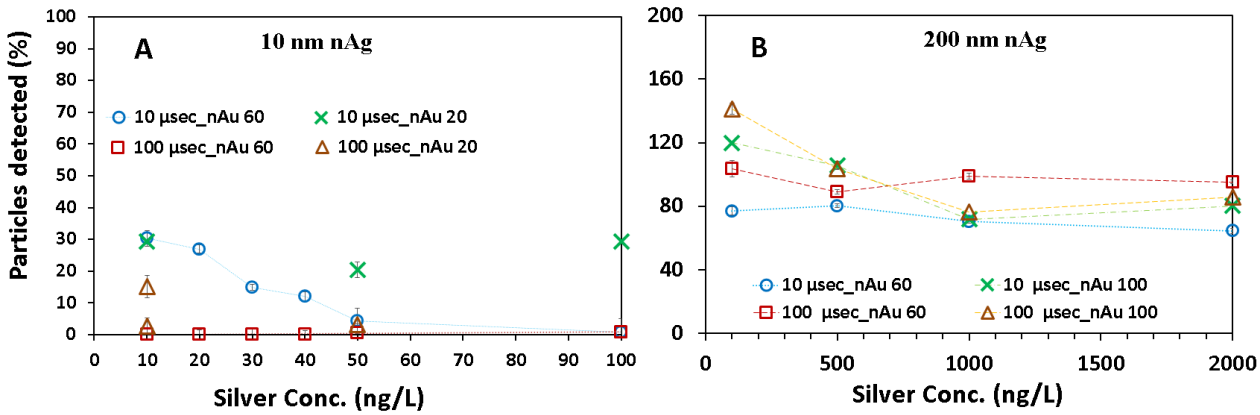

Figure 5-4- The impact of dwell time and silver mass concentration on particle counting efficiency of (A) 10 and; (B) 200 nm nAg, at two different transport efficiencies.

The particle counting of 10 nm nAg with spICP-MS was also greatly impacted by both the transport efficiency and the dwell time. The number of particles detected in a NP suspension by spICP-MS was determined at various dwell times (10 to 3000 µs) and normalized to the

nominal particle number concentration to attain percent of particles detected. Increasing the silver mass concentration in the solution from 10 to 50 ppt, the particle counting efficiency decreased to below 10% at 10 µs dwell time and only 1% of total number of particles were detected at the dwell time 100 µs (Figure 5-4A). The sample of 10 nm nAg suspension in DI water contains 2.55×10^7 particles/mL that is equal to 100 ppt silver mass concentration. At such a high particle number concentration, the risk of particle coincidence substantially increased which resulted in poor counting efficiency. Furthermore, recalculating the transport efficiency by 20 nm nAu improved the counting efficiency to 24.5±2.5 and 27.9±0.2 % for the analysis for nAg suspensions at 50 and 100 ppt respectively at 10 µs dwell time.

Similar to 10 nm nAg, the change in dwell time affected the particle counting of 200 nm nAg but in a less dramatic fashion. The number of particles detected in a suspension containing 200 nm nAg (100-2000 ppt) was determined at various dwell times (10 to 3000 µs) (Figure 5-4B). Number of particles decreased as the silver mass concentration in the solution increased at a certain dwell time. spICP-MS analysis of 200 nm nAg suspension in DI water at 100 and 2000 ppt mass concentration at 10 µs dwell time attained 76.9±2.3 and 64.4±0.9 % counting efficiency respectively, whereas it improved to 103.4±6.4 and 95.3±8.7 % counting efficiency for the analysis of the respective samples at 100 µs.

Similar experiments were conducted to evaluate the counting efficiency of 80 nm nAg at various dwell times by spICP-MS. It was observed that, more than one order of magnitude increase in initial silver mass concentration (100 to 2000 ppt) had little impact on the particles number concentration at a certain dwell time (Figure 5-13 S8 D).

5.3.5. Analysis of an unknown sample with spICP-MS

spICP-MS can be used for the detection of nAg in an unknown environmental sample or characterization of nAg in a spiked sample. However, certain preliminary analyses are required to determine the most optimum condition (dwell time, transport efficiency) are discussed in this section (Figure 5-5).

Long dwell time adversely affects the precision of mean size and particle size distribution as previously discussed (Figure 5-17 S12). Therefore, to start the shortest possible dwell time to analyze an unknown environmental sample is chosen. The matrix effect can be easily eliminated by diluting the sample prior to the analysis with pure water. Dilution with DI water also helps to avoid multi-counting due to particle coincidences in the spiked samples with high concentration of nAg (Figure 5-18 S13). However, environmental samples often contain trace concentration of nAg and further dilution of the sample can result in poor counting statistics, or no detection.

Thus, a recommended procedure for analysis is as follows. First, calculate the transport efficiency using 60 nm reference nAu and conduct a standard dissolved silver calibration. Then, analyze the sample at 0-2 time dilution at a sample data collection time between 50 and 100 sec. If the mean size obtained from the analysis is smaller than 80 but larger than 30 nm, and the counting statistics falls in an acceptable range (300-700 peaks), repeat the analysis at one or two larger dilutions with DI water to remove any matrix effect. In addition, run the analysis at one or two other dwell times, one larger and one smaller than the initial dwell time, in order to verify the mean size attained. Unless, the counting statistics is far below the acceptable range, then repeat the analysis only by choosing one or two other dwell times.

If the mean size of nAg obtained from the preliminary analysis is larger than 80 nm and the counting statistics falls in an acceptable range, conduct a standard NP calibration using three

or more standard nAg with well-characterized mean size. Dilute the sample a few times (2-10x) and repeat the analysis using the same transport efficiency and the dissolved and NP calibration curves and the sample data collection time of 180-200 s for both diluted and original sample. However, if the counting statistics is poor, concentrate the sample by centrifugal ultrafiltration, collect the NPs on the filter and repeat the analysis after dilution, 2-100 time, depending on the number of particles detected in the preliminary analysis. Recalculate the mean size and particle distribution by applying NP calibration. In addition, increase the sample data collection time to 180-200 s to increase the number of peaks detected.

If the mean size of nAg obtained from the preliminary analysis is smaller than 30 nm, recalculate the transport efficiency by using 10 or 20 nm standard nAu. Choose the shortest dwell time (i.e. 10 μs) in order to omit any particle coincidences. If the counting statistics fall in the acceptable range, dilute the samples between 10-1000 times, and repeat the analysis using new transport efficiency and 10 μs dwell time. If the counting statistics is poor, concentrate the specimen by centrifugal ultrafiltration, choose a longer dwell time, increase the sample time to 180-200 s and repeat the analysis using the modified transport efficiency. Once the counting statistics improved after second analysis, repeat the analysis for the third time at 10 μs dwell time in order to verify the mean size obtained and reduce the chance of particle coincidence due to improperly long dwell time.

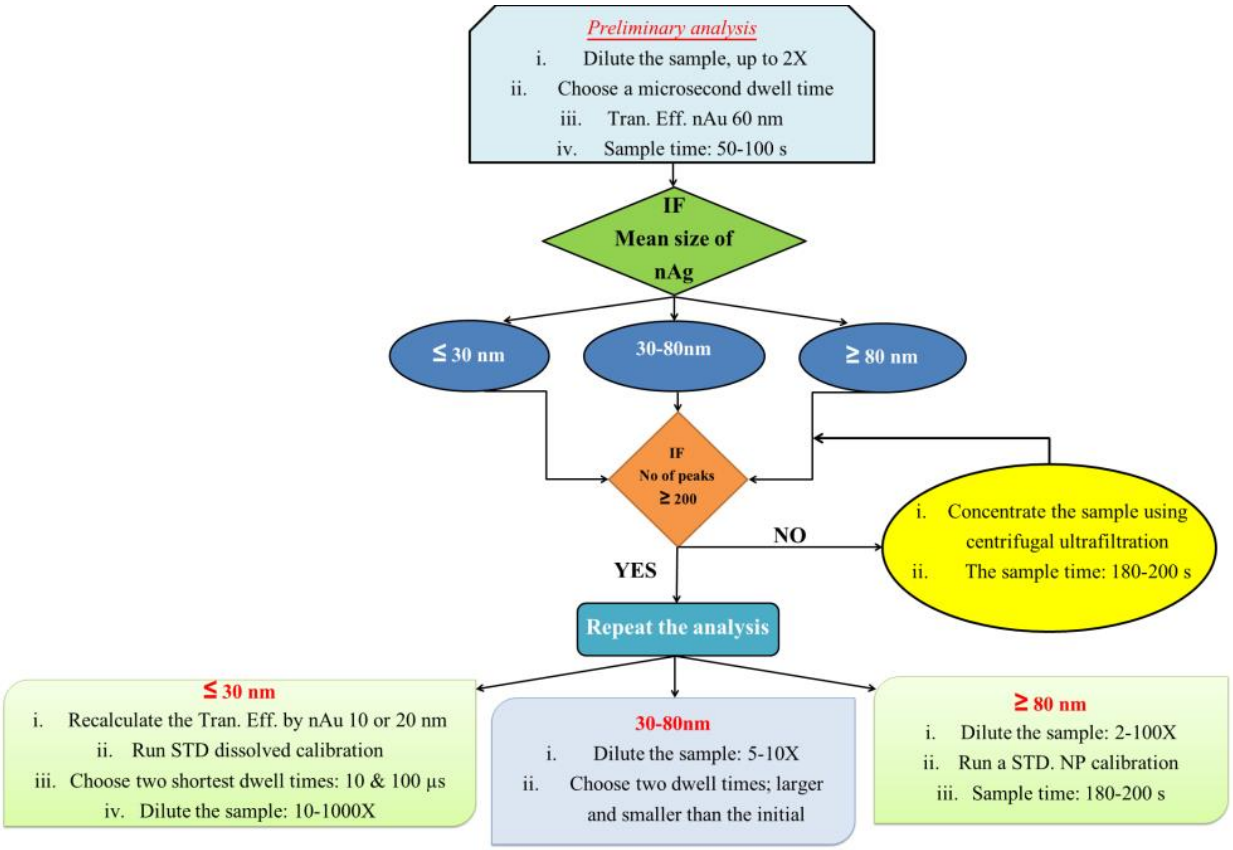

Figure 5-5- Schematic for the detection of nAg in unknown environmental samples with spICP-MS

5.4. Conclusion

This paper for the first time provided a procedure for detection of nAg 10 nm while previous literature reported that the smallest detectable nAg has been 13 nm. Using 20 nm standard nAu instead of the conventional 60 nm NIST nAu to determine the transport efficiency combined with dwell time of 10 µs greatly improved the particle mean size of 10 nm nAg. While for the smaller nAg, 10 and 20 nm, 10 µs dwell time significantly improved the sizing and counting efficiency of nAg as compared to the analysis at 100 µs dwell times, the sizing and counting accuracy of nAg of 200 nm at both dwell times were comparably similar.

The influence of transport efficiency, the optimum dwell time, sample data collection time, and dilutions with DI water on the accuracy of particle mean size and particle counting efficiency was investigated for several nAg suspensions (10, 20, 80 and 200 nm). Moreover, this paper for the first time suggested a procedure for the detection of nAg in an unknown environmental. The result suggest that for the analysis of unknown samples, first run a preliminary analysis to find out the size range of nAg; below 30 nm, 30-80 nm, or above 80 nm. Then according to the size range, recalculation of the transport efficiency, addition of standard NP calibration, manipulation of data collection time, and further dilution or concentration of the sample may be required.

5.5. Acknowledgments

We thank David Liu, McGill, for TEM analysis of nAg. Funding from Natural Sciences and Engineering Research Council, Canada (Grants STPGP 430659 – 12), Environment and Climate Change Canada, Perkin Elmer Health Sciences Canada, and SNC Lavalin Environnment, is gratefully acknowledged.

5.6. Supplementary data

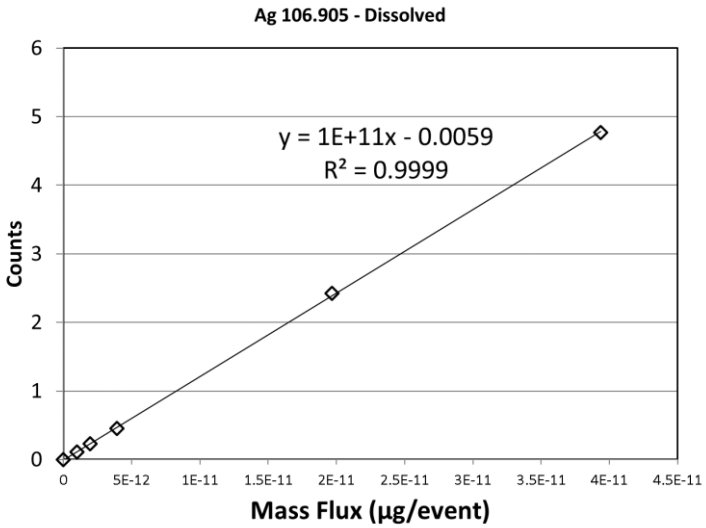

Figure 5-6 S1- Standard dissolved silver calibration

Table 5-2 S1- NexIon 300X ICP-MS Instrumental Parameters

Parameter	Value
Sample Uptake Rate	0.295 mL/min
Nebulizer	Glass Concentric
Spray Chamber	Glass Cyclonic
RF Power	1600 W
Analyte	Ag107
Analysis time	50-180 sec
Dwell time	10, 50, 100, 1000 & 3000 µsec

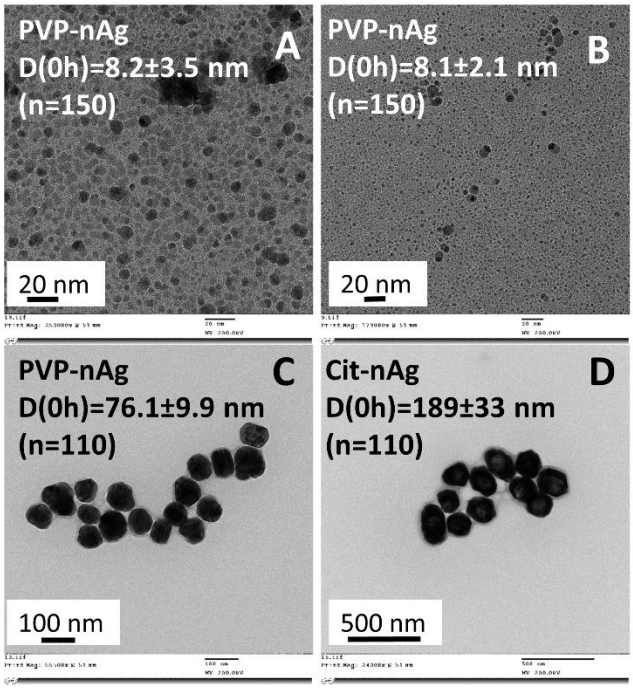

Figure 5-7 S2- nAg with nominal sizes of 10, 20, 80 (PVP-coated) and 200 nm (Cit-coated) analyzed with TEM and the mean size was calculated with sizing more than 100 NPs.

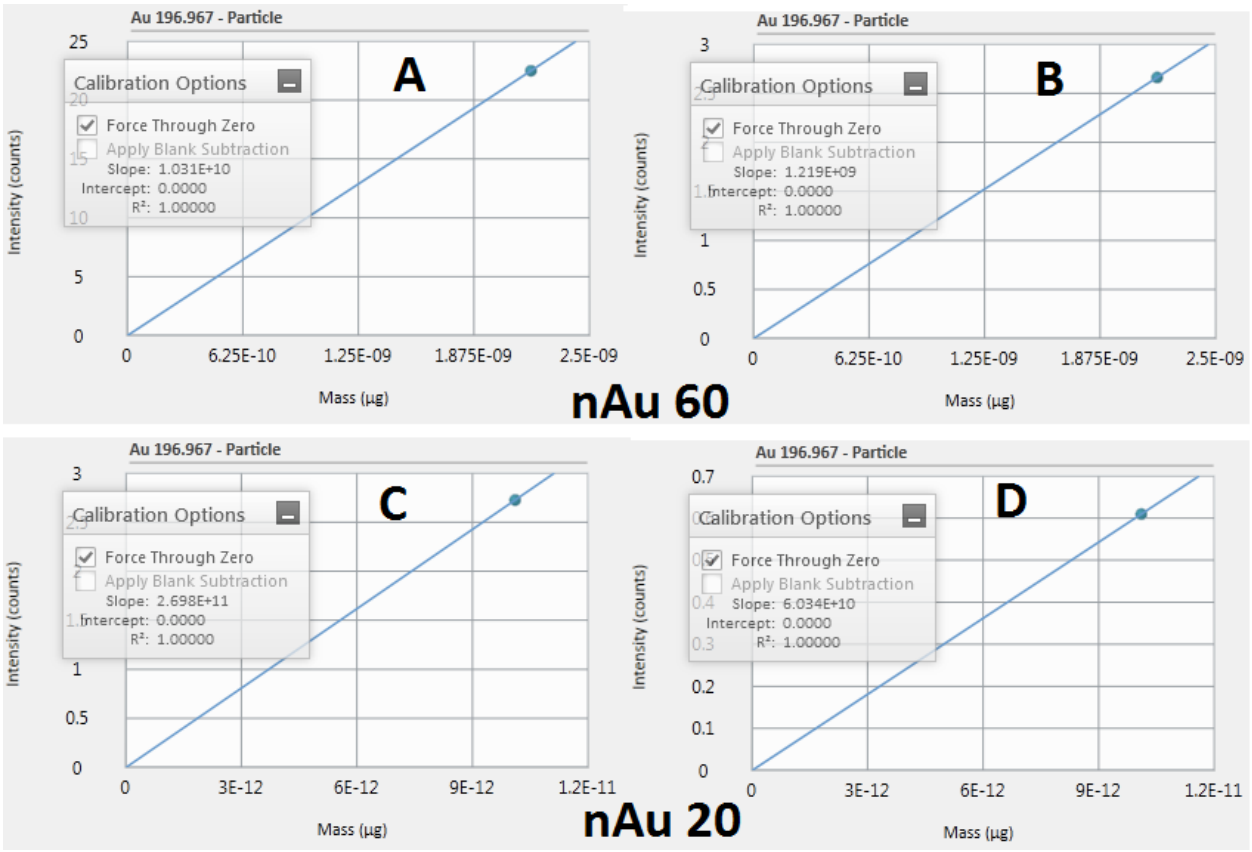

Figure 5-8 S3- The nAu signal intensity versus the mass of standard nAu to determine the transport efficiency; 60 nm nAu at dwell time (A)100 µs, and (B) 10 µs; 20 nm nAu at dwell time (C) 100 µs, and (D) 10 µs.

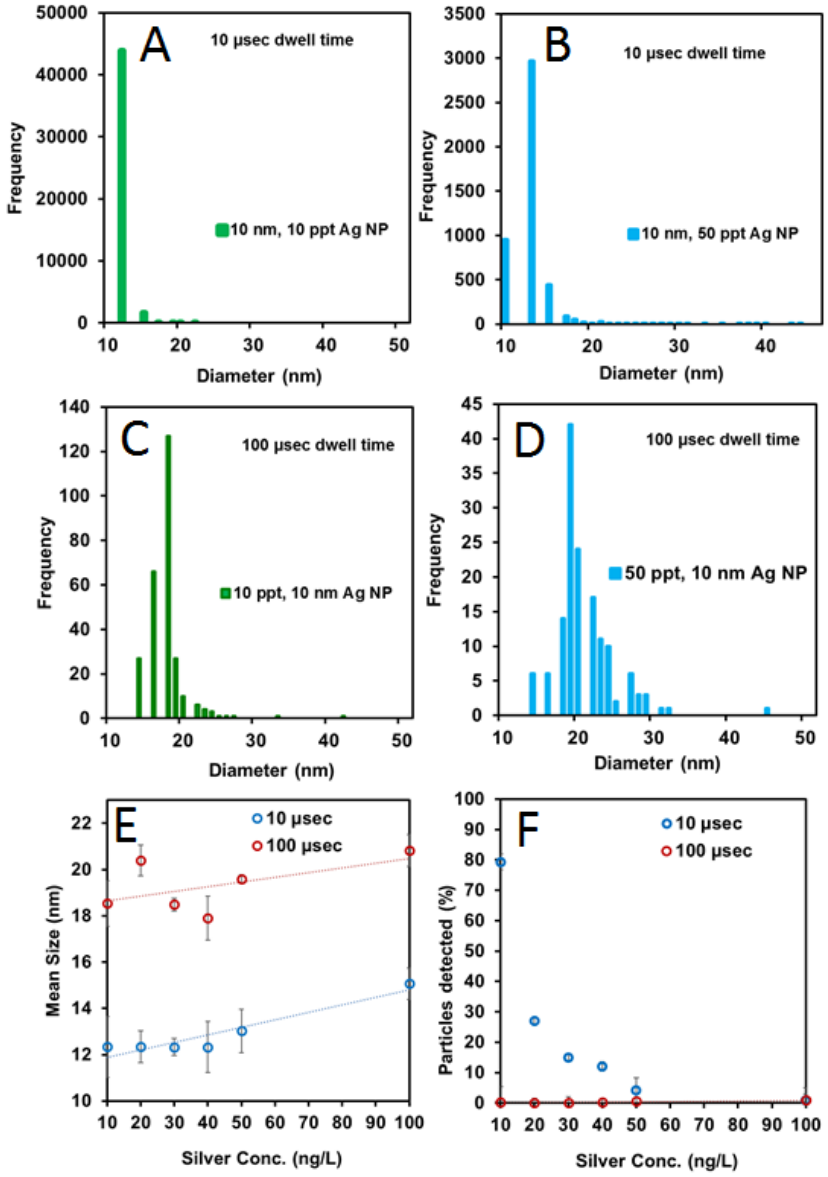

Figure 5-9 S4- The particle size distribution of 10 nm nAg at two dwell times (A, B) 10 µs ; and (C, D) 100 µs; (E) The change in particle mean size with the increase in silver mass concentration at two different dwell times, 10 and 100 µs; (F) The counting efficiency of 10 nm nAg with the change in silver mass concentration at two dwell times.

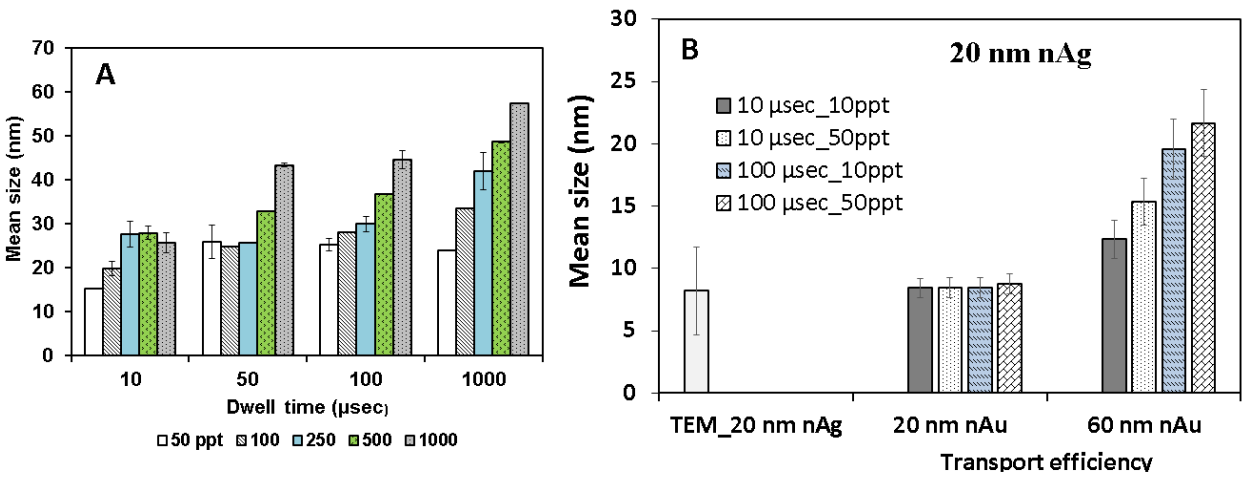

Figure 5-10 S5- Characterizing 20 nm PVP-Ag NPs with spICP-MS at (A) various dwell times and silver mass; (B) two different transport efficiency using 20 nm and 60 nm reference nAu.

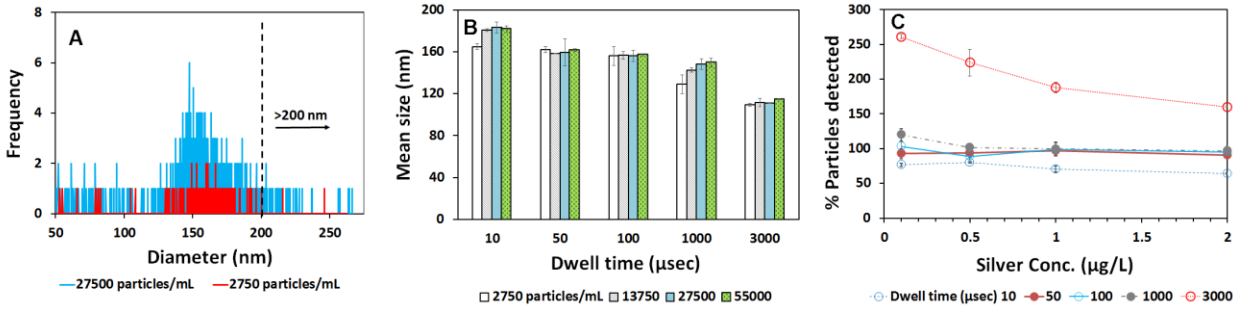

Figure 5-11 S6- 200 nm PVP- nAg characterized with spICP-MS in DI water (A) particle size distribution of nAg prepared at two particle number concentrations; 2750 and 27500 particles/mL; (B) The impact of dwell time and silver mass concentration on particle sizing; (C) The impact of dwell time and silver mass concentration on particle counting.

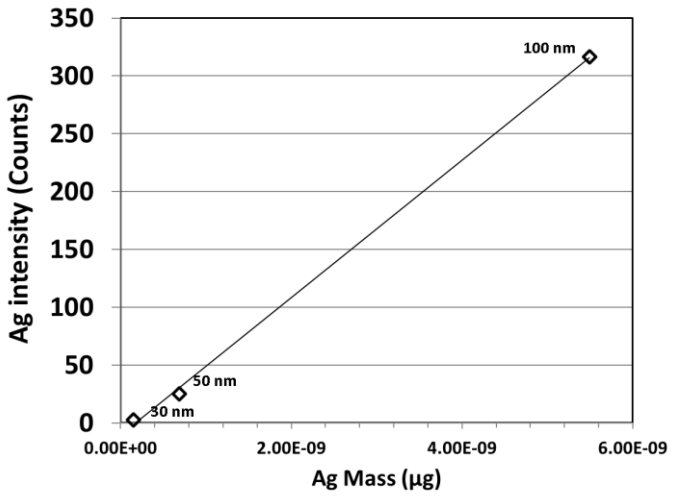

Figure 5-12 S7 – Nanoparticle diameter/mass calibration vs ^{107}Ag intensity (counts)

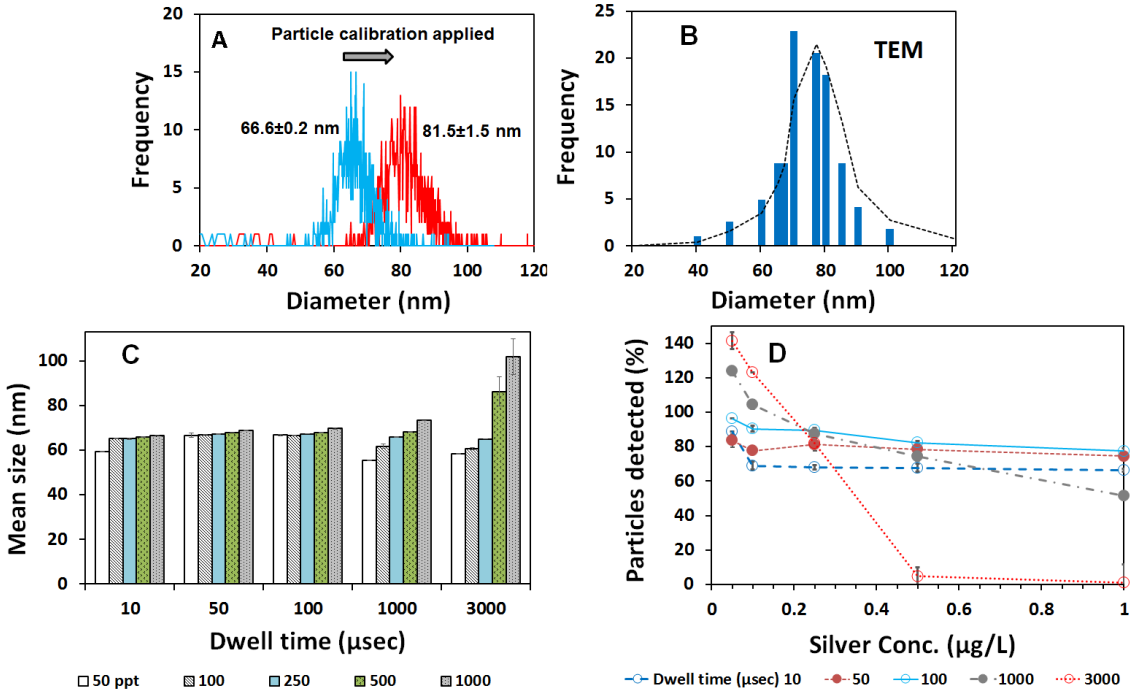

Figure 5-13 S8- 80 nm PVP- nAg characterized with spICP-MS in DI water. (A) The particle size distribution of PVP-nAg applying the dissolved and particle calibration with a silver concentration of 100 ppt at dwell time 100 µs; (B) Particle size distribution with TEM; (C) The impact of dwell time and silver mass concentration on particle sizing; (D) The impact of dwell time and silver mass concentration on particle counting.

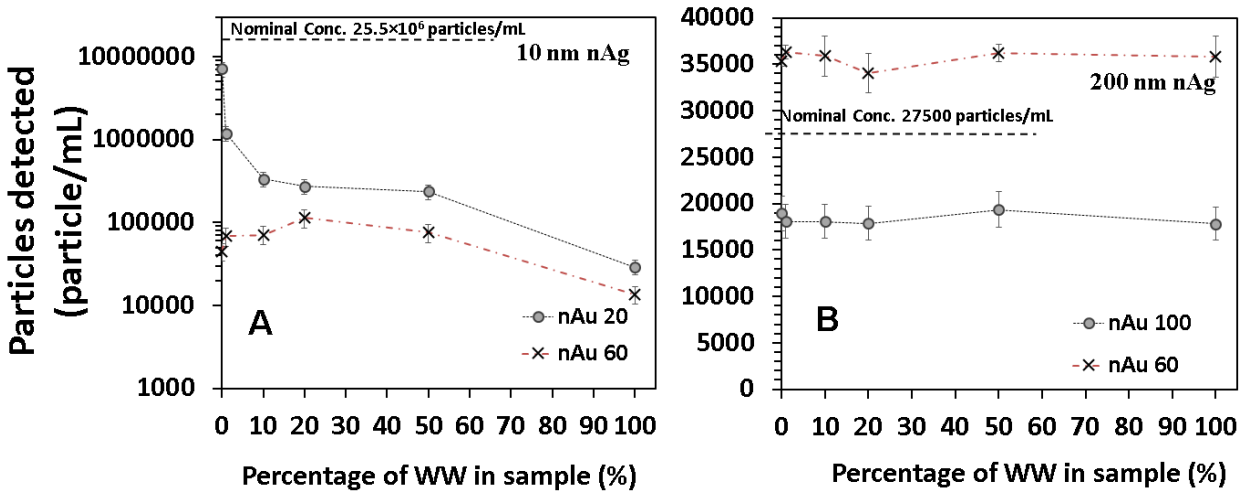

Figure 5-14 S9 – The particle number concentration of (A) 10 nm; (B) 200 nm, in WW mixed liquor sequentially dilutes from 1 to 100% in DI water.

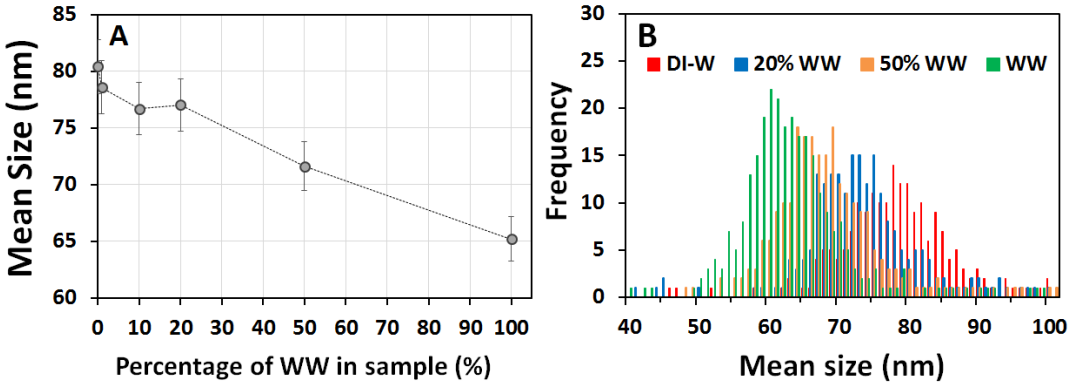

Figure 5-15 S10 – The impact of WW matrix on the particle sizing and particle size distribution of 80 nm PVP-nAg.

Sample time. The impact of the sample time is investigated by suspending the sulfidated 30 nm nAg (1 ppb) in DI water to simulate a common chemical transformation for nAg in the environment (Levard et al. 2013a). The particle size distribution of nAg freshly diluted in DI water is shown in Figure S11 and the mean size was measured at 29.7±2.1 nm by spICP-MS at 100 µs dwell time. The sulfidated nAg was analyzed after 30 days (Figure S 11B&C) in two sample times of 100 and 150 s. At a sample time of 100 s the particle size distribution showed an arbitrary peak at around 20 nm however by increasing the sample time to 150 s this peak disappeared. By increasing the sample time, acceptable number of events for 30 nm nAg was detected (Figure 11C) and the particle histogram showed the mean size of nAg at 33.3±0.6 nm which confirmed that the initial peak was incorrect.

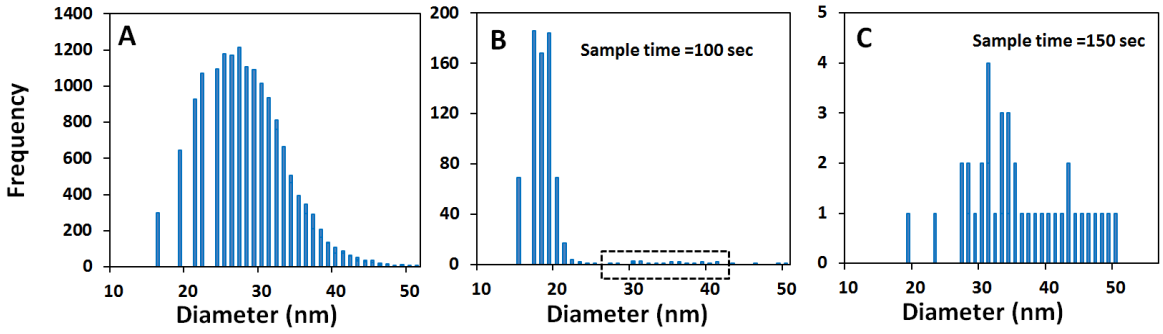

Figure 5-16 S11- Characterization of 30 PVP-nAg with spICP-MS in DI water. (A) Particle size distribution of nAg freshly suspended at 100 ppt in DI water analyzed at 100 µs dwell time; Particle size distribution of 30-day aged nAg in 250 ppt Na_2S solution with spICP-MS analyzed at 100 µs dwell time and two sample times of (B) 100 sec (C) 150 sec.

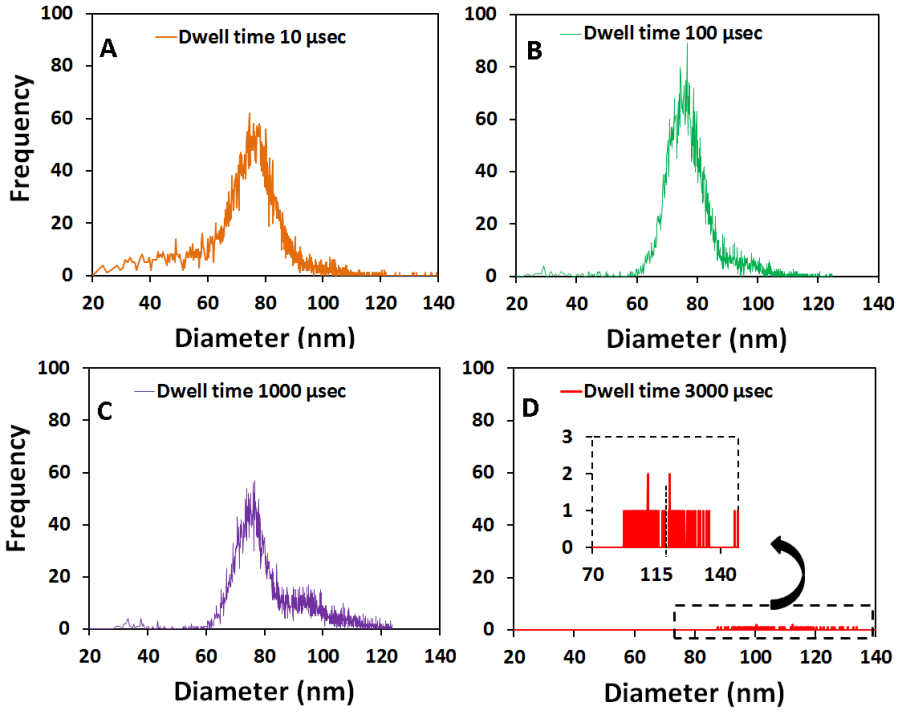

Figure 5-17 S12- Particle size distribution of 80 nm PVP-nAg at silver mass concentration of 1000 ppt analyzed at various dwell times (A) 10 (B) 100 (C) 1000 (D) 3000 µs.

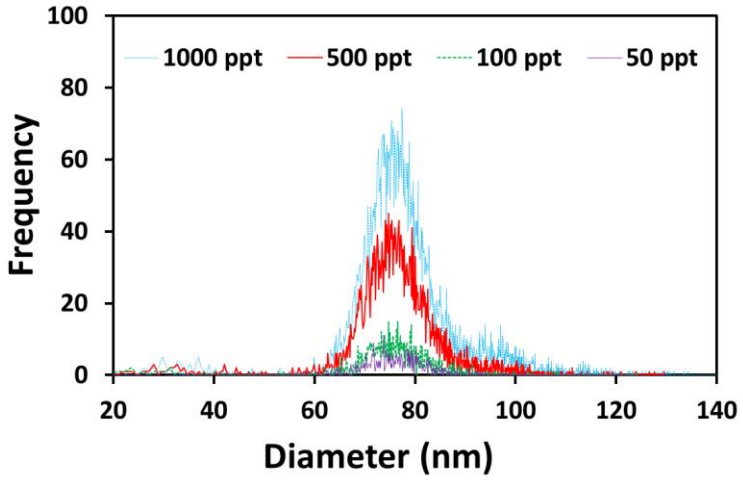

Figure 5-18 S13- The effect of serial dilutions on the particle size distribution for the 80 nm PVP-nAg in DI water analyzed at dwell time 100 µs.

5.7. References

1. Dunphy Guzman, K.A., Taylor, M.R. and Banfield, J.F. (2006) Environmental risks of nanotechnology: National nanotechnology initiative funding, 2000-2004. Environmental Science & Technology 40(5), 1401-1407.
2. Mueller, N.C. and Nowack, B. (2008) Exposure modeling of engineered nanoparticles in the environment. Environmental Science & Technology 42(12), 4447-4453.
3. Nowack, B. and Bucheli, T.D. (2007) Occurrence, behavior and effects of nanoparticles in the environment. Environmental Pollution 150(1), 5-22.
4. Mock, J., Barbic, M., Smith, D., Schultz, D. and Schultz, S. (2002) Shape effects in plasmon resonance of individual colloidal silver nanoparticles. The Journal of Chemical Physics 116(15), 6755-6759.
5. Liu, X., Dai, Q., Austin, L., Coutts, J., Knowles, G., Zou, J., Chen, H. and Huo, Q. (2008) A one-step homogeneous immunoassay for cancer biomarker detection using gold nanoparticle probes coupled with dynamic light scattering. Journal of the American Chemical Society 130(9), 2780-2782.
6. Kammer, F.v.d., Legros, S., Hofmann, T., Larsen, E.H. and Loeschner, K. (2011) Separation and characterization of nanoparticles in complex food and environmental samples by field-flow fractionation. TRAC Trends in Analytical Chemistry 30(3), 425-436.
7. Montaño, M.D., Olesik, J.W., Barber, A.G., Challis, K. and Ranville, J.F. (2016) Single Particle ICP-MS: Advances toward routine analysis of nanomaterials. Analytical and Bioanalytical Chemistry 408(19), 5053-5074.
8. Pace, H.E., Rogers, N.J., Jarolimek, C., Coleman, V.A., Gray, E.P., Higgins, C.P. and Ranville, J.F. (2012) Single particle inductively coupled plasma-mass spectrometry: A performance evaluation and method comparison in the determination of nanoparticle size. Environmental Science & Technology 46(22), 12272-12280.
9. Tuoriniemi, J., Cornelis, G. and Hassellöv, M. (2012) Size discrimination and detection capabilities of single-particle ICPMS for environmental analysis of silver nanoparticles. Analytical Chemistry 84(9), 3965-3972.
10. Telgmann, L., Metcalfe, C. and Hintelmann, H. (2014) Rapid size characterization of silver nanoparticles by single particle ICP-MS and isotope dilution. Journal of Analytical Atomic Spectrometry 29(7), 1265-1272.
11. Olesik, J.W. and Gray, P.J. (2012) Considerations for measurement of individual nanoparticles or microparticles by ICP-MS: determination of the number of particles and the analyte mass in each particle. Journal of Analytical Atomic Spectrometry 27(7), 1143-1155.
12. Gray, E.P., Coleman, J.G., Bednar, A.J., Kennedy, A.J., Ranville, J.F. and Higgins, C.P. (2013) Extraction and analysis of silver and gold nanoparticles from biological tissues using single particle inductively coupled plasma mass spectrometry. Environmental Science & Technology 47(24), 14315-14323.
13. Dan, Y., Zhang, W., Xue, R., Ma, X., Stephan, C. and Shi, H. (2015) Characterization of gold nanoparticle uptake by tomato plants using enzymatic extraction followed by single-particle inductively coupled plasma–mass spectrometry analysis. Environmental Science & Technology 49(5), 3007-3014.
14. Witzler, M., Küllmer, F., Hirtz, A. and Guenther, K. (2016) Validation of Gold and Silver Nanoparticle Analysis in Fruit Juices by sp-ICP-MS Without Sample Pre-Treatment. Journal of Agricultural and Food Chemistry.
15. Furtado, L.M., Hoque, M.E., Mitrano, D.M., Ranville, J.F., Cheever, B., Frost, P.C., Xenopoulos, M.A., Hintelmann, H. and Metcalfe, C.D. (2014) The persistence and transformation of silver

nanoparticles in littoral lake mesocosms monitored using various analytical techniques. Environmental Chemistry 11(4), 419-430.
16. António, D.C., Cascio, C., Jakšić, Ž., Jurašin, D., Lyons, D.M., Nogueira, A.J., Rossi, F. and Calzolai, L. (2015) Assessing silver nanoparticles behaviour in artificial seawater by mean of AF4 and spICP-MS. Marine environmental research 111, 162-169.
17. Mitrano, D.M., Rimmele, E., Wichser, A., Erni, R., Height, M. and Nowack, B. (2014) Presence of nanoparticles in wash water from conventional silver and nano-silver textiles. ACS nano 8(7), 7208-7219.
18. Mitrano, D.M., Arroyo Rojas Dasilva, Y. and Nowack, B. (2015) Effect of variations of washing solution chemistry on nanomaterial physicochemical changes in the laundry cycle. Environmental Science & Technology 49(16), 9665-9673.
19. Verleysen, E., Van Doren, E., Waegeneers, N., De Temmerman, P.-J., Abi Daoud Francisco, M. and Mast, J. (2015) TEM and SP-ICP-MS analysis of the release of silver nanoparticles from decoration of pastry. Journal of Agricultural and Food Chemistry 63(13), 3570-3578.
20. Peters, R., Herrera-Rivera, Z., Undas, A., van der Lee, M., Marvin, H., Bouwmeester, H. and Weigel, S. (2015) Single particle ICP-MS combined with a data evaluation tool as a routine technique for the analysis of nanoparticles in complex matrices. Journal of Analytical Atomic Spectrometry 30(6), 1274-1285.
21. Hadioui, M., Merdzan, V. and Wilkinson, K.J. (2015) Detection and characterization of ZnO nanoparticles in surface and waste waters using single particle ICPMS. Environmental Science & Technology 49(10), 6141-6148.
22. Mitrano, D.M., Lesher, E.K., Bednar, A., Monserud, J., Higgins, C.P. and Ranville, J.F. (2012a) Detecting nanoparticulate silver using single-particle inductively coupled plasma–mass spectrometry. Environmental Toxicology and Chemistry 31(1), 115-121.
23. Yang, Y., Long, C.-L., Li, H.-P., Wang, Q. and Yang, Z.-G. (2016) Analysis of silver and gold nanoparticles in environmental water using single particle-inductively coupled plasma-mass spectrometry. Science of the Total Environment 563, 996-1007.
24. Proulx, K., Hadioui, M. and Wilkinson, K.J. (2016) Separation, detection and characterization of nanomaterials in municipal wastewaters using hydrodynamic chromatography coupled to ICPMS and single particle ICPMS. Analytical and Bioanalytical Chemistry, 1-9.
25. Degueldre, C. and Favarger, P.-Y. (2003) Colloid analysis by single particle inductively coupled plasma-mass spectroscopy: a feasibility study. Colloids and Surfaces A: Physicochemical and Engineering Aspects 217(1), 137-142.
26. Degueldre, C. and Favarger, P.-Y. (2004) Thorium colloid analysis by single particle inductively coupled plasma-mass spectrometry. Talanta 62(5), 1051-1054.
27. Degueldre, C., Favarger, P.-Y. and Wold, S. (2006) Gold colloid analysis by inductively coupled plasma-mass spectrometry in a single particle mode. Analytica Chimica Acta 555(2), 263-268.
28. Laborda, F., Bolea, E. and Jiménez-Lamana, J. (2016) Single particle inductively coupled plasma mass spectrometry for the analysis of inorganic engineered nanoparticles in environmental samples. Trends in Environmental Analytical Chemistry 9, 15-23.
29. Laborda, F., Jiménez-Lamana, J., Bolea, E. and Castillo, J.R. (2011) Selective identification, characterization and determination of dissolved silver (I) and silver nanoparticles based on single particle detection by inductively coupled plasma mass spectrometry. Journal of Analytical Atomic Spectrometry 26(7), 1362-1371.
30. Pace, H.E., Rogers, N.J., Jarolimek, C., Coleman, V.A., Higgins, C.P. and Ranville, J.F. (2011) Determining transport efficiency for the purpose of counting and sizing nanoparticles via single particle inductively coupled plasma mass spectrometry. Analytical Chemistry 83(24), 9361-9369.

31. Lee, S., Bi, X., Reed, R.B., Ranville, J.F., Herckes, P. and Westerhoff, P. (2014) Nanoparticle size detection limits by single particle ICP-MS for 40 elements. Environmental Science & Technology 48(17), 10291-10300.
32. Mitrano, D.M., Barber, A., Bednar, A., Westerhoff, P., Higgins, C.P. and Ranville, J.F. (2012b) Silver nanoparticle characterization using single particle ICP-MS (SP-ICP-MS) and asymmetrical flow field flow fractionation ICP-MS (AF4-ICP-MS). Journal of Analytical Atomic Spectrometry 27(7), 1131-1142.
33. Hineman, A. and Stephan, C. (2014) Effect of dwell time on single particle inductively coupled plasma mass spectrometry data acquisition quality. Journal of Analytical Atomic Spectrometry.
34. Montano, M., Badiei, H., Bazargan, S. and Ranville, J. (2014) Improvements in the detection and characterization of engineered nanoparticles using spICP-MS with microsecond dwell times. Environmental Science: Nano 1(4), 338-346.
35. Tuoriniemi, J., Cornelis, G. and Hassellöv, M. (2015) A new peak recognition algorithm for detection of ultra-small nano-particles by single particle ICP-MS using rapid time resolved data acquisition on a sector-field mass spectrometer. Journal of Analytical Atomic Spectrometry 30(8), 1723-1729.
36. Liu, J., Murphy, K.E., MacCuspie, R.I. and Winchester, M.R. (2014) Capabilities of single particle inductively coupled plasma mass spectrometry for the size measurement of nanoparticles: a case study on gold nanoparticles. Analytical Chemistry 86(7), 3405-3414.
37. Laborda, F., Jiménez-Lamana, J., Bolea, E. and Castillo, J.R. (2013) Critical considerations for the determination of nanoparticle number concentrations, size and number size distributions by single particle ICP-MS. Journal of Analytical Atomic Spectrometry 28(8), 1220-1232.
38. Hotze, E.M., Phenrat, T. and Lowry, G.V. (2010) Nanoparticle aggregation: challenges to understanding transport and reactivity in the environment. Journal of environmental quality 39(6), 1909-1924.
39. Pal, T., Sau, T.K. and Jana, N.R. (1997) Reversible formation and dissolution of silver nanoparticles in aqueous surfactant media. Langmuir 13(6), 1481-1485.
40. Cornelis, G. and Hassellöv, M. (2014) A signal deconvolution method to discriminate smaller nanoparticles in single particle ICP-MS. Journal of Analytical Atomic Spectrometry 29(1), 134-144.
41. Smith, D.D. and Browner, R.F. (1982) Measurement of aerosol transport efficiency in atomic spectrometry. Analytical Chemistry 54(3), 533-537.
42. Olson, K., Haas Jr, W. and Fassel, V. (1977) Multielement detection limits and sample nebulization efficiencies of an improved ultrasonic nebulizer and a conventional pneumatic nebulizer in inductively coupled plasma-atomic emission spectrometry. Analytical Chemistry 49(4), 632-637.
43. Gustavsson, A. (1984) The determination of some nebulizer characteristics. Spectrochimica Acta Part B: Atomic Spectroscopy 39(5), 743-746.
44. Gottschalk, F., Sonderer, T., Scholz, R.W. and Nowack, B. (2009) Modeled environmental concentrations of engineered nanomaterials (TiO2, ZnO, Ag, CNT, fullerenes) for different regions. Environmental Science & Technology 43(24), 9216-9222.
45. Keller, A.A., McFerran, S., Lazareva, A. and Suh, S. (2013) Global life cycle releases of engineered nanomaterials. Journal of Nanoparticle Research 15(6), 1-17.
46. Levard, C., Hotze, E.M., Colman, B.P., Dale, A.L., Truong, L., Yang, X., Bone, A.J., Brown Jr, G.E., Tanguay, R.L. and Di Giulio, R.T. (2013) Sulfidation of silver nanoparticles: natural antidote to their toxicity. Environmental Science & Technology 47(23), 13440-13448.

Chapter 6 SUMMARY, CONCLUSIONS, AND FUTURE WORK

6.1. Summary and Conclusions

The overall goal of this thesis is to understand better the parameters that influence the dissolution of nAg in WW and natural waters and explore the impact of major constituents such as inorganic sulfides and DOC compounds in those aqueous matrices on the dissolution behavior of nAg.

Dissolution of nAg was supressed upon contact with municipal WW in batch systems as compared to similar systems containing DI water. In Chapter 3, it was shown that acid volatile sulfides and DOC were abundantly present in WW effluent and mixed liquor, and upon interaction with the surface of nAg, dissolution was inhibited. Extensive characterization of nAg surface with XPS, EDX, and ToF-SIMs confirmed presence of amine, and thiol-containing organics associated with nAg. It was observed that initial particle concentration, and availability of dissolved oxygen plays a considerable role in the dissolution extent and rate of nAg. Increasing the particle concentration from 5×10^{6} to 5×10^{8} particle/mL decreased the dissolution rate from 3.77×10^{-8} to 1.63×10^{-8} g cm^-2 sec^{-1} at 72 h. In addition, stripping off the dissolved oxygen (DO) levels to 5.3 and 2.2 mg/L in WW effluent and mixed liquor, caused the dissolved silver concentration to decrease by more than 50%, compared to DI water systems. This study also for the first time found that dissolved Ag^{+} ions were complexed with inorganic sulfides or organosulfur compounds and reformed into small nAg_xS_y particles after 120 h of exposure time of the parent nAg. Ag^{+} ions contacted with cysteine also resulted in plasmonic Ag nanoparticles whereas contacting Ag^{+} ions with various concentrations of Suwannee River humic and fulvic acids under same experimental condition did not show any formation of NPs.

In Chapter 4, presence of DOC, such as humic substances, prior to or simultaneous with the addition of the mixture of metal sulfides, inhibited the sulfidation of nAg. The results from

long-term (684 h) dissolution experiments of nAg showed that the presence of humic substance and alginate in post-sulfidated systems enhanced the dissolution of nAg up to 500 and 212 %, respectively, for 30 nm PVP-nAg. Humic substances improved the dissolution of nAg in post-sulfidated systems compared to sulfidated nAg, by two pathways: first, interaction of the humic substances with the nAg surface blocked active sites for sulfidation reaction, and second, by sorbing the sulfides in solution and thus reducing the availability of sulfides to react with nAg. Alginate was not able to limit reactions of sulfides in pre-sulfidated systems or when alginate was added simultaneously with alginate. Experiments confirmed that alginate was not able to bind dissolved sulfides and therefore when sulfides were present with or before the alginate molecules were added, the sulfidation reaction readily inhibited the dissolution of nAg almost completely. nAg in the presence of a mixture of amino acids (cysteine, and methionine) was readily aggregated and precipitated out of solution, and UV-vis absorbance spectra changes confirmed particle size growth. Formation of secondary nAg in the cysteine and methionine solution was observed which confirmed that silver ions after release were reduced by amino acids. Furthermore, this study showed for the first time that nAg dissolved in HA/FA and alginate to a similar extent as DI water when the contact time was long enough (648 h) although, during the first several hours of contact with HA/FA and alginate, the dissolution of nAg was supressed. Prior studies did not examine the dissolution extent over long times and concluded that HA/FA and alignate reduced the solubility of nAg.

Results from Chapter 5 suggests that spICP-MS is capable of detecting nAg, 10 nm and 200 nm, with high accuracy in complex matrix of WW. This study for the first time developed a method to improve the sizing accuracy by spICP-MS for small nAg (10 and 20 nm) and large nAg (200 nm). The results showed that the size of reference gold NP for determination of

transport efficiency is significantly important. The results showed that the transport efficiency changed with the size of reference gold NP as well as with the change in dwell time. Therefore, choosing long dwell times (>1000 μs), and 60 nm reference gold NP to calculate the transport efficiency resulted in overestimation of the size of 10 nm nAg. The transport efficiency was recalculated using a reference gold NP (20 nm nAu) that has a diameter comparable to that of target nAg. Using this new transport efficiency, the dissolved Ag standard calibration was repeated and then re-analyzed and the nAg suspension was characterized at dwell times of 10 and 100 μs. The mean size attained by this modified method matched with the mean size obtained by TEM. Moreover, this study showed that assuming 100% ionization efficiency and using the dissolved standard silver calibration instead of the NP calibration for large nAg (80 and 200 nm) is not reliable. We applied the NP calibration using three standard nAg and reanalyzed 80 and 200 nm nAg using this new calibration and the mean size attained was in very good agreement with the NP mean size obtained with TEM. Applying the dissolved standard silver calibration resulted in underestimation of the mean size for 200 nm nAg.

Overall, this research demonstrates that:

(i) Inorganic sulfides in the form of metal sulfides that are persistent in oxic municipal WW and DOC compounds heavily interacted with nAg surface and impacted the dissolution rates and extents;

(ii) inorganic sulfides supressed the dissolution of nAg to various extents depending on the S to Ag mole ratio, but the presence of humic substances can suppress the interactions of sulfides with nAg by first, creating a physical barrier due to strong interactions with nAg surface, and second, by binding free sulfides in solution;

(iii) spICP-MS is a powerful technique for thorough investigation of nAg dissolution because it provides NPs size and concentration data simultaneously with the dissolved silver concentrations, and the detection of nAg in pure and environmental water samples can be improved by recalculating the transport efficiency using gold reference NP of sizes similar to the nAg in target samples.

6.2. Future work

Understanding the dissolution behavior of nAg in environmental matrices is significant for assessing their fate and potential risks to environmental receptors. nAg dissolves in the presence an oxidizing source, and releases Ag^+ ions which are shown to be toxic to various biota. We have demonstrated in this research that nAg dissolved in WW even when considerable concentration of acid volatile sulfides were present. The sulfidation reaction in WW could be inhibited due to the presence of DOC compounds as was observed in Chapter 4. However, this study was conducted in batch systems and the presence of large amounts of suspended solids, sludge and extracellular polymeric substances can greatly influence the oxidation and dissolution of nAg. It is important to investigate the potential of ion release and extent of dissolution in pilot scale and real WW treatment systems. nAg attachment to biofilm, and EPS can affect the surface chemistry of nAg which needs to be investigated in a larger scale treatment process of WW.

Reformation of nanoparticulate silver from the dissolved silver can have very different toxicological implications as compared to pristine nAg due to their significantly smaller size than the parent nAg and different surface chemistry. Therefore, it would be important to examine the toxicity of these secondary particles, sulfidated nAg, and nAg complexed with DOC, on some microorganisms typical to WW and compare it with the toxicity of pristine nAg.

Our results show that organic and inorganic sulfides were associated with secondary particles generated from dissolved Ag. Characterization of WW specimen for DOC, and acid volatile sulfides confirmed the presence of ppm levels of these compounds in WW systems. Our experiments showed that organics such as humic substances were not able to form nAg in similar conditions (i.e. light, temperature, dissolved oxygen) as WW systems, whereas amino acids such as cysteine reformed free Ag^{+} into nanoparticulates of silver within several hours of contact. A thorough investigation of WW DOC structure can help to shed light on the identity of these organic carbons to know which dissolved organics play a major role in the reformation of nAg.

This research investigated the characterization of nAg of several various diameters by spICP-MS and developed the optimum conditions to detect and track nAg and its dissolution in complex environmental matrices using this technique. However, spICP-MS has been less explored for the characterization of several other ENPs such as copper and zinc oxide NPs. Therefore, it would be interesting to optimize characterization of copper and zinc NPs using spICP-MS and examine the accuracy of this technique to determine the mean size, and particle concentration. Furthermore, this study focused on development of methodologies to improve data acquisition by spICP-MS. Future research should focus on improvements to the nebulization systems and its impact on the characterization of transport efficiency.